

ScholarWorks@GSU

Genetic, Biochemical, and Functional Characterization of Heme Metabolism in Group A Streptococcus

Authors	Sachla, Ankita J
Citation	Sachla, Ankita J. 2015. "Genetic, Biochemical, and Functional Characterization of Heme Metabolism in Group A Streptococcus." Georgia State University. https://doi.org/10.57709/7882491
DOI	https://doi.org/10.57709/7882491
Download date	2026-04-13 11:01:53
Link to Item	https://hdl.handle.net/20.500.14694/1957

GENETIC, BIOCHEMICAL, AND FUNCTIONAL CHARACTERIZATION OF HEME
METABOLISM IN GROUP A STREPTOCOCCUS

by

ANKITA J. SACHLA

Under the Direction of Zehava Eichenbaum, PhD

ABSTRACT

Heme is vital to a variety of cellular functions in bacteria ranging from energy generation to iron reserve. Group A streptococcus (GAS) is a prevalent bacterial pathogen that is responsible for an array of human diseases ranging from simple, self-limiting, mucosal and skin infections to invasive and systemic manifestations. GAS needs iron for growth and can satisfy this nutritional requirement by scavenging the metal from heme. The pathogen produces powerful hemolysins that facilitate heme release during infection. Heme is captured and relayed through the GAS cell wall and cytoplasmic membrane by dedicated receptors and transporters. To-date, the fate of the acquired heme is unknown in Streptococci. Although heme is nutritionally beneficial for GAS growth, its pro-oxidant and lipophilic nature makes it a liability

with damaging effects on cellular components. The conundrum associated with heme use is particularly pertinent to GAS pathophysiology since invasive GAS infections involve massive hemolysis and the generation of unescorted heme in excess. In this dissertation, I aimed to describe the mechanisms that GAS uses for heme catabolism while managing its toxicity. I conducted a biochemical characterization of a new enzyme, HupZ in GAS that degrades heme *in vitro*. Similar to the heme oxygenase-1 (HO-1), HupZ activity leads to the formation of iron, CO, and a biliverdin-like product. I also investigated the impact of heme on GAS physiology and identified key mediators in the repair and detoxification process. This study demonstrated that heme exposure leads to a general stress response that involves the activation of antioxidant defense pathways to restore redox balance. Further, I studied a 3-gene cluster, *pefRCD* (*porphyrin-regulated efflux RCD*), which was activated by environmental heme, and provided support to my hypothesis that the *pefRCD* gene encodes a heme-sensing regulator (PefR) and heme efflux system (PefCD). I showed that the *pef* system protects GAS cells from heme-induced damage to the membrane and DNA by preventing cellular accumulation of heme. In conclusion, this dissertation addresses key knowledge gaps in GAS physiology and provides new insights into heme metabolism of GAS.

INDEX WORDS: Heme tolerance, Group A streptococcus, Gram-positive, heme sensing, mutational analysis, heme toxicity, heme tolerance, PefRCD transporter, heme efflux, heme degradation, HupZ protein, UV-vis spectroscopy, iron and CO release.

GENETIC, BIOCHEMICAL, AND FUNCTIONAL CHARACTERIZATION OF HEME
METABOLISM IN GROUP A STREPTOCOCCUS

by

ANKITA J. SACHLA

A Dissertation Submitted in Partial Fulfillment of the Requirements for the Degree of

Doctor of Philosophy

in the College of Arts and Sciences

Georgia State University

2015

Copyright by
Ankita J. Sachla
2015

GENETIC, BIOCHEMICAL, AND FUNCTIONAL CHARACTERIZATION OF HEME
METABOLISM IN GROUP A STREPTOCOCCUS

by

ANKITA J. SACHLA

Committee Chair: Zehava Eichenbaum

Committee: Parjit Kaur

Adam Wilson

Chung-Dar Lu

Electronic Version Approved:

Office of Graduate Studies

College of Arts and Sciences

Georgia State University

December 2015

DEDICATION

I dedicate my scientific work and achievements to my wonderful parents, Jagdish and Jyoti Sachla for granting me this exceptional opportunity to study abroad. I am greatly indebted to their relentless support, unconditional love, guidance, and encouragements in all my endeavors. They have truly nurtured my dreams and provided me with the life long vision of success. Thank you for always putting my needs and desires on top priorities, I feel absolutely blessed to have both of you in my life.

I also dedicate this dissertation to both my sisters for being marvelous friends and cheerleaders all along this doctorate journey, starting from GRE preparation to regular pep talks.

Special thanks to Dr. Timothy Bartness for teaching me all the necessary tools to survive in academia and Dr. Lois Borek for her warmth and kindness towards me. Thank you Gargi for showing me the ropes when I came to the US.

This work is possible due to lovely interactions that I had with all my friends that I have made throughout this process at Georgia State University and at Mumbai.

Above all, special dedication to almighty god for the gift of life and guidance all through out.

“And, when you want something, all the universe conspires in helping you to achieve it.” - Paulo

Coelho

ACKNOWLEDGEMENTS

The Webster's dictionary defines mentor as an experienced and trusted advisor, and it was after meeting Dr. Zehava Eichenbaum that I truly understood and cherished its meaning. I express my heartfelt gratitude to Dr. Eichenbaum for being an exceptional and passionate advisor throughout my doctoral program. Thank you for welcoming me in your laboratory with great warmth and consistently supporting all of my scientific ventures. I consider her to be a trailblazing scientist with a keen eye for details. Her mentorship has enabled me to be an original writer and independent thinker. Thank you for nurturing my career and creating all the opportunities. I am grateful to Molecular Basis of Disease (MBD) Area of Focus fellowship for all the awards and support, especially to Dr. Susanna Greer for her professionalism and insight on career after graduate school. I would like to extend my thanks to our collaborators Dr. Giovanni Gadda for help with biochemical analysis of HupZ protein. All of the HupZ (spectral) work was carried out in conjunction with Dr. Elvira Guzman of Gadda lab, where I learned a great deal of biochemistry and troubleshooting skills from her. The friendly working environment and welcoming spirit of Eichenbaum and Gadda lab members has been instrumental in my progress. Additionally, my appreciation to Dr. Jiafeng Geng of Aimin Liu's lab for conducting electron paramagnetic resonance analysis on HupZ and being a cohesive interdisciplinary team while writing and presenting MBD seed grant. I am also thankful to my committee members: Dr. Parjit Kaur, Dr. Adam Wilson, and Dr. Chung-Dar Lu on helpful discussions, feedbacks, and cooperation during various meetings. Lastly thanks to all who made this work possible. *"Perfection is not attainable, but if we chase perfection we can catch excellence"* - Vincent Lombardi.

TABLE OF CONTENT

ACKNOWLEDGEMENTS	V
1 GENERAL INTRODUCTION.....	1
1.1 Group A streptococcus	1
1.2 GAS burden.....	1
1.3 GAS virulence.....	2
1.4 Dissertation objectives and significance.....	4
2 CHAPTER 1. THE CORNUCOPIAS INTERACTIONS OF PORPHYRIN-HEME IN A BACTERIAL SYSTEM	5
2.1 Iron, heme, and infection in mammalian systems.....	5
2.2 Heme.....	7
2.3 Heme uptake.....	9
2.4 Heme degradation.....	12
2.5 The redox-active nature of heme.	14
2.6 Heme tolerance.....	15
3 CHAPTER 2- IN VITRO HEME BIOTRANSFORMATION BY THE HUPZ ENZYME FROM GROUP A STREPTOCOCCUS.....	19
3.1 Introduction.....	19
3.2 Materials and Methods.....	23
3.2.1 <i>Bacterial strains, media and antibiotics</i>	23
3.2.2 <i>Recombinant HupZ</i>	23
3.2.3 <i>Protein expression and purification</i>	23
3.2.4 <i>Heme reconstitution</i>	24
3.2.5 <i>Heme degradation assays</i>	24
3.2.6 <i>Myoglobin differential spectroscopy</i>	25
3.2.7 <i>Ferrozine differential spectroscopy</i>	25
3.2.8 <i>Crystallization and data collection</i>	26
3.2.9 <i>Structure determination</i>	26
3.3 Results	27
3.3.1 <i>HupZ is a new heme binding protein</i>	27

3.3.2	<i>Heme degradation by HupZ proceeds with the production of CO, ferrous iron, and a chromophore that absorbs at 660 nm</i>	29
3.3.3	<i>Crystal structure of HupZ</i>	31
3.4	Discussion	34
4	CHAPTER 3- HEME TOXICITY AND TOLERANCE IN GAS	39
4.1	Introduction	39
4.2	Materials and Methods	43
4.2.1	<i>Bacterial strains and growth conditions</i>	43
4.2.2	<i>Determination of the minimal inhibitory concentration (MIC). Agar dilution method</i>	43
4.2.3	<i>Thiobarbituric acid-reactive-substances (TBARS) assay for lipid damage</i>	44
4.2.4	<i>Detection of protein damage</i>	45
4.2.5	<i>RNA extraction</i>	45
4.2.6	<i>Microarray analysis and Real-Time RT-PCR validation</i>	46
4.2.7	<i>Quantification of expression by real-time RT-PCR</i>	48
4.2.8	<i>In silico analysis</i>	48
4.2.9	<i>Cloning, overexpression, and purification of PefR</i>	49
4.2.10	<i>Heme and PPIX binding assay</i>	49
4.3	Results	50
4.3.1	<i>Excess of heme is inhibitory to the growth of GAS</i>	50
4.3.2	<i>Exposure to sub-lethal heme levels cause lipid peroxidation in GAS</i>	51
4.3.3	<i>Exposure to heme damaged membrane proteins</i>	52
4.3.4	<i>GAS demonstrates adaptation response to heme</i>	53
4.3.5	<i>Identification of the pefRCD locus in GAS</i>	55
4.3.6	<i>GAS PefR binds heme and PPIX with high affinity</i>	56
4.4	Discussion	57
5	CHAPTER 4 - THE PEFC D IS A MDR SYSTEM THAT EXPORTS HEME AND CONFERS RESISTANCE TO HEME AND DOXORUBICIN IN GAS	63
5.1	Introduction	63
5.2	Materials And Methods	67
5.2.1	<i>Bacterial strains and growth conditions</i>	67

5.2.2	<i>Nucleic acid methods.</i>	67
5.2.3	<i>Construction of plasmids, GAS mutants and complementation strains:</i>	68
5.2.4	<i>Heme and doxorubicin sensitivity assay</i>	68
5.2.5	<i>Determination of lipid peroxidation using TBARS assay</i>	69
5.2.6	<i>DNA damage detection</i>	69
5.2.7	<i>Determination of intracellular heme content</i>	70
5.3	Results	71
5.3.1	<i>The pefCD genes encode a conserved Class-1 ABC exporter</i>	71
5.3.2	<i>Inactivation of pefCD resulted in a growth phenotype and hypersensitivity to heme and doxorubicin.</i>	73
5.3.3	<i>Inactivation of the pefCD system is associated with elevated levels of heme-induced damage to cellular constituents</i>	74
5.3.4	<i>The pefCD prevents cellular heme accumulation</i>	76
5.4	Discussion	77
REFERENCES		84
APPENDIX		102
Appendix A: Tables		102
Appendix B: Figures		111
Appendix C: Supplementary Tables		151
Appendix D: Supplementary Figures		166

1 GENERAL INTRODUCTION

1.1 Group A streptococcus

Group A streptococcus (GAS) also commonly known as *Streptococcus pyogenes* is a Gram-positive, beta-hemolytic, obligate human pathogen that can adapt and flourish in numerous micro environments within the human body. GAS infections are realized in a range of manifestations from superficial, self-limiting infections of the mucous membranes and skin (pharyngitis, pyoderma, impetigo, etc.) to more severe and rare invasive infections (bacteremia, necrotizing fasciitis, streptococcal toxic shock syndrome, etc.) (1, 2). In certain patients GAS can cause autoimmune complications in the form of glomerulonephritis or acute rheumatic fever (3, 4). Occurrences of rheumatic fever is linked to rheumatic heart disease and neurological complications (5).

1.2 GAS burden.

GAS infections are ranked among the top 10 causes of infectious mortality (1). Worldwide, GAS causes ~700 million infections every year of which 1.8 million are invasive manifestations with 25% mortality rate (~450,000 patients succumb to death) (6). The non-invasive infections are treated with the β -lactam group of antibiotics; however, the invasive manifestations of GAS are rapid, aggressive, and difficult to manage. Often surgical amputation is the only available alternative that significantly impairs the lifestyle of the patients and requires extensive care (7). Manifestations of acute-rheumatic fever following GAS pharyngeal infections cause damage to joints and heart and account for a significant morbidity (~223,000 cases worldwide) (3, 4). In the absence of efficacious and licensed vaccines made for human practices, the understanding of the GAS-host interactions is an important strategy that may facilitate the design of novel therapeutics for combating GAS infections (8).

1.3 GAS virulence

The pathophysiology of GAS is very complex; GAS is a versatile pathogen that is armed with more than 50 identified virulence factors, some are shared by all strains (consisting of the core virulon) while others are strain-specific. GAS virulence factors contribute to the different stages of infection and pathologies, occasionally serving redundant functions. The highlights of some of GAS core virulence factors are as follows:

M protein: The M protein is the major surface and virulence determinant in GAS, it protects the bacterium from phagocytosis and facilitates adherence to the host epithelium (2). The cell wall anchored M protein is encoded by the *emm* gene. The hyper variability of M protein is the basis for GAS serotyping. There are more than 200 M protein types identified in GAS up to date (6).

Capsule: GAS produces hyaluronic acid capsule that coats the bacterial cell and protects it from complement deposition and phagocytosis (9-11). Capsule biosynthesis in GAS is brought about by the *hasABC* operon, which codes for membrane bound synthase leading to the assembly of a linear hyaluronic acid polymer made out of alternating units of glucuronic acid β -1,-3 linked to N-acetylglucosamine (12, 13). The capsular gene expression is increased during GAS growth in blood

Cytolysins: GAS cells produce two hemolysins, SLO and SLS. SLO is an oxygen-labile, cholesterol-dependent toxin that is produced throughout the exponential phase of growth (14). The SLO protein oligomerizes in the membrane of the host cells, creating large pores (25-30 nm) and leading to cellular damage and activation of apoptotic pathways (15). SLS, which consists of a peptide, is an oxygen stable toxin used by GAS to resist immune killing. This toxin can create hydrophilic pores in the neutrophils membrane. SLS biosynthesis and export is encoded by the *sagA-I* operon, which is expressed during the stationary phase of growth (16, 17).

SpeB: The Streptococcal pyrogenic exotoxin B is a cysteine protease secreted by GAS cells from the late exponential to stationary phase (18, 19). In the activated form, the SpeB zymogen aids in immunoglobulin degradation and the establishment of GAS in skin and soft tissue niches (20-22).

Peptidases: The C5a peptidase called ScpA is a serine protease that cleaves C5a chemoattractant. The ScpA protein prevents the recruitment of neutrophils to the site of infection and the generation of the peroxide burst associated with the phagocytosis process occurring subsequent to neutrophil infiltration (23, 24). ScpC is another cell wall anchored peptidase, which inactivates cytokines (e.g. interleukin-8) and impairs the recruitment of neutrophils (25).

Streptodornases (deoxyribonucleases): The neutrophil extracellular traps (NET) are excessive extracellular DNA network produced by neutrophils. The NET captures bacteria and facilitates their killing using the antimicrobial effectors associated with it and enables bacterial detection by the cells of the immune system. GAS produce and secret two DNases, Sda1 and Sda2, which act to dissolve the NET and thus prevent subsequent detection (by TLR9) and clearance (26, 27).

In addition to the virulence factors described above, GAS secretes a number of proteins capable of modifying the host molecules and tissues and help in the pathogen dissemination and/or subversion of the host immune response. For example the streptokinase (Ska) protein is a plasminogen activator secreted by GAS during invasive infections. Ska converts the host plasminogen to the active protease, plasmin. Plasmin is then recruited and used by GAS to dissolve the host extracellular matrix (ECM) and facilitates the bacterial spread (28).

Like the majority of pathogens, GAS requires iron for growth and this elemental requirement is linked to the virulence potential of GAS (29-31). During infections heme and hemoproteins serve as a largest reserve for metal iron. GAS is endowed with a number of molecular mechanisms to acquire iron from the host heme (and or hemoproteins) (30, 32, 33). In this respect, heme metabolism is central for the survival and success of GAS as a human pathogen; yet significant knowledge gaps regarding this aspect in GAS physiology exist.

1.4 Dissertation objectives and significance

The purpose of this dissertation is to describe the mechanisms for heme homeostasis in GAS. In chapter 1, I laid the theoretical foundation for my studies by providing a review on the current understanding of heme, its juxtaposing nature and interactions in bacterial systems. In chapter 2, I addressed the fate of the intracellular heme in GAS by characterizing a new enzyme, named heme utilization protein Z (HupZ). Dr. Mahamoudou Ouattara, a former member and colleague in Dr. Eichenbaum's lab, cloned and began describing this enzyme. I devoted my efforts in 1) optimizing the heme degradation process, 2) identifying the products of heme catabolism and 3) conducting *in-silico* analysis to establish the phylogenetic placement of HupZ. The elucidation of heme biotransformation by HupZ could serve as a novel pathway for heme catalysis in streptococcal pathogens. Successful mammalian infections involve evasion of the host defenses, here streptococcus is exposed to highly oxidative environment and reactive species (34). In addition, as a hemolytic pathogen that spreads through the blood, GAS is likely to encounter toxic levels of heme during infection. In Chapter 3, I described the impact of environmental heme on GAS physiology. I illustrated the toxic implications of environmental heme, characterized GAS response to heme stress, and identified GAS mechanisms for heme tolerance. In Chapter 4, I aimed to describe the function of a new pathway, named *pefRCD* (*porphyrin-regulated efflux RCD*) and its contribution to heme tolerance in GAS. This investigation revealed that the PefCD protein consists of an ABC-type transporter that exports heme and defends GAS cellular components from heme damage. Together, this dissertation provides new insights into heme metabolism in GAS and in Streptococcus overall. Because of the importance of these new pathways to streptococcal biology and interactions of GAS with its human hosts, they consist of potential targets for new therapeutic modalities against streptococcal infections.

2 CHAPTER 1. THE CORNUCOPIAS INTERACTIONS OF PORPHYRIN- HEME IN A BACTERIAL SYSTEM

Summary for mini-review: There is a significant portion of research dedicated to heme acquisition, uptake, and utilization in bacteria. However, the important part that heme plays in the production of redox stress and cellular damage in bacterial systems is less understood. The purpose of this mini-review is to provide insights into heme metabolism in bacteria. This paper is centered on the biochemical attributes of heme, heme interactions that lead to toxicity, and the bacterial mechanisms for heme tolerance. A special focus is given in this review to the group A streptococcus (GAS).

2.1 Iron, heme, and infection in mammalian systems.

Iron, the first-row transition metal, participated early in the evolution of life and to date remains an essential element for the vast majority of organisms including bacteria. The human body, for example, contains about 3-4 grams (gm) of iron. However, under normal physiological conditions, iron that partitions within mammalian system is not readily available (35, 36). Mammals have evolved multiple ways of sequestering iron in both the extracellular and the cellular compartments not only to keep it soluble and transferable but also to prevent the toxicity that is associated with the free metal. In addition, since the majority of bacteria require about 10^{-6} to 10^{-7} M of iron for growth (37, 38), iron withholding also serves as a form of nutritional immunity in response to infection.

The extracellular fluids in the body are rich with oxygen and have a neutral pH. Under these conditions, the iron is in the ferric form, which is extremely insoluble and therefore must be bound to carrier proteins. The hepatic glycoproteins, transferrin and lactoferrin, transport the ferric iron in the blood and body secretions (e.g. milk, tears, sweat, nasal secretion, and saliva) respectively. The low solubility and the high binding affinity of ferric iron to transferrin and lactoferrin (association constant of about 10^{36}) leave the interstitial fluids with an extremely low concentration of free metal [10^{-18} M] (39). Transferrin-iron complexes circulate in the blood (with only 20-45% of transferrin binding sites being filled) and the iron is eventually delivered to various cells by binding to the transferrin receptors and subsequent endocytosis of the receptor-transferrin complexes. In the intracellular compartment, most of the inorganic iron is stored in the protein ferritin, which is mostly found in the cells of the liver and heart. It is heme however, that represents the largest reserve of iron in the body (~80%). In the heme molecule, the iron is coordinated by protoporphyrin IX (PPIX) that serves to solubilize the metal and increases its catalytic activity by several folds (40). The majority of the heme in the body is bound in hemoglobin and myoglobin, and found in erythrocytes and muscle tissues (41). When heme and/or hemoglobin are released to the extracellular compartment due to the lysis of erythrocytes or of other cells, heme components are quickly bound by the carrier proteins hemopexin and heptoglobin and transported to the liver for recycling.

The daily iron requirements in humans are about 20-23 milligrams (mg). On average, only 1–2 mg of dietary iron is absorbed daily. The recycling of iron reserves generally from aging erythrocytes accounts for the rest of the metal iron (Figure 1). Iron recovery from hemoglobin in senescent erythrocytes occurs in the macrophages of the lymphoid tissues. A transporter named ferroportin mediates the export of iron from cells (such as macrophages and the intestinal enterocytes) into circulation. Hepcidin, a peptide hormone secreted by the liver, controls this process and therefore manages the overall extracellular availability of iron (42, 43). Hepcidin functions by binding to ferroportin and causing its eventual degradation.

In response to signals generated during infection processes, the liver secretes elevated amounts of hepcidin, which in turn acts to reduce the export of cellular iron into circulation. The liver also releases more hemopexin, heptoglobin to sequester heme and hemoglobin from the serum. In addition, apo-lactoferrin is secreted by neutrophils and macrophages are induced to enhance their uptake of iron and its further storage within ferritin (44). Collectively, this response leads to hypoferremia, further reducing the availability of iron at the extracellular compartment.

2.2 Heme.

Porphyryns (literal translation of Greek word porphura refers to the color “purple”) are a universal class of heterocyclic compounds that support a myriad of biological processes. The chemical composition of porphyryns can be best described as an aromatic, 16 carbon atom ring scaffold which contains 4 nitrogen atoms obtained by the linking of 4

tetrapyrrolic subunits with 4 methine bridges. This macrocycle, utilizes inwards facing nitrogen atoms to coordinate various metal ions forming secure metalloporphyrins (Figure 2) (45). The stable complexes between transition metals cations and porphyrins are attributed to the aromaticity of the heterocyclic compound. It is the porphyrin portion that accounts for the increased solubility and catalytic activity in the biological systems for the metal component. The high stability of the porphyrins with transition metals is exemplified by Zn-tetraphenylporphyrin (ZnTPP), which has a stability constant of 10^{29} (46, 47). Iron-porphyrins (heme) are known for their redox reactions. Heme and heme-proteins have versatile biological functions including serving as sensors and transporters of diatomic gases, biotransformation and detoxification of metabolites, chemical catalysis (serving as a 'source' or 'sink' of electrons in redox reactions), and an important iron reserve on which invading pathogen often rely (48).

The photoactive nature of porphyrin makes it a highly useful target in spectroscopy. The chief characteristic absorption peak of protoporphyrins is around 380-400 nm (Figure 3). This peak, known as the Soret or B-band, arises due to fully conjugated aromatic π -system that allows transition from the ground state to a second excited state. The Q bands are weaker absorbance peaks that occur after the Soret band. This region consists of a weak transition of electrons to the first excited state and ranges between 500-750 nm (49). Protonation of the inner nitrogen atoms of protoporphyrins, which occurs during insertion of metal ions, causes strong changes in the visible absorption spectrum. Minor variations in absorption spectrum can take place due to distal substituents. In addition, the absorbance maxima are greatly influenced by the electronic state of iron, interactions

with small ligands, and contact with amino acid side chains in the heme-binding pocket or with axial ligands in a protein-bound heme. Figure 3 illustrates the various absorbance spectra of free PPIX and heme as well as heme bound to the PefR protein of group A *Streptococcus*. Holo-PefR depicts Soret absorbance between 404-430 nm and β , α bands of heme absorb between 500-600 nm (50). Spectroscopic analysis provides a powerful tool in analyzing the function of proteins and enzymes that use heme as a prosthetic group or cofactor. The ability to depict and monitor spectral behaviors has facilitated studies of diverse reactions including heme binding, transfer, and degradation that have enhanced our understanding of protein structures and functions.

2.3 Heme uptake.

With only few exceptions (e.g. *Borrelia burgdorferi* and some *Lactococcal species*), iron is an indispensable micronutrient for all organisms. Successful colonization, therefore, demands from invading bacteria to have means to obtain the nutrient iron from the host environments. Consequently, bacterial pathogens often obtain iron from heme and have evolved mechanisms to capture heme during infection. Gram-negative bacteria deploy secreted hemophores or outer membrane receptors that can capture free heme or scavenge it from host hemoproteins (such as hemoglobin and hemopexins). In both mechanisms, the heme is delivered through the outer membrane and into the periplasmic space by Ton-dependent receptors using the proton motive force of the cytoplasmic membrane to energize this process (51, 52). Hemophore-mediated uptake of heme for pathogenic bacteria such as *Pseudomonas aeruginosa*, *Yersinia pestis*, and *Hemophilus influenza* has been demonstrated (53-55). The outer-membrane receptors HmbR and HpuA of *Neisseria*

species and HutA of *Vibrio Cholerae* were shown to capture heme directly from host proteins (56-58). In the periplasmic compartment, heme is captured by heme-binding proteins and delivered across the inner membrane via dedicated ABC transporters, using ATP hydrolysis to support the transport process.

Like Gram-negative bacteria, Gram-positive organisms also employ secreted hemophores or dedicated surface receptors to capture heme from the extracellular milieu or to seize it from the host hemoproteins. Nevertheless, significant differences in the nature of this process and acquisition machinery exist, reflecting the differences in the cell envelope of Gram-negative and Gram-positive organisms. Gram-positive bacteria are missing the selective barrier provided by the outer membrane. On the other hand, the delivery of heme to the cytoplasmic membrane has to overcome the challenge imposed by the thick and dense Gram-positive peptidoglycan cell wall. A common approach that evolved among Gram-positive organisms is the use of a protein relay apparatus that facilitates heme shuttling from secreted hemophores or surface exposed receptors through the peptidoglycan layers to heme-binding proteins in the cytoplasmic membrane. Not surprisingly, the ABC-type transporters involved in this process are homologous to those used by Gram-negative bacteria to mediate the transport through the cytoplasmic membrane.

A few heme-capture and relay mechanisms have evolved independently among Gram-positive organisms. The best understood machinery, named Isd (iron-regulated surface determinant), was first described in *Staphylococcus aureus*. Orthologous systems have

been recognized in a number of pathogens including *Bacillus anthracis*, *Bacillus cereus*, and *Listeria monocytogenes* (59). Heme uptake by Isd-like proteins, involves a protein module named NEAT (NEAr-iron Transporter), which is carried in one or more copies by the Isd and Isd-like proteins. After it is captured by a NEAT domain belonging to surface exposed Isd proteins, heme is relayed to the downstream NEAT domains of proteins located deeper in the cell wall, until it reaches the cytoplasmic membrane (41, 60, 61). While in most cases, the Isd proteins are anchored to the cell wall; *Bacillus anthracis* also employs NEAT-based hemophores, IsdX1 and X2, to capture labile heme (61, 62). NEAT independent mechanisms of heme relay were described in *Corynebacterium diphtheriae* (63) and *Mycobacterium tuberculosis*. However, the molecular bases for the function of these receptors are not fully understood.

The major heme uptake pathway in GAS is named the streptococcal iron acquisition (*sia*) system. The *Sia* machinery consists of 10-gene operon whose expression is directly repressed by an iron and manganese-dependent repressor named *MtsR* (64, 65). The streptococcal hemoprotein receptor (*Shr*) captures heme from hemoglobin via its NEAT domains and transports it to the NEAT-like domain of the streptococcal hemoprotein (*Shp*), which further delivers it to the binding protein *SiaA* (31, 33, 66). Other than the presence of NEAT and NEAT like domains, *Shr* and *Shp* do not share homology to Isd proteins, and unlike most Isd proteins they are anchored in the cell membrane instead of the cell wall. The transport of heme through the cytoplasmic membrane is completed by the membrane permease and ATPase encoded by the *siaB* and *siaC* genes respectively. A second ABC transporter named streptococcal iron uptake system (*siuABC*) contributes to

GAS growth in iron-depleted medium supplemented with whole blood or hemoglobin (30). However, heme binding or transport by the *SiuABC* was not directly demonstrated.

2.4 Heme degradation.

The recycling of iron from heme typically necessitates heme catalysis, which involves oxidative cleavage by heme oxygenases (HOs). In addition to HOs being key components in heme catabolism and iron homeostasis, these enzymes are associated with oxidative stress management, the synthesis of light harvesting pigments phytybilin in plants, algae, and cyanobacteria, and represent important iron acquisition pathways in bacterial pathogens (67). The majority of the bacterial HOs are homologous to the mammalian HO-1 enzyme. HO utilizes oxygen dependent reactions to cleave heme and generate equimolar amounts of biliverdin (BV) IX, iron, and carbon monoxide (CO). In this reaction heme acts as both substrate and a cofactor, and total of three oxygen molecules and seven electrons are consumed during this reaction. The reducing equivalents for heme catalysis are provided by NADPH (67).

Depending on the position of the eliminated carbon in the heme precursor, heme cleavage can produce four possible isomers of BV, i.e. α , β , γ , and δ . In mammals and plants, HOs preferentially initiate degradation at α -meso carbon to yield BV IX α (68). Degradation of heme by HO is a multi-step process that in most cases proceeds with intermediates like hydroxyheme and verdoheme to yield BV. In mammals, BV is further reduced by biliverdin reductase (BVR) to yield bilirubin (BR) (Figure 4 and 5) (48). The productions of BV, BR, and CO contribute to cytoprotection and have been targeted for developing

therapeutics (69, 70). The fate and the purpose of BV that is generated during bacterial heme catalysis are largely unknown, except for cyanobacteria (71). In eukaryotes, most HOs use NADPH in conjunction with cytochrome P450-reductase (CPR) for the transfer of electrons from NADPH. CPR is a flavin containing enzyme that facilitates the flow of electrons from NADPH to FAD, from FAD to FMN, and finally from FMN to HO (and cytochrome P₄₅₀) (72). Bacterial HOs can use CPR, Trolox, ascorbate, and or Ferredoxin/Ferredoxin reductase (for PigA, pa-HO, and BphO) as *in vitro* redox partners (67). The identity of the native redox partners is unknown for most bacterial HOs [except for *pigA* of *P. aeruginosa*, which can use pa-FPR for electron transfer during heme catalysis (73)].

The most extensively studied heme oxygenases are the human HO-1 and HO-2 enzymes. The gene encoding HO-1 is induced in response to iron limitations and other environmental cues in most tissues with the exception of the liver and spleen. HO-2 expression is typically constitutive (48). As expected from enzymes involved in iron supply, the vast majority of bacterial HOs are induced during growth in low iron conditions. HO-1 is a large (~36 kDa) membrane bound protein. Most of the characterized HOs in bacteria (including HemO, PigA, HmuO) share homology to HO-1. These enzymes however, are missing the C-terminus anchor residues, and are therefore smaller (~13-25 kDa) and located in the cytosol (67). The bacterial HOs that do not share homology with the eukaryotic enzymes (such as ChuS from *E. coli* O157, IsdG/I from *S. aureus*, MhuD from *M. tuberculosis*) are considered non-canonical. IsdG and IsdI from *S. aureus* are examples from a non-canonical HO group that has a homodimeric β -barrel

fold with two active sites at the dimer interface. Holo-IsdG shows significant ruffling (non-planarity) of the bound heme leading to distortion in tetrapyrrole. Unlike most HOs, IsdG catalyzes the liberation of one of the meso-carbons as formaldehyde instead of CO. This reaction produces staphylobilin, an oxo-bilirubin chromophore rather than BV (74-76). This unique chemistry implies not only different mechanism of oxygen activation but also a distinctive evolutionary path of IsdG and related enzymes such as IsdI. The HO of *M. tuberculosis*, MhuD, depicts heme-ruffling mechanism analogous to that of IsdG family. However, MhuD produces an unusual product termed mycobilin, in which the meso-carbon atom at the site of the ring cleavage remains attached as an aldehyde group (77).

A new family of bacterial HOs with no sequence conservation to HO-1 was recently identified. These enzymes include ChuZ of *C. jejuni*, HutZ of *V. Cholerae*, and HugZ of *H. pylori* (78-80). Enzymes from this family have a putative FMN-like binding site with a split β -barrel fold of homodimers. However, actual flavin binding is yet to be confirmed. The non-canonical HOs are currently in the spotlight due to unusual heme coordination, and production of unusual products with varied regiospecificity. GAS is able to thrive in iron-restricted medium as long as it is supplemented with hemoglobin or other hemoproteins. Heme utilization by GAS is quite evident but the catabolic enzyme(s) remains to be identified. Notably, the GAS genome does not share homology to any of the known canonical or non-canonical HOs.

2.5 The redox-active nature of heme.

The machinery for heme uptake and degradation can supply bacteria with the growth essential iron during infection. Paradoxically, this survival strategy can lead to cellular damage, and the toxicity may be augmented when high levels of heme are encountered at the infection site. The noxious effects of heme in bacteria are thought to be multifactorial. Heme iron can participate in redox reactions that can in turn induce oxidative stress. Oxidative stress occurs when the accumulation of free radicals exceeds the natural ability of an organism to protect itself from radical damage. Heme is able to catalyze the formation of reactive oxygen species (ROS) through multiple pathways (81). One of these pathways, known as the Fenton reaction, which occurs when either ferric or ferrous iron reacts with hydrogen peroxide (H_2O_2) to form hydroxyl radicals ($\bullet OH$) (82). This process, which is cyclic in nature, is not only damaging by itself but can also lead to initiation of vicious oxidative cascade due to interactions between the radical species and various biomolecules. In humans, prolonged time spent in oxidative stress is related to a multitude of disorders caused by damage to membrane lipids and proteins as well as deficiencies in cellular signaling (83, 84). Studies have shown that hemin, the oxidized version of heme, is cytotoxic due to its ability to aggregate in cell membranes and trigger cell death (83). GAS showed heme-induced damages to membrane proteins, lipid components, and chromosomes [(50), Eichenbaum unpublished data]. The prevention and detoxification of heme stress is not well understood in most bacterial species. including GAS.

2.6 Heme tolerance.

Heme degradation carried by HO seems to be an obvious defense choice for bacteria. (85). Sequestration of heme could be protective as well. In the *Plasmodium* parasite, free heme is removed by the heme detoxification protein (HDP), which forms an innocuous crystalized product called hemozoin (86). Sequestration of free iron by ferritin-like proteins is quite common among bacterial species (63). In addition, various cytoplasmic heme-binding proteins, such as HemS in *Y. enterocolitica*, function as interim heme chelating agents before shuttling it to a dedicated HO for breakdown (87). Proteins homologous to HemS that contribute to heme withholding and trafficking have been described in other Gram-negative bacteria. These include the ShuS protein of *Shigella* and the PhuS protein of *Pseudomonas* (88, 89). Active efflux is very useful in providing protection from heme toxicity in mammalian systems. Transporters that pump a single substrate (or a family of compounds) are considered dedicated transporters. Other systems, which exhibit more promiscuous nature and are able to extrude structurally distinct compounds, are referred to as multidrug resistance (MDR) efflux systems (90). It is not uncommon for an MDR transporter to detoxify heme; for example the mammalian feline leukemic viral receptor (FLCVR) and ABCG2 transporters confer heme tolerance in erythroid cells by conducting the export of heme excess out of hepatocytes and enterocytes in the gut lining (91). The MRP-5/ABCC5 MDR, which is known for removing the monophosphate metabolites of fluorinated pyrimidine compounds in metazoans is also essential in maintaining systemic heme homeostasis and in alleviation of heme stress (92). For the majority of MDR transporters, ion motive force (H^+ or Na^+) drives the pumping mechanism, but there are increasing evidences for reliance on ATP hydrolysis in heme efflux as well (93).

Among bacterial systems, *S. aureus*, group B streptococcus (GBS), and *B. anthracis* combat heme toxicity by export. These pathogens encode the *heme-regulated transporter*, HrtAB, which pumps heme (at levels of 1-10 μM) and or toxic by-products of heme catabolism (94, 95). The regulatory network that controls heme tolerance in bacteria varies among different species. For example, the expression of the *hrtAB* genes in the pathogenic *S. aureus*, *B. anthracis*, and *C. diphtheria* is responsive to the two-components, HssSR, system. The non-pathogenic *L. lactis*, utilizes HrtR, a TetR family of regulator in heme hemostasis (96). In addition to putative *hrtAB* genes, the opportunistic GBS employ a five-gene regulon that is referred to as '*porphyrin-regulated efflux (pef)*' in managing the intracellular pools of heme and PPIX (95). A MarR-like protein, named PefR, repressed the *pef* regulon in a heme dependent manner. PefR disengages from its cognate operator sites upon binding to heme or PPIX. The *pef* regulon is expressed in response to lower levels of heme (0.1-10 μM) than the putative *hrtAB* genes (10 μM), and is thus proposed to function in the fine-tuning of intracellular heme levels. Knockout strains of *hrtAB* and *pef* systems are ultrasensitive to heme exposure, an observation that highlights a critical and an intricate regulatory mechanism for heme tolerance in pathogenic strains (95). Exporters from the general multiple transferable-resistance (*mtr*) family were also implicated in providing protection from heme stress in *S. aureus* and GBS (97).

In GAS, we have recently shown that the transcription of a *pefRCD*-like operon is induced in response to environmental heme and demonstrate that the putative repressor,

PefR, specifically binds heme and PPIX *in-vitro*. *In-silico* analyses revealed a high degree of conservation of the Pef proteins among the 20 GAS genomes that are available in the database. In addition, the genomic organization of the *pef* locus is conserved among the streptococci from the pyogenic cluster (*S. pyogenes*, *S. agalactiae*, *S. iniae*, and *S. equi*). *In vivo* data collected with strains defective in functional *pefCD* genes illustrated an increased sensitivity to heme and anthracyclic compounds. Additionally, the lack of the PefCD proteins in GAS leads to increased heme-induced damage in lipids and DNA (Eichenbaum unpublished data, chapter 4). Thus, the *pef* system is the first type of efflux system linked to heme tolerance in GAS. Now, that we have established that labile heme causes cellular mayhem in GAS and GAS employs activation of protective pathways including *pef* system; it would be noteworthy to examine the mechanisms of pathogen heme-sensing and tolerance used during host infections.

3 CHAPTER 2- IN VITRO HEME BIOTRANSFORMATION BY THE HUPZ ENZYME FROM GROUP A STREPTOCOCCUS

3.1 Introduction

Most of the iron in mammals is bound to protoporphyrin IX in heme molecules, which are found in complex with hemoglobin, myoglobin, and other proteins. Pathogenic bacteria often tap into the heme reservoir to overcome the severe iron scarcity, which they encounter during infection. These pathogens use elaborate systems to scavenge heme from host hemoproteins and transport it into the bacterial cell (41, 98-100). A few mechanisms allow bacteria to retrieve iron from heme. For example, the release of iron from heme without breaking the macrocyclic ring by enzymes belonging to the family of dye-decolorizing heme peroxidases (DyP) has been described in *Escherichia coli* (101) and *Staphylococcus aureus* (102). The most common pathway, however, relies on oxidative cleavage of the porphyrin ring by enzymes known as heme oxygenases (HOs) (103, 104). When supplied with oxygen and electron donors, canonical HOs (e.g., HO-1 in eukaryotes) break down heme through three sequential mono-oxygenation steps (105). In the first step, heme is reduced to the ferrous form and rapidly binds oxygen. A subsequent reduction and protonation generates ferric hydroperoxy species, which self-hydroxylate the tetrapyrrole at one of the meso carbons forming a hydroxyheme derivative (α -meso-hydroxyhemin). In the second step, the hydroxyheme reacts with another oxygen molecule and is converted to verdoheme with the release of a meso carbon as carbon monoxide (CO). In the third and rate-limiting step, the cyclic verdoheme is opened through a reaction with oxygen, producing biliverdin and iron. Like

HO-1, many bacterial HOs specifically hydroxylate the porphyrin at the α -meso carbon and eventually produce α -biliverdin. Some bacterial enzymes however, demonstrate different regiospecificity and produce alternative or a mixture of biliverdin isomers (103, 104).

The first bacterial HO to be discovered was HmuO, a homologue of the human HO-1 enzyme found in the pathogen *Corynebacterium diphtheriae* (106, 107). Other HOs that also show significant structural and functional similarities to HO-1 were identified and characterized in several bacteria including *Neisseria meningitidis* (HemO) (108, 109), *Clostridium* species (HemO) (110, 111) and *Pseudomonas aeruginosa*, PigA (pa-HO or HemO), and BphO (112, 113). Like the mammalian enzymes, these bacterial HOs have a single compact domain that consists mostly of α -helices, with the heme inserted in between two of the α -helices (104). These bacterial enzymes degrade heme to α -biliverdin, with the exception of PigA, which produces a mixture of β - and δ -biliverdin isomers (112-115). Most of the characterized HOs in bacteria are associated with iron acquisition and are negatively regulated by iron (41, 116). BphO, however, appears to be an exception as it is expressed independently of iron availability and serves only to produce the precursor for the phytochrome chromophore (113-115).

Bacteria also use HOs that evolved independently of HO-1 like proteins; ChuS from *E. coli* O157:H7, for example, is such a non-conventional HO (117). ChuS has a unique structure that consists of two central sets of antiparallel β -strands, each flanked by two pairs of α -helices (117). Several cytoplasmic heme-binding proteins share sequence

homology with ChuS including HemS from *Yersinia enterocolitica* (87, 118), *Bartonella henselae* (119) and PhuS from *P. aeruginosa* (120). However, heme degradation was demonstrated only for a few family members (117, 119). In addition, it has been established that PhuS does not degrade heme and instead specifically delivers its heme to a partner HO (120, 121). Therefore, different proteins from this group may function in intracellular heme trafficking rather than in direct degradation of heme.

IsdG from *S. aureus* is the prototype of a non-canonical HO group that has a distinctive homodimeric β -barrel fold with two separate active sites at the dimer interface (74, 122). IsdG catalyzes heme degradation by liberating one of the meso carbons as formaldehyde instead of CO; this reaction produces an oxo-bilirubin chromophore (staphylobilin) rather than biliverdin (123, 124). The unique catalytic mechanism of IsdG is attributed to the ruffling of the bound heme molecule and its impact on the chemistry of oxygen activation (123). *S. aureus* encodes two representatives of this family, IsdG and IsdI (74). Other members of the IsdG HO family include HmuD and HmuQ from *Bradyrhizobium japonicum* (125), IsdG homologues from *Bacillus anthracis* (75) and *S. lugdunensis* (126). MhuD from *Mycobacterium tuberculosis* is another HO related to IsdG with heme ruffling and which also degrades heme without CO release. However, MhuD produces a novel product named mycobilin, in which the meso-carbon atom at the site of the ring cleavage remains attached as an aldehyde group (77, 127).

A new family of bacterial HOs with no homology to previously described enzymes was recently uncovered in *Campylobacter jejuni* (ChuZ) (78), *Helicobacter pylori* (HugZ)

(80, 128) and *Vibrio cholerae* (HutZ) (79, 129). Proteins from this family form homodimers with a split β -barrel fold that is characteristic of FMN-binding proteins, but no FMN binding was demonstrated. Interestingly, like PigA, HugZ exhibits δ -meso regioselectivity for cleaving the ring in the heme molecule (80), whereas HutZ is suggested to have β - or δ -meso regioselectivity (79). The exact nature of the bilin produced by HutZ or ChuZ reactions were not defined.

The Group A Streptococcus (GAS) is a significant human pathogen that produces an array of clinical manifestations including infections of the mucosal membranes and the skin that are typically moderate, severe invasive infections, as well as post-infection sequelae (4, 130). GAS is a hemolytic bacterium that readily uses hemoglobin and other hemoproteins to satisfy its need for iron (131). A heme relay apparatus comprising Shr, Shp, and SiaABC (HtsABC) proteins mediates the capture and delivery of heme into GAS cell (32, 132-135). A second ABC transporter, SiuADBG, also contributes to heme acquisition in GAS through an unknown mechanism (30). Heme uptake is important for GAS pathogenesis and adaptation to the host environment. Accordingly, mutants in *shr*, *sia* or *siu* genes are attenuated for virulence (30, 31, 136).

Despite the strides made in the field of heme uptake in Gram-positive bacteria, the mechanism for heme catabolism and iron release remains unknown in GAS and the *Streptococcus* genus. Herein, we provide biochemical evidences for *in vitro* heme binding and degradation by HupZ. Moreover, our structural and bioinformatics data on

HupZ, suggest that this streptococcal protein represents a new split β -barrel enzyme functioning in heme biotransformation.

3.2 Materials and Methods

3.2.1 Bacterial strains, media and antibiotics

E. coli cells were grown aerobically, in Luria–Bertani (LB) medium at 37 °C supplemented with 100 μ g/ml of ampicillin. In certain experiments cells were grown in the presence of 25 μ g/ml of 5-aminolevulinic acid and 25 μ g/ml of ferrous sulfate at 37 °C under shaking conditions. The *E. coli* strains used in this study are listed in Table 1.

3.2.2 Recombinant HupZ

The *hupZ* gene was amplified from GAS using the pair of primers, ZE437-ATGATAACACAAGAAATGAAA / ZE438- GTTACTTTCACTGTTTATTTCTT. The plasmids used in this study are listed in Table 1. The construction of HupZ-His expression vectors was accomplished by TOPO® directional cloning according to the manufacturer instruction (Invitrogen, K101-01). The *hupZ* gene was amplified from GAS NZ131 chromosome using the ZE437/ZE438 primer set and introduced into the pET101/D-TOPO vector. The resulting plasmid, pZZ2, codes for a HupZ-His tag fusion protein expressed from the T7 RNA polymerase promoter.

3.2.3 Protein expression and purification

Expression of the recombinant His-tagged proteins was induced overnight at 27 °C (or 5 hours at 37 °C) with 1 mM isopropyl β -D-1-thiogalactopyranoside. Cells were harvested

and re-suspended in an extraction buffer (20 mM Tris-HCl, pH 8.0, 100 mM NaCl, 0.1% Triton X-100) with the addition of 0.5 mg/mL Complete, mini-EDTA-free protease inhibitor cocktail tablets (Roche), then lysed by sonication. The cells' pellet was centrifuged and the cleared lysate was then applied to a 5 mL HisTrap HP affinity column (nickel column) and purified using a FPLC. Purified protein was dialyzed in sodium phosphate buffer (SPB, 20 mM sodium phosphate, 500 mM NaCl, pH 7.4) prior to its use for experiments. Western blot analysis of the recombinant His-tagged protein was carried out using anti-His antibodies from mouse (Sigma).

3.2.4 Heme reconstitution

Heme reconstitution experiments were conducted as described in (134). Hemin chloride, the oxidized form of heme, was used in all experiments. For simplicity, in this manuscript we refer to iron-protoporphyrin complex in both redox states as heme.

3.2.5 Heme degradation assays

Heme-HupZ complex was prepared at a heme:protein ratio of 1.5:1 and excess heme was removed by filtration through a PD-10 column (GE Healthcare). Degradation of bound heme by HupZ was carried in the presence of NADPH [with NADPH regeneration system for heme degradation (Figure 7B) and iron release (Figure 9) or without regeneration system for heme degradation (Figure 7A) and the detection of CO (Figure 8)] and human NADPH-cytochrome P450 reductase (CPR) or ascorbic acid. Ascorbic acid was added to a final concentration of 20 mM. In the NADPH-CPR system, heme-HupZ protein (20 μ M) was added to 0.4 μ M of recombinant CPR. The reaction was

initiated by adding 100 μM of NADPH to the system and spectra were recorded from 250 nm to 700 nm every 10 min for 1 h and every 60 min for additional 5 hours. Catalase (bovine liver, Sigma-Aldrich) was added to the reaction systems at a final concentration of 2 μM . The heme degradation reaction with ferredoxin reductase (FNR) and ferredoxin (Fdx) typically contained 20 μM Holo-HupZ, 10 μM Fdx, 0.1 unit/mL spinach FNR, 2 μM catalase and 500 μM NADPH, in 1 mL SPB. The UV-visible absorption spectra were recorded before and at 10, 20, 30, 50 and 60 min after the addition of NADPH.

3.2.6 Myoglobin differential spectroscopy

5 μM holoHupZ, 2 μM catalase, 0.4 μM CPR were mixed in 20 mM sodium phosphate buffer, pH 7.4, containing 500 mM NaCl. The reaction mixture was used as the blank and 4 μM of myoglobin solution was added immediately to the reaction. The UV-visible absorption spectrum of myoglobin was acquired over 16 min at 30 s intervals where reaction was initiated by the addition of 500 μM NADPH. The reference reaction was carried out similarly, except that instead of holoHupZ an equal volume of buffer was added, blanked, prior to adding 4 μM of myoglobin and 500 μM NADPH. The reaction was carried out at 25 $^{\circ}\text{C}$.

3.2.7 Ferrozine differential spectroscopy

20 μM of holoHupZ, 2 μM catalase, 200 μM NADPH, 6.5 mM glucose-6-phosphate, 1 unit/mL glucose-6-phosphate dehydrogenase, 0.4 μM CPR and 1 mM ferrozine were mixed and the reaction was followed for several hours (spectra were recorded frequently for the first hour; then every 60 min for a total 5 hours. One time point was taken after 22

h). The reaction was carried out at 25 °C in a final volume of 750 μ L. The reaction was blanked with catalase, glucose-6-phosphate, glucose-6-phosphate dehydrogenase, CPR and ferrozine in 50 mM MOPS buffer containing 500 mM NaCl (pH 7.4).

3.2.8 Crystallization and data collection

Crystals of HupZ were grown in hanging drops at room temperature by mixing 1 μ L of protein solution (6 mg/mL of protein) and 1 μ L of reservoir solution (20% PEG 3350, 0.2 M lithium acetate). The crystals were cryo-cooled with a cryo-protectant containing 22% glycerol in addition to the mother liquor. The X-ray diffraction data were collected at 100 K on beamline 22-ID of the Southeast Regional Collaborative Access Team (SER-CAT) at the Advance Photon Source, Argonne National Laboratory. The data were integrated and scaled with HKL2000 (137).

3.2.9 Structure determination

The crystal structure of HupZ was solved by molecular replacement employing PHASER (138, 139). The published structure of putative pyridoxamine 5'-phosphate oxidase (PNPOx, PDB ID: 2HTD) sharing 28% sequence identity with HupZ was used as the initial model. Successful structure solution was obtained by pruning the N-terminal eight residues of the initial model and also using serine instead of the dissimilar amino acids in the HupZ sequence compared with the 2HTD sequence. The HupZ structure was constructed from the molecular replacement phases using the Arp/wArp program (140, 141), which fitted 84% of the amino acid residues into the electron density. The model was subjected to several rounds of refinement in REFMAC (142) and the rest of the

protein structure was manually built with COOT (143). Solvent molecules were inserted at stereochemically reasonable positions using 2Fo-Fc and Fo-Fc maps at 1 and 3 sigma levels, respectively. The R_{work} and R_{free} values of the final refined structure are 17.0 % and 21.7 %, respectively. The data collection and refinement statistics are summarized in Table 2. The final refined structure has excellent protein geometry with no disallowed ϕ/ψ values on the Ramachandran plots. Structures were superimposed by secondary structure matching using SUPERPOSE (144) in CCP4 suite. The HupZ crystal structure was deposited with PDB ID 4NU4.

3.3 Results

3.3.1 HupZ is a new heme binding protein

GAS growth in an iron-depleted medium is restored when the medium is supplemented with whole blood or various heme-containing proteins, indicating that the hemolytic pathogen can retrieve iron from heme (30, 32, 131, 134). Yet, bioinformatics analysis failed to locate homologs of characterized HOs in the GAS genome, suggesting that a new type of enzyme may be involved. In a recent microarray analysis we identified a putative gene (*spy49_0662*) that is repressed by MtsR, the global iron-dependent regulator of GAS (65). *Spy49_0662* encodes a 15.9 kDa ORF containing the signature domain of PNPOx, found in FMN binding enzymes and evidently without any secretion signals. We therefore hypothesized that the iron-repressed *spy49_0662* encodes a cytoplasmic enzyme involved in iron metabolism.

To begin testing the function of *Spy49_0662*, we cloned and purified it from *E. coli* as a C-terminal end fusion to hexa-histidine tag. SDS-PAGE and Western blot examinations

revealed the presence of a single protein band that migrated to the expected size (Figure 6A) and reacted with anti-His tag antibody (data not shown). UV-visible absorption spectrum of the purified protein did not exhibit significant absorption other than at 280 nm (apo-HupZ, Figure 6B). However, when the HupZ was purified from cells grown in the presence of the heme precursors, 5-aminolevulinic acid and iron, it had a brown color and UV-visible scanning suggested that it was bound to heme (Figure 6C). To test if indeed heme serves as a ligand for Spy49_0662, we incubated it with heme (30 min at 1:1.5 molar ratio, pH 7.4). After excess heme was removed, Spy49_0662 demonstrated absorption peaks at 414, 530, and 560 nm characteristic of a heme-bound protein (Heme-HupZ, Figure 6B). The absorption maximum at the Soret region (390-430 nm) and the β and α bands (500-600 nm) exhibited by Spy49_0662 following incubation with heme are indicative of heme-protein complex formation and are clearly distinguishable from the spectrum of free heme in solution (Free heme, Figure 6B). Heme binding by Spy49_0662 was investigated further by titration of the apo protein with increasing amounts of free heme. A growing Soret band at 414 nm appeared in the resultant solution with incremental addition of heme (Figure 6D). The plot of the differential absorbance at 414 nm as a function of heme these data established that *spy49_0662* encodes a protein that specifically binds heme. We therefore named Spy49_0662 as HupZ (for heme utalization protein). The molar extinction coefficient for heme-bound HupZ was determined at 414 nm using the pyridine hemochromogen method (145) and resulted in $\epsilon_{414 \text{ nm}} = 110,000 \text{ M}^{-1} \text{ cm}^{-1}$.

3.3.2 Heme degradation by HupZ proceeds with the production of CO, ferrous iron, and a chromophore that absorbs at 660 nm

Heme binding by HupZ, a likely cytoplasmic protein, supported the notion that it may be involved in heme trafficking or metabolism. We therefore asked if HupZ is capable of heme degradation. Oxidative cleavage of heme by HOs requires a source of reducing equivalents, which is provided in mammals by NADPH and CPR (146). While the native redox partner for most bacterial HOs is unknown, CPR is typically used to support heme catabolism by these enzymes *in vitro*. Heme degradation by holoHupZ was assessed first in a reaction containing human CPR and NADPH as reductants. The reaction was incubated at room temperature and the change in the UV-visible absorption spectrum was recorded at 10 min intervals for 1 hour (Figure 7A). Catalase was included in the reactions to prevent non-enzymatic degradation of heme by hydrogen peroxide. As shown in Figure 7A, the absorbance at 414, 530, and 560 nm decreased over time. The absorption peak at 340 nm, which is indicative of NADPH, also decreased rapidly during incubation (Figure 7A), suggesting that the pyrimidine nucleotide may be a limiting factor in the catalysis under our experimental conditions. We therefore included an NADPH regeneration system consisting of glucose 6-phosphate and glucose-6-phosphate dehydrogenase in the reaction (147). This addition allowed us to follow heme degradation without exhausting the NADPH (Figure 7B). Although the decrease in the Soret region was more rapid in the first 10 minutes, the Soret band continued to decrease for two-three hours. A growing peak at 660 nm followed the drop in the Soret peak and became more pronounced during the second hour of incubation (Figure 7C). Importantly, no significant spectral changes were observed during incubation of either free heme or a

control hemoprotein (holoShp) in the reaction buffer, indicating that heme in solution or in complex with protein does not react with NADPH under our experimental conditions (Figure 7D). The changes in the spectral properties of holoHupZ (during incubation with NADPH and CPR) imply that this enzyme progressively degrades the bound heme to form a product that absorbs at 660 nm. Our studies also show that human CPR can serve as an *in vitro* redox partner of HupZ. Some bacterial HOs can use alternative redox partners such as Fdx, FNR and/or ascorbate. We found however, that the inclusion of spinach Fdx and FNR or ascorbic acid instead of CPR in the HupZ reaction did not lead to spectral changes (Fig. 8 and data not shown).

While canonical HOs release one of the meso carbons as CO during heme degradation, two bacterial enzymes were recently reported to catalyze heme breakdown by alternative mechanisms that involve the release of formaldehyde instead of CO (123) or the retention of the carbon atom after the ring cleavage (77). To test for CO formation by HupZ we used an established method that relies on the spectral signature of myoglobin-CO complex (107) and monitored the differential absorption spectrum of myoglobin during heme degradation. Myoglobin affinity for CO is 200 times higher than that for dioxygen (148), therefore if CO is released during heme breakdown in the presence of myoglobin it is likely to be captured. As can be seen in Figure 9, a shift in the absorption maximum from 410 to 420 nm was observed during the reaction. This spectral change was accompanied by the appearance of bands at 540 and 580 nm. The generated peaks at 420, 540 and 580 nm are characteristic of myoglobin-CO complex (107). The plot of the absorbance at 410 and 420 nm as a function of time, demonstrates the conversion of the

starting myoglobin state (ferrous-dioxygen) to myoglobin-CO complex during the reaction course (Figure 9, insert). No changes in the spectrum of myoglobin were observed in control reactions without holoHupZ (Figure 9 insert, control reaction). Together, these experiments indicate that like the canonical enzymes, HupZ generates CO as one of the reaction products.

To test whether HupZ releases iron from heme, we used the iron-indicator ferrozine. Ferrozine forms a stable magenta-colored solution with the ferrous iron, which exhibits a single sharp peak with maximum absorbance around 564 nm (149). Differential spectroscopy of HupZ catalysis of heme degradation in the presence of ferrozine demonstrated that the decrease in the Soret peak at 414 nm was accompanied by the concomitant increase of a peak at 564 nm, suggesting the formation of iron-ferrozine complex (Figure 10A). When free heme was incubated with ferrozine under the same conditions, no significant changes in absorbance were noticeable even after a long incubation period (Figure 10B). This observation indicates that ferrozine is able to capture iron only from solution but not from intact heme molecule. Using a standard curve, we determined that 20 μ M holoHupZ generated about 20 μ M iron over the course of the reaction, suggesting complete degradation of the bound heme (Fig. 10C).

3.3.3 Crystal structure of HupZ

HupZ was crystallized in the triclinic space group of P1 with two dimers in the unit cell. The crystallographic data and refinement statistics are summarized in Table 2. The structure was refined to the resolution of 2.0 Å with R and R_{free} of 16.7% and 20.8%,

respectively. The final structure has 119 residues per monomer with good electron density. Fourteen residues at the C-terminal end are disordered in the electron density maps and cannot be modeled unambiguously. The asymmetric unit consists of two HupZ homodimers (Figure 11A). All four monomers are essentially identical and can be superimposed with low pairwise RMSD values of 0.2-0.4 Å. The two dimers also superimpose with a very low RMSD of 0.2 Å, and the description here forth applies to both the dimers. The structure of the HupZ monomer contains six β strands, three α helices and forms a typical split-barrel fold (Figure 11B). The six strands form an antiparallel β-barrel. The first two helices lie across and block the two open ends of the β barrel. The third helix is packed against the side of the β barrel. HupZ dimerizes by stacking the β-barrel from two monomers at an angle of ~90°.

The new HupZ crystal structure was compared with known structures of other bacterial HOs. Comparison of HupZ with HugZ (128) [PDB ID: 3GAS], an HO from *H. pylori*, shows that the two dimers can be superposed by secondary structure matching to give an RMSD of 2.5 Å for 218 Cα atoms. HupZ is smaller and lacks the 80 residues N-terminal domain of HugZ, but the two proteins share the same split barrel fold for the C-terminal domain (Figure 11C). A heme moiety was observed in HugZ bound at the dimer interface, where it mainly interacts with the C-terminal residues. The flexible C-terminal region of HugZ plays an important role in heme binding and in particular His245 is involved in heme iron coordination and is conserved in related heme-utilization proteins (128). HupZ has a shorter C-terminal region that is truncated by 28 amino acids compared to HugZ. In addition, HupZ has no histidine in the superimposed structures

corresponding to His245 that coordinates heme iron in HupZ. In fact, the only histidine present in the HupZ sequence is located at the surface of the monomer and distal from the dimer interface. HupZ bears Arg166, which forms a water-mediated interaction with heme iron coordinating azide, and is essential for its activity (128). Substitution of Arg166 to Ala in HupZ results in loss of HO activity of HupZ. However, the amino acid structurally equivalent to Arg166 in HupZ is a glycine, which cannot form the equivalent interactions. The absence in HupZ of these crucial amino acid residues in HupZ emphasizes differences in the heme binding mechanism of the two enzymes.

Comparison of HupZ with ChuZ (78) [PDB ID: 3SWJ] another HO from *C. jejuni*, shows that the monomers from the two structures can be superposed to an RMSD of 2.2 Å for 108 C α atoms based on secondary structure matching. Similar to HupZ, ChuZ has a smaller 82 residue N-terminal domain, which is absent in HupZ, and a larger 169 residue C-domain with a split barrel fold resembling those in HupZ and HupZ (Figure 11D). The ChuZ crystal structure contains two bound heme molecules. The first heme binds at the dimer interface and is coordinated by His245 at the flexible C-terminal loop as seen in HupZ. The azide coordination of the other side of this heme and water mediated interaction with Arg166 are also conserved in ChuZ and HupZ indicating a common heme binding and reaction mechanism for these two enzymes. However, the ChuZ structure features a second surface heme bound to the N-terminal domain through residues His9 and His14. Alanine mutation of these two surface histidines together with Arg166 eliminates the heme degradation activity of ChuZ by blocking heme binding at the dimer interface and the non-enzymatic oxidation of the surface bound heme. His9 and

His14 of the N-terminal domain are conserved in both ChuZ and HugZ, which also indicate a conserved binding site. No equivalent histidines are present in HupZ, suggesting a different mechanism for heme binding.

The third heme degrading protein with a split barrel fold, HutZ (79, 129) [PDB ID: 3TGV] from *V. cholerae* also can be superimposed with HupZ to an RMSD of 2.1 Å for 218 C α atoms in the dimer by secondary structure matching. However, the HutZ crystal structure has no bound heme. Also, the first 12 residues at the N-terminal end and 25 residues in the C-terminal end including the heme-Fe coordinating His were removed during cloning to prevent crystal twinning observed with the full length protein. Hence, this HutZ structure can yield little information on heme binding.

3.4 Discussion

Previous studies established that GAS uses dedicated surface receptors and membrane transporters to capture heme from host hemoproteins and relay it through the peptidoglycan layers and into the cytoplasm (30, 32, 132-135). GAS imports heme to satisfy nutritional requirements for metal iron (131, 134). Bacteria typically employ cytoplasmic HOs to release the iron from the porphyrin center. These enzymes catalyze the oxidative cleavage of one of the porphyrin *meso* carbon bridges at α , β , γ or δ positions and usually produce free iron, CO, and biliverdin (103, 104). To date, no HOs have been identified in GAS and the fate of the imported heme remained obscure. In this study, we describe a new GAS enzyme, HupZ, which binds and degrades heme *in vitro*. The recombinant HupZ can be isolated from *E. coli* in the apo form, which readily binds exogenous heme to saturation at a 1:1 ratio (Figure 6B and 6C) or in complex with heme

(after growth in medium containing 5-aminolevulinic acid and iron) (Figure 6D). The addition of NADPH to heme-bound HupZ (in the presence of CPR and NADPH regeneration system) triggered a progressive decrease of the protein absorption at the Soret region, 530, and 560 nm with an absorption peak at 660 nm (Figure 7). These spectral changes suggest the conversion of the heme bound to HupZ to a bilin that absorbs at 660 nm. Since catalase, which can scavenge hydrogen peroxide that may be produced in the reaction, was included in all reactions, catalytic conversion of the heme rather than coupled oxidation is responsible for the observed changes in the absorption spectrum. The absence of similar changes in reaction samples containing heme, free or bound to Shp, without HupZ shows that HupZ is required for this conversion.

Spectroscopic assessment of myoglobin-CO complex formation during the HupZ reaction confirmed the release of CO from heme by HupZ (Figure 9) and suggests that HupZ heme degradation proceeded through the first two steps of a typical HO reaction. The last step in a standard HO reaction involves protonation and reduction of the iron in the ferric-biliverdin complex, which does not have significant spectroscopic features to produce free ferrous iron and biliverdin (which absorbs at the 640 to 680 nm range) (104, 105, 150). The formation of the broad band at 660 nm by the HupZ reaction suggests therefore that this enzyme is able to carry on and liberate the iron. The demonstration of ferrous iron release is provided by titration with ferrozine. The magenta color and the band at 564 nm formed during the reaction indicate the formation of ferrozine-iron complex (Figure 10). Moreover, a direct correlation between heme consumption and the development of the ferrozine-iron complex was observed. Together, these observations

suggest that HupZ degrades heme in the presence of reducing equivalents (NADPH and CPR) and produces CO, ferrous iron, and an unidentified chromophore. Moreover, CO production implies that the catalytic mechanism of HupZ follows the canonical pathway and not those mediated by IsdG- or MhuD-type enzymes (77, 124).

While HupZ quantitatively liberates iron from heme, this reaction is very slow and takes several hours to complete under our experimental conditions (Figure 9). Difficulties in releasing iron from the linear tetrapyrrole *in vitro* were reported for several HOs (73, 107, 114, 124). The efficiency of this final step in heme catalysis often appears to depend on the nature of the redox partner. For example, in the presence of ascorbate, the human HO-1 enzyme produces ferric-biliverdin complex and not free iron as it does with NADPH and CPR (150). The HO-1 like enzyme from *C. diphtheriae* (HmuO) catalyzes the formation of biliverdin and free iron with either NADPH/CPR or ascorbate. With ascorbate, however, the last step of the reaction is slow. Free biliverdin is observed only after two hours of incubation (107). Finally, many bacterial HOs cannot reduce and liberate the iron *in vitro* and thus catalyze the formation of ferric-biliverdin complex as the final product. These include HemO from *N. meningitidis* (109), BphO from *P. aeruginosa* (73), PigA from *Pseudomonas* species (114), and HutZ from *V. cholerae* (79). Considering the absence of sequence homology between HupZ and HO-1, it seems likely that the interactions between HupZ and the eukaryotic CPR are inefficient which may explain the sluggish iron release. Fdx/FNR or ascorbate could not support heme degradation by HupZ under our experimental conditions (Figure 8 and data not shown). Therefore, at this time, only NADPH/CPR was demonstrated to drive HupZ catalysis *in*

vitro. The identity of the cognate redox partner of HupZ remains elusive. The use of cognate redox partner in the HupZ reaction instead of CPR may allow for more efficient heme degradation *in vitro*, as was seen with the IsdI and IsdG enzymes while paired with IruO, their probable redox partner *in vivo* (151).

HupZ does not share significant sequence homology with characterized HOs. To gain molecular insights into this new enzyme we solved the crystal structure of HupZ. The apo protein was crystallized as a homodimer with a split β -barrel conformation in each monomer, which contains six β strands and three α helices (Figure 11A). The structure of HupZ is similar to the common structural domain shared by the ChuZ, HugZ and HutZ proteins (Figure 11B-C) (78, 128, 129). Despite the overall structural resemblance, several important differences occur between HupZ and HOs from this family. HupZ is smaller and lacks the 80-residue N-terminal of HugZ and ChuZ, which is proposed to mediate coupled oxidation of heme (78). In addition, HupZ lacks the heme iron coordinating histidine residue (His245) that is conserved in both ChuZ and HugZ. The corresponding His170 in HutZ, however, was found to be unnecessary for heme binding (129). A phylogenetic tree was generated from the multiple sequence alignment of several HOs from various organisms (Figure 12). Members of the different families of HOs were grouped with their known respective relatives with high bootstraps values for the external nodes. This analysis located HupZ to a branch that is separated from the other HOs, indicating it belongs to a new subfamily of split β -barrel enzymes. The low bootstraps values for the internal nodes suggest that the bacterial HOs evolved independently and that this tree does not reliably represents the evolutionary direction of

this process. Putative ORFs that are homologous to HupZ are found in the genomes of GBS, *Streptococcus dysgalactiae* and other streptococci suggesting that HupZ is possibly a representative of a new family of enzymes in *Streptococcus* species.

In conclusion, we identified a new streptococcal enzyme that degrades heme *in vitro* generating CO, free ferrous iron, and unidentified chromophore. HupZ adopts a split β -barrel fold, thus it structurally resembles members of a recently characterized family of bacterial HOs. The structurally related HugZ produces δ -biliverdin, but final product of ChuZ and HutZ remained to be described (79, 80, 152). The significant differences observed between HupZ and these bacterial HOs indicate that HupZ may be a representative of a separate family of bacterial enzymes. The vast majority of HOs in bacteria are associated with iron uptake. Regulation by a metalloregulatory protein (such as Fur or DtxR) is one of their hallmarks (41, 116); other than BphO, the expression of bacterial HOs enzymes is enhanced during growth in low iron conditions. Likewise, MtsR, the global metal-dependent regulator in GAS represses the expression of *hupZ* gene [*spy49_0662*] (65). Regulation by iron availability supports the notion that HupZ degrades heme to provide GAS with iron. However, further analysis is necessary to unequivocally determine the role of HupZ in GAS physiology.

4 CHAPTER 3- HEME TOXICITY AND TOLERANCE IN GAS

4.1 Introduction

Heme is vital to many biological systems, ranging from planktonic marine microorganisms to the highly complex and evolved humans. The heterocyclic ring in heme, protoporphyrin IX (PPIX), co-ordinates metal iron (Fe^{+2}); this architectural arrangement supports a wide array of roles upon presentation of an appropriate microenvironment. Hemoglobin and myoglobin, for example, use heme as a prosthetic moiety for the transport and storage of oxygen and other diatomic gases. A multitude of redox enzymes engages heme as a catalyst of electron transfer. Heme is also associated with energy conservation and biotransformation in processes such as photosynthesis and respiration. In addition, signal transduction pathways are integrated via heme due to its ability to bind gaseous ligands such as oxygen, carbon dioxide, carbon monoxide, and nitric oxide (81, 153, 154). Notably, heme in hemoproteins constitutes a major iron reserve used by invading microorganisms during infection (41, 155). Blood in particular is an immediate source of iron and heme for the majority of pathogens. Invading bacteria are often able to obtain heme directly from the circulating pool of hemoproteins. Some pathogens also deploy hemolysins to trigger erythrocyte destruction and hemoglobin release (41, 156, 157).

Ironically, while heme is essential for many functions, the transitional nature of the coordinated iron renders it a significant pro-oxidant that can harm many cellular entities including DNA, proteins, cytoskeleton, and membranes (81, 158, 159). To prevent cellular damage and to control infections, mammals restrict the pool of free circulating

hemoproteins through scavenger proteins such as serum albumin, hemopexin (for heme), and heptoglobin (for hemoglobin) (160, 161). To minimize oxidative damage, the cellular levels of heme are managed by heme oxygenases. These enzymes degrade heme to biliverdin, which is then reduced to the cytoprotectant molecule bilirubin (162). Since heme could act as a menace, it is advantageous only in amounts that meet the bacterial requirements and, as long as it remains sequestered, preventing access to susceptible macromolecules (85). Bacteria that are exposed to heme and take advantage of it during infection had to develop strategies to manage its toxic effects. While we do not fully understand how bacteria avoid and manage the negative ramifications of heme exposure, recent studies have begun to shed light on some of the molecular mechanisms that are involved in this process (85, 95, 163).

Heme tolerance in bacteria is typically based on tight regulation of heme uptake and degradation. Often bacteria employ Fur- or DtxR-like metallorepressors to orchestrate heme metabolism in response to iron availability (41, 164). In some cases, auxiliary defense systems that facilitate repair, detoxification, and expelling of heme surplus are activated when the cellular mechanisms for heme homeostasis are overwhelmed. A number of two-component systems (TCS) that coordinate the response to heme stress have been described in bacteria. The Heme Sensor System (HssRS) is a TCS that activates the expression of a heme efflux transporter (*hrtAB*) in *Staphylococcus aureus*, *Bacillus anthracis*, and possibly the Group B Streptococcus (GBS) (95, 165, 166). In response to heme pressure, the ChrAS TCS from *Corynebacterium diphtheria* inhibits the heme biosynthetic gene, *hemA*, and activates the transcription of the heme oxygenase

gene, *hmuO*, required for heme catabolism (167-170). Interestingly, in addition to putative HssRS TCS, GBS also codes for *pefR*, a heme-responding repressor (95). PefR binding to heme leads to derepression of two heme export systems, namely *pefAB* and *pefCD* (95). It is suggested that GBS uses PefR to fine-tune heme homeostasis, while it deploys the HssRS system in response to high heme exposure.

As mentioned above, bacteria often detoxify, using active export systems that directly eliminate accumulated heme or its toxic byproducts. The efflux system, MtrCDE, in *Neisseria gonorrhoea*, is crucial for bacterial resistance to hydrophobic agents and heme; overexpression of this machinery leads to increased bacterial burden in vaginal fluids (171, 172). GBS mutants in *pefAB* or *pefCD* genes are over-sensitive to heme and demonstrate increased accumulation of intracellular heme and PPIX (95). Respiration-linked studies in *Lactococcus lactis* incriminated the *hrtAB* homologous genes *ygfAB* in heme efflux (173). A family of cytoplasmic proteins that bind and sequester heme forms another facet of heme tolerance. The proteins HemS of *Yersinia enterocolitica*, ShuS of *Shigella dysenteriae*, PhuS of *Pseudomonas aeruginosa*, and HmuS of *Y. pestis* are established members of this family (87, 120, 174-177). Interestingly, the enzymes SodC of *Haemophilus ducreyi* and AhpC of the GBS have both heme sequestration roles in addition to enzymatic activity (174, 178). Bacteria also degrade heme to alleviate toxicity. Heme oxygenases were described in several pathogenic bacteria (103, 179-181). Despite the clear role heme metabolism has in pathogenesis, our understanding of heme tolerance is lacking in numerous pathogens.

The Group A Streptococcus (GAS) is a Gram-positive obligate human pathogen. GAS infections range from mild diseases such as pharyngitis and impetigo to invasive and systemic manifestations, including necrotizing fasciitis and streptococcal toxic shock syndrome. GAS can also produce post-infection complications such as glomerulonephritis and rheumatic fever (182). In the absence of a vaccine, GAS infections are commonly treated with β -lactam antibiotics. However, due to the swift progression rate and extent of tissue damage, surgical intervention is often required to manage invasive GAS infections (183). The grave nature of invasive GAS infection is attributed to many virulence factors, including its β -hemolytic property that causes massive erythrocyte and tissue lysis (184). GAS requires iron for growth and the pathogen can fulfill its needs for the metal by acquiring heme from lysing erythrocytes (30, 131). Heme acquisition is mediated by the *sia* (*streptococcal iron acquisition*) operon that facilitates heme relay and transport across the bacterial membrane (32, 132, 133, 185, 186). *In vivo* studies on a second operon named *siu* (*streptococcal iron uptake*) linked it to the uptake of heme and ferric ion (30). Although heme receptors and transport proteins have been identified, our understanding of heme metabolism in GAS is still incomplete. The focus of this study was to fill in the knowledge gaps in GAS heme tolerance. Here, we show that excess heme is inhibitory for the growth of GAS *in vitro*; heme exposure caused a global transcriptome shift wherein it significantly up regulated genes that are important for redox stress, which includes sensing and management along with protein damage and rescue.

4.2 Materials and Methods

4.2.1 Bacterial strains and growth conditions.

Strains and plasmids used in this study are listed in Table 3. GAS was grown under static conditions at 37 °C in Todd-Hewitt broth with 0.2% (wt/vol) yeast extract (THY broth, Difco Laboratories) or in C-medium consisting of 0.5% Proteose Peptone #3 (BD), 1.5% yeast extract (BD), 10 mM K₂HPO₄, 0.4 mM MgSO₄, 17 mM NaCl, adjusted to pH 7.5 (187). In some experiments, hemin chloride (Sigma) from stock solutions prepared in DMSO was added to the growth media at different concentrations. *E. coli* cells were used for cloning and protein expression purposes. *E. coli* was grown aerobically in a Luria-Bertani medium (pH 7.0) supplemented with kanamycin (30 µg/ml) at 37 °C.

4.2.2 Determination of the minimal inhibitory concentration (MIC). Agar dilution method

This procedure was performed as described in (188) with minor modifications. Briefly, the turbidity of overnight grown cultures in C-media was adjusted to OD_{600nm} = 0.08-0.1, representing the turbidity of 0.5 MacFarland's acidified barium chloride standard as described (Washington, 1974) and spotted (1 µL) onto C-medium agar containing varying concentrations of heme. The plates were incubated overnight at 37 °C and the minimal heme concentration that did not allow for significant bacterial growth was determined. **Broth macrodilution method:** this method was performed as per the instruction of (188). In brief, THYB containing heme at a range of 0-100 µM in 5 µM intervals was inoculated with GAS cells (OD_{600nm} = 0.05) and incubated at 37 °C for 17

hours. The minimal heme concentration that did not support growth ($OD_{600nm} \leq 0.2$) was determined. **Disc diffusion method:** this procedure was adapted from (189). Briefly, sterile Whatman filter paper discs (8.0 mm diameter and 1.2 mm width) were submerged in 10 mM heme (in DMSO) and impregnated onto C-media agar that was plated with 0.1 ml of GAS culture (final $OD_{600nm} = 0.1$). The plates were incubated at 37 °C for 17 hours and the zone of clearance around the discs were measured.

4.2.3 Thiobarbituric acid-reactive-substances (TBARS) assay for lipid damage.

GAS culture samples with equal cell numbers were harvested 30, 60, and 90 min following treatment with 4 μ M heme (in 0.035% DMSO) or with mock (0.035% DMSO, control) and washed twice with phosphate buffer saline, pH 7.4 (PBS). The resulting cell pellets were resuspended in 5 ml of PBS with lysozyme (1 mg/ml, Sigma) and 400 U of mutanolysin (sigma) and incubated at 37 °C for 30 min. The cells were then subjected to sonication (5 sec., 10% amplitude). TBARS formation in the membrane samples was quantified using the TBARS assay kit (ZeptoMetrix Corporation) according to the manufacture's recommendations. Briefly, 100 μ l cell lysate samples were treated with 100 μ l of SDS and 2.5 ml of the TBA reagent and incubated at 95 °C for 60 min. The sample supernatant was collected following 10 min incubation on ice by centrifugation (15 min at 835 \times g). The absorbance at 532 nm (indicative of TBARS) was measured using the DU 730 Life Science UV/Vis spectrophotometer. The amount of TBARS in the experimental samples was derived from a standard curve generated using the malondialdehyde (MDA) reagent supplied with the kit.

4.2.4 Detection of protein damage.

The TBARS assay was followed as above except the cell pellets were washed twice with TSM buffer (100 mM Tris, 500 mM sucrose, 10 mM MgCl₂, pH 7.0), resuspended in 0.5 ml of TSM with 400 U of Mutanolysin (Sigma) and incubated at 37 °C for 30 min. The protoplasts were centrifuged at 20,000×g for 5 min at 4 °C, suspended in 0.2 ml of lysis buffer (50 mM Tris-HCl, 60 mM KCl, 10 mM MgCl₂, pH 7.0, 2% β-mercaptoethanol) and subjected to sonication (10 Sec. 10% amplitude). The membrane components were collected by centrifuged at 100,000×g for 30 min at 4 °C. The supernatant was retained as a cytoplasmic fraction and pellets were resuspended in 0.2 ml of lysis buffer and were considered as the membrane fractions. Protein damage was detected using the OxyBlot™ protein oxidation detection kit (Millipore) according to the manufacturer's instructions. In this assay, oxidized proteins are derivatized with 2,4-dinitrophenylhydrazine (DNP), which is then detected with primary antibodies specific for DNP and secondary antibody conjugated to horseradish peroxidase (HRP) using a chemiluminescence protocol. The intensity of the signal in individual lanes was quantified using ImageQuant LAS 4000 and the ImageQuant TL software (GE).

4.2.5 RNA extraction.

Cell samples were harvested 30, 60, and 90 min following heme or mock treatment by centrifugation (5000×g for 20 min) at 4 °C. RNA was extracted from the cell pellet using the RiboPure™ RNA purification kit (Ambion) followed by DNaseI digestion (Ambion) performed according to manufacturer's instructions. Microarray analysis was performed with total RNA extracted from 90 min post treatment cell samples. Real-time RT-PCR

transcript analysis for selected genes was performed using total RNA extracted from all three-time points post treatments.

4.2.6 Microarray analysis and Real-Time RT-PCR validation.

The GAS microarray used in this study (190) consists of 2,328 70-mer oligonucleotide probes targeting unique non-repetitive ORFs from the sequenced genomes of serotypes M1 (SF370), M3 (MGAS315), and M18 (MGAS8232). Probes were synthesized by Qiagen Operon with a melting temperature of 76 ± 5 °C, $\leq 70\%$ cross-hybridization identity to another gene within the same strain, ≤ 20 contiguous bases in common with another gene, and probe location within 3' end of ORF. Microarrays were printed at Microarrays Inc. (<http://www.microarrays.com>), with 10 pl of each oligonucleotide probe spotted onto slides (UltraGAPS2; Corning) using a 12-pin contact printer. The microarray hybridization was performed as previously described (191). Briefly, 10 µg of DNase I-treated total RNAs to be compared were used for reverse transcription into single-stranded cDNA using 200 U Superscript II reverse transcriptase (Life Technologies), 6 µg random hexamers, 1X first strand buffer, 10 mM dithiothreitol (DTT), 0.5 mM dATP, 0.5 mM dCTP, 0.5 mM dGTP, 0.3 mM dTTP and 0.2 mM of amino-allyl dUTP. The mixture was incubated at 42 °C for 2 h and the reaction stopped by addition of 10 µl 0.5 M EDTA and 1 M NaOH. Amine-modified cDNA was purified by ethanol precipitation followed by chemical labeling with Cy3- or Cy5-NHS-ester fluorescent dyes (GE Healthcare) in a final step. Yield and incorporation of dye was determined using a Nanodrop ND-1000 (Thermo Scientific). Slides were pre-hybridized in a 50 ml solution of 5X SSC, 0.1% SDS and 1% BSA for 30 min at 42 °C, washed 4X in water

and once in isopropanol, then dried by brief centrifugation. Labeled probes were resuspended in hybridization buffer (30% formamide, 5X SSC, 0.1% SDS, 0.6 µg/µL salmon sperm DNA) and hybridized to the microarray slides in a 42 °C water bath for 16-20 h. Slides were washed twice in a low stringency buffer (2X SSC, 0.1% SDS) at 55 °C for 5 min, twice in a medium stringency buffer (0.1X SSC, 0.1% SDS) at room temperature for 5 min and finally twice in a high stringency buffer (0.1X SSC) at room temperature for 5 min, and then dried by brief centrifugation. Synthesized cDNA from each RNA sample from three independent cell cultures was hybridized on three separate microarray slides (biological replicates), and independently synthesized cDNA from each of these same RNA samples was hybridized in a repeat dye-swap experiment (technical replicates) to test technical reproducibility. Slides were scanned using an Axon 4100A personal array scanner and GenePixPro 6.0 software (Molecular Devices). Data obtained from MGAS5005 cells incubated in the presence of DMSO or 4 µM of heme were compared for twofold changes in expression, ≥ 2.0 or ≤ 0.50 with Acuity 4.0 software (Molecular Devices). Using a ratio-based normalization, data were normalized by the ratio of the means (635/532) and samples were removed when four out of the six experiments did not show significance. Data was validated on 11 independent genes by real-time RT-PCR as described below. Correlation coefficients for the arrays were determined by plotting the log value of the array on the x-axis to the log value of the real-time RT-PCR on the y-axis. An equation determining the line of best fit was determined, and the resulting R^2 value was calculated to be 0.889. Array data was submitted to the Gene Expression Omnibus (GEO) at the National Center for Biotechnology Information under the accession number GSE61415.

4.2.7 Quantification of expression by real-time RT-PCR.

For microarray data validation, real-time RT-PCR analysis was carried out using primers in Table 4 as follows: 25 ng of DNaseI-treated total RNAs were added to SYBR green master mix (AB) containing 5 µg of each specific real-time primer for the one-step protocol. The real-time RT-PCR experiments were completed using a LightCycler 480 instrument (Roche), and levels represent the ratio of non-treated to treated experimental values relative to the level of expression of *gyrA* transcript as an endogenous control. For expression of the *pefRC* operon, a SYBR Green based quantitative PCR reactions were performed using the Power SYBR® Green RNA-to-Ct™ 1-Step Kit (AB) on 7500 Fast Real-Time PCR machine (AB) according to the manufacturer's specifications. Briefly, the reaction mixture (20 µl) contained, 10 µl of RT-PCR Mix (final 1X), 10 nM of each forward and reverse primers, 25 ng of total RNA, and RT enzyme Mix in 1X final concentrations. The relative quantification with comparative $\Delta\Delta\text{CT}$ method was employed to calculate differences in *pefRC* expression levels at different times after heme exposure. The relative expression levels of *pefR* and *pefC* genes were normalized to the level of *rpsL* transcript as an endogenous control. The levels of transcripts in heme treated samples were compared to the control samples.

4.2.8 *In silico* analysis.

The PefR binding motif was identified within the putative promoter region of MGAS5005 *spy_0195* (*pefR*) using Multiple Em for Motif Elicitation (MEME) suit hosted by the National Biomedical Computation Resource (192). The outcome was

further analyzed by the MAST application of MEME for its genome wide occurrence within the upstream sequences of GAS under both the stringent (E value ≤ 0.01) and relaxed (E value ≤ 10) parameters. All of the sequences were acquired from Kyoto Encyclopedia of Genes and Genomes (KEGG) database (193) for comparative sequence analysis; sequences were aligned using ClustalW (194).

4.2.9 Cloning, overexpression, and purification of PefR.

The *spy_0195* ORF was amplified from GAS MGAS5005 genomic DNA by PCR using primers ZE515 and ZE516 (Table 4). To generate pAJS11 plasmid (Table 3), the PCR fragment with *pefR* ORF was cloned into the pRhamTM expression vector (Lucigen) by ExpressioneeringTM technology and introduced into *E. cloni*® 10G competent cells. The cloning was confirmed by sequence analysis. For PefR expression, cells harboring pAJS11 were induced at OD_{600nm} = 0.8 with 0.2% rhamnose. The cells were harvested (8,000×g for 5 min at 4 °C) following 16 hours incubation at 28°C. The resulting pellets were resuspended in extraction buffer (20 mM Tris pH 8, 100 mM NaCl, 0.1% Triton X-100) containing 0.5 mg/mL Complete, mini-EDTA-free protease inhibitor cocktail (Roche), sonicated and the cell debris were removed by centrifugation. The resulting lysate was purified over 5 ml HisTrapTM HP (GE) nickel affinity column. Protein fractions were dialyzed overnight in sodium phosphate buffer (SPB: 20 mM sodium phosphate, 500 mM NaCl pH 7.4). Expression of the recombinant PefR was evaluated by SDS-PAGE and western blot analysis with mouse anti-His antibodies (Sigma).

4.2.10 Heme and PPIX binding assay.

Heme binding by PefR was assessed spectroscopically as described in (125, 185) with minor modifications. Briefly, an increasing concentration of hemin chloride (2-30 μM) was added to both the test cuvette containing 10 μM of PefR protein in SPB and the reference cuvette (containing SPB alone) and the changes in absorbance across the wavelength of 250 – 700 nm region were recorded every 6 min. The PefR to heme stoichiometry and dissociation constant (K_d) were determined by plotting the absorbance at 435 nm as a function of the heme concentrations. The extinction coefficient (ϵ_{max}) for PefR was calculated from the hemocromogen method described in (195). All of the spectroscopic measurements were made using the DU730 Life Science UV/Vis spectrophotometer (Beckman Coulter). PPIX binding was tested by titrating PefR (5 μM) with 0-6 μM PPIX (in 0.5 μM increments) prepared in acidified methanol:dimethylformamide (1:1). The changes in absorbance were recorded.

4.3 Results

4.3.1 Excess of heme is inhibitory to the growth of GAS.

Host heme is the immediate source of iron during infection for invading pathogens such as GAS. Recent studies demonstrated that bacteria must maintain the intracellular levels of heme at equilibrium in order to benefit from its nutritional value, while eluding the toxicity that is associated with heme overload (95, 166, 196). In this work, we began evaluating the impact of heme on GAS physiology. We found that the addition of a disc saturated with 10 mM heme onto agar plates seeded with a confluent lawn of GAS resulted in a zone of clearance similar to those observed with antibiotic-impregnate discs.

This observation indicates that heme can have a bacteriostatic effect on GAS (Table 5). To compare the sensitivity to heme among GAS isolates we determined the MIC values of heme using two common methods (Table 5). The agar dilution assay employs solid C-medium containing varying concentrations of heme. We determined that the heme MIC in this method is between 10 to 20 μM with the nephritogenic M49 GAS skin isolate, NZ131 (197, 198), exhibiting the highest sensitivity of all GAS strains tested. The highly pathogenic MIT1 MGAS5005 strain (199) as well as clinical isolates from patients with invasive diseases (Table 3) demonstrated higher heme tolerance. In the broth dilution assay, we measured bacterial growth in THYB supplemented with varying heme concentrations. This method resulted in higher values of heme MIC (30-50 μM) for MGAS5005 and the clinical isolates. However, both methods indicated that the invasive strains were more resistant to heme than NZ131.

4.3.2 Exposure to sub-lethal heme levels cause lipid peroxidation in GAS.

To learn why heme is detrimental for GAS growth, we investigated its impact on GAS macromolecules. Heme is reported to damage directly or through the generation of reactive oxidative species the integrity of membrane lipids (81, 200). Therefore, we evaluated the extent of lipid peroxidation in GAS following heme exposure. Using low heme concentration that could still support cell growth when applied at the early logarithmic phase allowed us to examine the kinetics of damage production and later the bacterial transcriptome response to heme. As seen in Figure 13A, the addition of 4 μM heme to MGAS5005 at the early logarithmic phase of growth did not result in a significant change in the bacterial growth profile. To detect lipid peroxidation, we used

an established method that relies on the tendency of oxidized lipids to react with a thiobarbituric acid (TBA) reagent to form adducts (named TBARS) that absorb at 532 nm (201). The time course of TBARS production in GAS cells exposed to heme (or in control samples) was quantified using a standard curve (Figure 13B). Significantly higher occurrence of lipid peroxidation was observed in all of the heme-treated samples compared with control samples (Figure 13C). Lipid peroxidation was the highest (22.5 fold over background) 30 min after heme treatment; while lower levels (~5 fold over background) were found in the samples collected 60 and 90 min post-heme treatment (Figure 13C), indicating possible repair mechanism. In eukaryotes, membrane repair involves enzymes such as phospholipase A2 that hydrolyse peroxidized fatty acid esters and glutathione peroxidase (202, 203).

4.3.3 Exposure to heme damaged membrane proteins.

We next evaluated the effect of heme on GAS proteins. Oxidation introduces carbonyl groups into protein side chains that can then react with 2,4-dinitrophenylhydrazine (DNPH) to generate 2,4-dinitrophenylhydrazone (DNP) derivatives (204). To monitor protein oxidation in GAS, membrane and cytoplasmic proteins were extracted from culture samples collected at 30, 60, and 90 min post treatment and allowed to react with DNPH. Oxidation was then visualized by immunoblot with antibodies specific for DNP and the damage was quantified by densitometry. Analysis of the membrane fractions revealed that the anti-DNP antibody strongly reacted with all of the samples from heme exposed cells (Figure 14A, upper panel). While general staining confirmed the presence of proteins in all samples (Figure 14A, bottom panel), protein oxidation was only

observed in the heme-treated cells in the early sample. At the later time points (60 and 90 min) some background oxidation also occurred in the control samples. In all cases though, a significantly higher amount of protein damage was observed in the heme-exposed cells compared to the controls (Figure 14C). In addition, the degree of protein oxidation was the highest in the 90 min samples. Similar analysis of cytoplasmic proteins did not reveal detectable damage (Figure 14B); therefore, protein oxidation following heme exposure is primarily linked to the membrane fraction under our experimental conditions.

4.3.4 GAS demonstrates adaptation response to heme.

When overnight cultures of NZ131 grown in heme-free medium were inoculated into medium containing 1 μ M heme, which is below the growth inhibiting concentrations at the early logarithmic phase, an extended lag phase that lasted for more than 8 hours was observed (Figure 15). Although exposure to heme inhibited growth initially, the cultures reached after overnight incubation the cell density observed in cultures that grew in heme-free medium (data not shown). To test for possible adaptation to environmental heme, GAS cells were grown overnight in the presence of 0.1 μ M heme before they were inoculated into medium with 1 μ M heme. Indeed, pre-exposure to low heme level eliminated the extended lag period (Figure 15). These observations suggest that the treatment with low level of heme-triggered adaptation to environmental heme.

In light of recent evidence that bacteria can sense and respond to heme (95, 163, 196, 205) and with evidence for a similar response in GAS, we wanted to gain insight into the

pathogen's mechanisms for heme sensing and tolerance. We examined the differential global gene expression pattern between GAS cells subjected to heme stress (4 μ M) and control treatment. Total RNA was isolated from cells 90 min post treatment and analyzed using a 70-mer oligonucleotide microarray (representing GAS genomes M1, M3 and M18) (190). Our data showed a significant shift in the transcript profile of different genes and operons in response to heme stimulus; referred to as the 'GAS heme stimulon'. This stimulon involved changes in 163 total genes, including 79 genes that were up regulated and 84 genes that were down regulated (Figure 16 and Supplementary Table 1). The array analysis was validated by quantitative RT-PCR (qPCR) on 11 differentially regulated genes (Supplementary Table 1), showing a strong correlation, with an R^2 value of 0.889 (Supplementary Figure 1).

Genes that were down regulated significantly in response to heme are found in the categories of metabolic pathways, sugar and metabolite transport, and two-component system (TCS, Figure 16A). Of particular interest is the down regulation of the TCS, *trxSR*. The response regulator, TrxR activates the Mga virulence regulon in GAS, and a *trxR* mutant is attenuated for virulence in a murine infection model (206, 207). Therefore, environmental heme may impact the expression of key virulence factors in GAS via the TrxSR/Mga pathway. Since the TrxSR system is implicated in asparagine sensing, our observations also imply that the damage to the cell envelope introduced by heme is associated with increased levels of asparagine (or other amino acids) (206, 207). In contrast, heme-activated genes and highly expressed transcripts encode for protein folding and degradation (such as *groEL/ES* ~8 fold, *DnaJ/K* 3-4 fold, and *clpE/L* ~4 fold)

and components of the Clp protease machinery (*clpCP*- 2.5 fold) (208, 209) (Figure 16B). In addition, the GAS heme-activated stimulon includes genes whose functions are linked to regulation of redox stress management, including *spx* (5 fold) and *ctsR* (2.5 fold) (210, 211). Accordingly, members of the downstream genes of these regulators were also activated by heme such as thioredoxin (*trx* ~2.5 fold) and oxidoreductases (3 fold). Finally, the expression of two TCSs was also up regulated in response to heme exposure, including the pneumococcal-like TCS homologous system, *ciaHR* (~2.3 fold) (212) and the *ihk/irr* TCS (2.5 fold) involved in GAS response to oxidative stress and survival within phagocytes (213).

4.3.5 Identification of the *pefRCD* locus in GAS.

The transcriptomic analysis also revealed that several putative efflux proteins also showed an increase in transcriptional activity in response to heme stress. These included a 3-gene cluster (MGAS5005 *spy_0195*, *0196*, and *0197*) with homology to the *pefRCD* genes from GBS (95). Since the *pefRCD* genes are important for the management of heme stress in GBS, we focused our attention on their heme-induced homologs in GAS. Comparative sequence analysis demonstrated that the putative GAS genes, *spy_0195* (84% similarity; 56% identity), *spy_0196* (76% similarity; 48% identity), and *spy_0197* (76% similarity; 51.3% identity) show significant sequence homology to the GBS *pefRCD* genes, respectively (Figure 17). In addition to the high sequence homology demonstrated by each of these GAS genes, the genomic arrangement of the GBS *pefRCD* locus and its immediate chromosomal location are also conserved in all of the published GAS genomes (Figure 18A). Moreover, using the MEME algorithm, we identified a 17-

bp inverted repeat region within the putative promoter of *spy_0195* that shared 76% identity with the PefR binding site from GBS (Figure 18A). Based on this sequence conservation and the observed induction by heme, we hypothesized that like GBS, the above-mentioned GAS genes encode a heme dependent repressor (*spy_0195*) and an ABC heme exporter (*spy_0196* and *spy_0197*) and named them *pefRCD*, respectively.

We examined the time course of *pefRC* expression in response to heme by qPCR (Figure 18B). As seen in the microarray analysis, the expression of *pefR* and *C* was comparable to one another in all of the time points, supporting an operon structure. Heme exposure resulted in an increase of *pefR* and *pefC* expression over time, reaching 2.5 fold over background at 30 min, 4.5 fold at 60 min and remained high at 90 min post treatment. This temporal increase in *pef* expression in response to heme insinuates an active participation of these genes in heme tolerance.

4.3.6 GAS PefR binds heme and PPIX with high affinity.

In GBS, PefR is a MarR-like repressor that binds to DNA and blocks the transcription of both *pefRCD* and *pefAB* operons. In this system, heme acts as an inducer that binds to PefR protein to alleviate repression. The GAS protein shares 43% identity and 74% similarity with PefR from GBS (Figure 17), implying the two proteins may function in a similar manner. We cloned the *pefR* gene from GAS and expressed it as an N-terminal hexahistidine (6x-His) fusion protein. SDS-PAGE and western blot analysis of the recombinant protein following purification from *E. coli* confirmed the presence of a single protein at the expected size that reacts with anti-his tag antibodies (Figure 19A and

data not shown). Interestingly, the purified PefR had a light brown color (Figure 19B, left inset) and exhibited an absorption in the Soret region (435 nm). Upon titration with free heme, PefR displayed a growing Soret band and concomitant increase in absorption at 530 and 560 nm (β and α bands of heme). These spectral features are characteristics of heme bound protein and are easily separated from the absorption displayed by heme that is free in solution (214). The holo-PefR maintained a bright red color after the removal of heme excess by gel filtration and dialysis (Figure 19B, right inset). Therefore, PefR was purified from *E. coli* with some heme and readily bound heme *in vitro*. The plot of changes in absorbance at 435 nm as a function of heme concentrations indicated a binding stoichiometry of 1:2 (PefR:heme, Figure 19C). We determined the dissociation constant (Kd) for PefR by fitting the plot of changes at 435 nm in the modified Hill's equation (215). We found the Kd to be 10 μM and Hill's coefficient (nH) to be 1.3, greater than 1 (216). The molar extinction co-efficient at 435 nm of holo-PefR was determined using the pyridine hemocromogen method (195) and resulted in $\epsilon_{435} = 30,407 \text{ M}^{-1}\text{cm}^{-1}$. Similarly, titration of PefR with PPIX indicated that it could also bind PPIX in 1:1 stoichiometry with Kd of 9 μM (Figure 20).

4.4 Discussion

It is the biochemical properties of heme that contribute to its characteristics as a double-edged sword in a variety of biological systems. Heme toxicity in humans stems from the lysis of erythrocytes due to disease, inflammation, or physical damage, which could raise the heme levels in the bloodstream up to 20 μM (217, 218). The generation of reactive

oxygen species, alteration in membrane permeability, damage to macromolecules, and decrease in the pool of reductants are some of the cellular mayhem that follows heme overload in eukaryotes (218). In bacteria, despite the importance of heme to physiology and pathogenesis, the molecular mechanisms for heme toxicity and tolerance are poorly understood (85). In this study, we probed these processes in GAS for the first time and established that heme stress is very significant to the physiology of the α -hemolytic pathogen; heme in excess inhibits GAS growth and exposure to low heme levels damages membrane lipids and proteins. We demonstrated the presence of an adaptation process to environmental heme in GAS and revealed a comprehensive transcriptome response to excess heme exposure. Finally, our findings also implicate a new gene cluster, *pefRCD*, in GAS heme sensing and tolerance.

We found that heme tolerance in GAS depends on medium type, growth conditions and genetic background (Table 5). Differences in bacterial metabolism, aeration, and cell-to-cell contact may all affect the bacterial sensitivity to heme. In addition, the THY medium is prepared from brain and heart infusion and is likely to contain some heme. Growth in THYB therefore, may allow for bacterial adaptation, possibly contributing to the higher heme MIC values observed in this medium. A significant variation in heme tolerance was exhibited by different strains of GAS; with NZ131, a serotype M49 skin isolate (197, 198), demonstrating the lowest heme tolerance, whereas the more invasive strains such as MIT1 MGAS5005 (199) and other clinical isolates showing higher heme resistance. It is tempting to speculate that these variations in heme sensitivity might add to the inclination of different GAS strains to colonize certain sites and to their invasive potential.

The absence of significant damage to cytosolic proteins in GAS suggests that the membrane is the primary target of heme in this bacterium (Figures 13 and 14). This observation is in accordance with findings made in *S. aureus* (219) and is likely to result from heme accumulation in the cell envelope. The negative regulation of the heme uptake machinery works to limit the amount of heme that can reach the GAS cytoplasm (30, 32, 220). In addition to active import, heme can diffuse through biological membranes, albeit with slow diffusion rates that can lead to accumulation in this compartment. Indeed it is well established that heme surplus tends to accumulate in the membranes of the eukaryotic cells, where it can be transformed into highly reactive species (81, 161). There is less information regarding heme localization in bacteria; however, studies in *S. aureus* suggest a similar buildup in the cell envelope (221). In addition to the preferential localization of heme outside of the cytoplasm, the reducing environment and the detox mechanism induced by heme (e.g. heat shock and redox factors) could mitigate some of the oxidative effects of the heme in this compartment. In this study we only probed the impact of heme at 4 μ M, a concentration that is below the MIC level in early exponential phase, and for 90 min post treatment. Further investigations are needed to determine if heme at higher concentrations or after longer exposure time is affecting other cellular compartments.

The extended lag period that is observed when naïve GAS cells are introduced into medium containing heme and the absence of the growth delay in cells that were pre-exposed to low heme levels (Figure 15) provide strong evidence for the presence of heme

sensing and coping mechanisms in GAS. Indeed, microarray analysis indicated that heme triggers comprehensive changes in GAS transcript levels (Supplementary Table 1 and Figure 16A). The shift in the expression of regulatory proteins such as *spx*, *ihk/irr*, *ctsR*, and *hrcA* and their downstream-regulated genes, suggests that heme leads to significant redox, oxidative, and protein damage (Figure 16B). Spx is an RNA polymerase binding protein with CXXC redox-sensing center that acts to restore thiol balance by controlling redox enzymes and antioxidants formation (222). The *ihk/irr* TCS regulates oxidative stress genes that protect GAS from killing by phagocytic cells and hydrogen peroxide (213, 223). The induction of this regulatory system is consistent with ROS formation and cell envelope damage following heme exposure. The master regulators CtsR and HrcA, originally classified as class III and class I heat shock gene regulators, respectively, have been associated with a wide variety of stresses such as temperature shifts, antibiotics, carbonyl, electrophiles, etc. (224, 225). Here we show their association with heme stress and the elevated expression of chaperones and *clp* proteases further corroborates our hypothesis of heme-induced protein unfolding and findings of protein oxidation.

Heme treatment also resulted in significant inhibition of the genes encoding lactate oxidase (*lctO*) and of a V-type ATP synthases system (*ntpKCFABD*). LctO reaction leads to hydrogen peroxide production that can exacerbate the damage induced by heme (226, 227). The down regulation of the proton pump may serve to increase the reducing power at the cell surface. Further selective down regulation of genes such as *citDEFX* and up-regulation of *fruRBA*, which are involved in import and utilization of citrate and fructose, respectively, could indicate a metabolic state that is more conducive to detoxification.

Le Breton *et al.* recently used a *mariner*-based transposon library to screen for genes that are important for GAS survival in human blood (228). Comparing the heme stimulon identified in this study to the findings of Le Breton *et al.* revealed significant overlap, including *clpE* and *L*, *fhs.2*, *fruA*, *citF*, *trxS*, *lacZ*, and the *has* operon. This comparison suggests that heme, directly or indirectly, act as a signal that mediates adaptation *in vivo* and that the management of heme toxicity is relevant to GAS pathogenesis, in particular during spread through the blood.

The heme stimulon in GAS also includes three genes (*spy_0195-7*) that share high homology to the GBS *pefRCD* genes. In GBS these genes code for a heme responsive repressor (PefR) from the MarR-like family (229) and to an ABC heme exporter (PefCD) (95). While the presence and genomic arrangements of *pefRCD* are highly conserved among different GAS strains (Figure 17 and 18), we failed to identify homologues to *pefAB* (and *hrtAB*) that also participate in heme tolerance in GBS and other Gram-positive bacteria. The high degree of sequence similarity and the temporal increase in expression in response to heme stress (Figure 18B) suggest that the 3-gene locus encodes for a true homologue of the *pef* operon. This hypothesis is further supported by the identification of a putative PefR heme-binding box that is highly comparable to that of PefR from GBS (Figure 18A) (95) and by our heme and PPIX reconstitution experiments (Figures 19 and 20). The ability of PefR to coordinate two heme molecules and curve fitting data demonstrating positive Hill's coefficient of cooperativity most likely suggest that the binding of heme at one binding site increases the affinity of heme binding at

another site (215, 216). Further experiments are underway to determine if and how heme and PPIX are modulating PefR binding to DNA and to establish the role of this 3-gene cluster in heme and protoporphyrin tolerance in GAS.

To the best of our knowledge our work is 1) the first effort to characterize GAS mechanisms for heme toxicity and tolerance; 2) shows that environmental heme constitutes a significant redox stress in GAS with damaging effects on membrane lipids and proteins; 3) provides evidence for heme sensing and adaptation that involves global transcriptome shifts; and 4) links heme stress to several key regulators and TCS systems of this important human pathogen.

5 CHAPTER 4 - THE PEFCD IS A MDR SYSTEM THAT EXPORTS HEME AND CONFERS RESISTANCE TO HEME AND DOXORUBICIN IN GAS

5.1 Introduction

Streptococcus pyogenes or Group A Streptococcus (GAS) is a Gram positive, β -hemolytic, human pathogen transmitted via respiratory droplets and direct contact. GAS is responsible for a diverse spectrum of diseases ranging from superficial (e.g., pharyngitis, impetigo and pyoderma) to severe invasive infections and systemic manifestations (such as necrotizing fasciitis and streptococcal toxic shock syndrome). In addition, simple GAS infections can trigger autoimmune reactions in some patients leading to neurological disorders, glomerulonephritis, or acute rheumatic fever (3, 4). GAS encodes a large collection of virulence factors, which act to promote infections and pathologies by various means such as bacterial adherence and invasion, evasion of the host immune surveillance and nutrient acquisition (230). Due to the high morbidity associated with GAS related illnesses, this pathogen is ranked 9th among the world's leading infectious agents (231). Recent global estimates suggest that every year about 600 million GAS infections occur, accounting for ~ 600,000 deaths (232). The reported increase in antibiotic resistance, emergence of new strains, and absence of vaccine programs suggest that the disease burden inflicted by GAS is likely to rise (6, 233).

GAS requires iron for growth and can retrieve the metal from heme (131). The cytolysins produced by GAS provide the pathogen with access to the host intracellular pool of hemoproteins. GAS proceeds with heme uptake using the streptococcal iron acquisition

(*sia*) operon: heme is extracted and captured on the bacterial surface by the streptococcal hemoproteins receptor (Shr), relayed to the streptococcal hemoprotein (Shp), and subsequently to the substrate binding protein, SiaA (HtsA). The SiaBC importer then internalizes the heme (32, 133-135, 186). Although heme is nutritionally beneficial, its pro-oxidant nature renders it hazardous in surplus quantities (85). We recently observed that exposure to sub-lethal heme concentrations elicits a global stress response in GAS (50). This observation underscores the harmful potential of heme. Heme toxicity seems particularly relevant to the patho-physiology of the β -hemolytic pathogen, and could impose as a significant challenge for GAS growth during invasive infections.

Heme-mediated cell injuries are primarily accredited to the coordinated iron element. The dynamic existence of iron in two redox and spin states within heme allows it to react with multiple biological entities including proteins, nucleic acids and lipids. This effect is exacerbated by the participation of iron in Fenton reactions, which lead to generation of radicals or reactive oxygen species (234). In addition to iron toxicity, the lipophilic nature of the protoporphyrin-ring (PPIX) is associated with photosensitivity and insertion of heme into membranes. This process was shown to undermine membrane permeability and further potentiates the release of free-heme from erythrocytes (235, 236). In mammals, increased and persistent flux of free-heme in the vascular system is associated with significant inflammation and pathology (237).

To manage heme toxicity, bacteria carefully control heme uptake according to cellular demands. In GAS for example, a metalloregulatory protein named MtsR, directly

represses the expression of the *sia* operon in the presence of iron (65). In addition to limiting heme uptake, bacteria employ various sequestration, degradation, and active efflux mechanisms. The export of heme excess and its role in protection against toxicity has been increasingly recognized in bacteria. The multiple-transferable-resistance (MtrCDE) efflux system from *Neisseria gonorrhoea* which, expels hydrophobic antibacterial agents (238), also facilitate resistance to PPIX, heme, and other porphyrin-based compounds. Inactivation of the *mtrCDE* pump resulted in increased gonococci sensitivity to porphyrins and metalloporphyrins, while overexpression of this system endowed cells with an increased tolerance to porphyrin based compounds (239). The *E. coli* MacAB pump is another example of an active exporter with broad specificity that contributes to heme tolerance. MacAB (with the TolC outer membrane channel protein) enables enterotoxin secretion and confers resistance to macrolides (240, 241). In addition, MacAB-TolC serves as the major PPIX exporter in *E. coli* (242).

In Gram-positive organisms, the archetype of an exporter that mediates heme tolerance in several bacteria including *Bacillus anthracis* and *Lactococcus lactis* was identified first in *Staphylococcus aureus* and named heme-regulated transporter (HrtAB) (94, 96, 243, 244). Work performed in *L. lactis* suggested that this system exports heme directly from the membrane, acting to limit heme accumulation in this compartment (96, 245). The expression of the *hrtAB* genes is tightly regulated according to heme availability via the two-component system HssRS (in *S. aureus* and *B. anthracis*) or the heme-dependent repressor, HrtR (*L. lactis*) (94, 96, 246). The presence of the HrtAB transporter and the associated regulatory network bestows bacteria with elevated heme sensing and

resistance capacity. Studies in mouse infection model demonstrated that the *HrtAB* promoter in *B. anthracis* is induced *in vivo*, suggesting that the HrtAB transporter is recruited during infection, presumably to alleviate heme toxicity (94). Interestingly, while both species exhibit similar sensitivity to environmental heme, the loss of *hrtA* in *B. anthracis* has a more pronounced impact than in *S. aureus*, implying that heme sensing and/or detoxification by the HssRS and HrtAB systems are more effective in *B. anthracis* than in *S. aureus*. (94). The genome of Group B streptococcus (GBS) contains putative *hrtAB* homologs that are regulated by heme availability. However, contribution of these genes to heme efflux and tolerance in GBS has yet to be determined. In addition, GBS carries a regulon called *porphyrin regulated efflux (pef)* whose expression is controlled by PefR, a MarR-like repressor (95). Heme or PPIX allow for transcriptional activation of the *pef* regulon by relieving PefR binding to its operator. The *pef* regulon consists of at least two separate gene clusters (*pefAB* and *peRCD*) that encode two distinct transporters, *pefAB* and *pefCD*. Inactivation of the GBS *pef* transport system results in increased sensitivity to heme and intracellular buildup of heme and PPIX. Overexpression of these systems led to heme depletion and a defect in both respiratory metabolism and virulence (95). In *Listeria monocytogenes*, an ATP-dependent transporter, FrvA (Fur regulated virulence factor A), was implicated in heme export and protection from heme toxicity (247). Notably, the FrvA transporter is essential for the systemic infections in mice models.

Mechanisms of heme tolerance are poorly understood in GAS. We recently identified a three-gene operon in GAS that shares significant similarity to the GBS *pefRCD* genes.

We demonstrated that these genes are up regulated in response to heme exposure and implicated the PefR homolog in heme sensing and regulation of the gene cluster (50). In this study, we set to determine the function of the *pefCD* genes in GAS physiology.

5.2 Materials And Methods

5.2.1 Bacterial strains and growth conditions

Plasmids and strains used in this study are listed in Table 6 and the primers are described in Table 7. *E. coli* cells were used for cloning and propagation of plasmids. *E. coli* was grown aerobically in Luria-Bertani medium (BD) at 37 °C (pH 7.0). GAS was grown under static conditions in Falcon tubes or nephelometer flasks in THYB: Todd-Hewitt broth (TH broth, Difco laboratories) with 0.2% (weight/volume) yeast extract (BD). Growth was measured using a Klett-Summerson colorimeter (A filter) and / or by viable counting. In some cases, hemin chloride (Sigma) prepared in DMSO (0.035% final concentration, Fisher BioReagents) was added to the cultures. Antibiotics were used at the following concentrations: Spectinomycin at 100 µg/ml for both *E. coli* and GAS, and kanamycin at 70 µg/ml for *E. coli* and 300 µg/ml for GAS.

5.2.2 Nucleic acid methods.

Chromosomal and plasmid DNA extraction and DNA manipulations including restriction digests, cloning, and DNA transformation were done according to the manufacturer's recommendations and with standard protocols as previously described (248). Plasmid DNA was isolated from *E. coli* using the Wizard Plus SV mini-prep system (Promega).

DNA was subjected to restriction digestion (SpeI-HF[®] and or EcoRI of NEBL), and fragments were gel purified from agarose using S.N.A.P. UV-free gel purification kit (Invitrogen). The digested and gel purified fragments were ligated using T4 DNA ligase (Roche) to generate a recombinant construct.

5.2.3 Construction of plasmids, GAS mutants and complementation strains:

The *pefC::pMZ1* mutant, ZE4951, was constructed in NZ131 background by Campbell insertion using plasmid pMZ1. Briefly, an internal 696 bp fragment from the *pefC* gene was amplified from NZ131 chromosome using ZE565 and ZE566 primers and ligated into the EcoRI site in pUC-Spec, which carries the spectinomycin resistance gene, *aad9* (249). The resulting plasmid, pMZ1, was introduced into NZ131 strain and spectinomycin resistant colonies were selected. The structure of the chromosomal *pefC::pMZ1* mutation was verified by PCR and sequence analysis. For complementation analysis, a 4336 bp fragment spanning the *pefRCD* operon including the promoter region was amplified from NZ131 chromosome with ZE634 and ZE635 primers and ligated into the SpeI site of the shuttle vector, pKSM201 (250), which carries the kanamycin resistance gene *aphA3*, generating pANKITA5b. The plasmids pKSM201 (empty vector) and pANKITA5b were introduced into ZEM4951 strain by selection for spectinomycin and kanamycin resistance.

5.2.4 Heme and doxorubicin sensitivity assay

GAS sensitivity was tested using the Disc Diffusion method as previously described (50). Briefly, sterile 8.0 mm Whatman filter paper discs (with 1.2 mm width) were submerged

in 10 mM heme or 1.6 mM Doxorubicin (prepared in water) solutions, dried and impregnated onto THYA that was plated with 0.1 ml ($OD_{600nm} = 0.1$) of overnight GAS culture. The plates were incubated at 37°C for 17 hours before the zone of clearance around the discs was measured.

5.2.5 Determination of lipid peroxidation using TBARS assay

Fresh THYB was inoculated with GAS cells collected from plates: the inocula consisted of cells grown overnight at 37°C on THYA and suspended in saline. Bacterial suspensions at $OD_{600} = 0.5$ were diluted 1:100 into fresh THYB, incubated at 37°C, and growth was monitored. Heme (1 μ M) was added at the logarithmic phase of growth (~ 60-70 Klett units) and samples (standardized according to cell density) were harvested by centrifugation (5000 \times g, 20 min at 4°C) at 30, 60, and 90 minutes post exposure. The cell pellets were washed and samples were prepared and analyzed for lipid peroxidation using OXI-TEK TBARS (Thiobarbituric Acid Reactive Substances) assay kit (ZeptoMatrix Corporation) as previously described (50). Sample absorbance at 532 nm was recorded using the DU 730 Life Science UV/vis spectrophotometer. The $A_{532\text{ nm}}$ obtained for the experimental samples were compared to a standard curve generated using the malondialdehyde (MDA) reagent supplied with the kit.

5.2.6 DNA damage detection

Fresh THYB medium was inoculated with GAS cells collected from THYA plates as described above. The cultures were treated with 5 μ M heme at the logarithmic phase of growth (~ 60-70 Klett units) and samples (standardized according to cell density) were

harvested at 0, 30 and 90 minutes post exposure. Genomic DNA was extracted from the cell pellet using the ArchivePure DNA extraction kit (5 PRIME). DNA purity and concentration were determined and 0.5 µg of DNA samples were used to quantify the formation of apurinic/apyrimidinic (AP) sites using the DNA damage detection kit (PromoKine) per the manufacture instructions. Briefly, DNA (500 ng) was incubated with aldehyde reactive probe containing biotin tag (ARP) solution for 1 hour at 37 °C. Glycogen and TE buffer were added to the solution, the DNA was allowed to precipitate at -20°C for 10 min and then collected by centrifugation at 13,000 rpm for 10 minutes at 4°C. The pellet of the biotin-tagged DNA was washed with 70% ethanol, air-dried, resuspended in 1ml of TE buffer. The DNA samples (60 µl) were added to 96 well ELISA plate and incubated overnight at room temperature with DNA binding solution. The signal was developed after incubation with horseradish peroxidase (HRP)-streptavidin solution and developer. The signal intensity was quantified spectroscopically at 650 nm. A standard plot depicting the absorbance at 650 nm as a function of the number of standard AP sites of standard solution (0, 8, 16, 24, 32, and 40 ARP sites/10⁵ bp solution) was used to determine the number of AP sites /10⁵ bp DNA fragment in experimental samples. As a positive control for AP site formation in GAS cells, we used cells exposed to 10 mM H₂O₂ solution for 1 hour at 37°C followed by genomic DNA extraction, labeling, and detection similar to standards and experimental samples (data not shown).

5.2.7 Determination of intracellular hemin content

Fresh THYB medium was inoculated with GAS cells collected from plates as described above. The cultures were treated with 3 µM heme at the logarithmic phase of growth (60-

70 Klett units) and samples (standardized according to cell density) were collected 90 minutes post exposure by centrifugation (8000×g for 20 min at 4 °C). The cell pellet was washed 5 times (10 ml phosphate buffered saline, pH 7.0 each), resuspended in 2 ml of DMSO, and subjected to sonication (20 % amplitude for 30 sec.). Heme content in the cell lysate was determined using the procedure described by Lombardo *et al* with small modifications (251). Briefly, 4 ml of experimental samples along with hemin standard solutions (0-5 μM, in DMSO) were subjected to acidified chloroform extraction as follows: addition of 2 ml of 50 mM glycine buffer, pH 2.0 then 0.1 ml of 4N HCl (pH 2.0), 0.2 ml of 5M NaCl (pH 2.0) and chloroform (2 ml) followed by vigorous mixing for 10sec (6 times). The reactions were incubated at room temperature for 1 minute and the absorbance by the organic phase was then determined. The absorbance at 388, 450 and 330 nm were recorded and fed into the correction equation $A_c = 2 \times A_{388} - (A_{450} + A_{330})$. The plot of A_c corrected for standard heme concentrations was used to extrapolate the hemin concentration in experimental samples.

5.3 Results

5.3.1 The *pefCD* genes encode a conserved Class-1 ABC exporter

We recently reported the transcriptional activation of a 3-gene cluster (MGAS5005 spy_0195, 0196, and 0197) ensuing GAS exposure to environmental heme. We named these GAS genes as *pefRCD* based on similarity in genetic organization, primary sequence, and regulation to the previously described *pefRCD* operon in GBS (50, 95) (Figure 21A). Here, our analysis showed that the *pefRCD* genes are highly conserved

among GAS strains exhibiting 100% identity for PefR, 98% identity for PefC, and 99% identity for PefD protein (for all 20 strains in the database). The *pefCD* genes are annotated in GAS genome as the subunits of a putative multi-drug resistance (MDR) system. Sequence analysis indicated that the *pefCD* genes code for the two subunits of a heterologous ATP-dependent exporter. Both ORFs contain, at the N terminus, an integral membrane (IM) permease domain from the superfamily of ATP binding cassettes fused to an ATP-hydrolyzing domain (ABC, also referred to as the nucleotide binding domain) (Figure 21B). This domain organization is of the Class-1 ABC-type transporter family (252). This transporter class is comprised of systems with fused IM and ABC domains and contains the vast majority of ABC-type export systems (252). Our recent BLAST analysis against the transporter classification (TC) database (<http://www.tcdb.org>) (253) revealed that the PefCD proteins consists of a transporter from the drug exporter-4 sub class (3.A.1.135). Importantly, this analysis revealed that PefCD exporter is identical to a previously described transporter from the GAS strain JRS4, named Rsc (regulated by stress and Cov) after its regulation by the response regulator CovR (254). The substrate(s) of the Rsc system was not identified but the transporter was found to be required for bacterial growth at high temperature. The nearest relatives of the PefCD (RscAB) proteins are the components of the MDR transporters, SatAB of *S. suis* (255), PatAB from *S. pneumonia* (256), and LmrCD (aka YdaG and YdbA) from *L. lactis* (257). For simplicity we continue in this manuscript to refer to the GAS exporter as the PefCD system. Further *in-silico* analysis performed on genomes of streptococci identified putative homologs of the *pefRCD* gene cluster in *S. equi*, *S. uberis*, *S. suis*, and *S. iniae* (258-262). A high degree of conservation in genetic organization and

sequence exhibiting 54% amino acid similarity for the PefR, 60% for the PefC, and 64% for the PefD protein among all the candidates tested by ClastalW pairwise alignment tool (263), (Figure 21A).

5.3.2 Inactivation of *pefCD* resulted in a growth phenotype and hypersensitivity to heme and doxorubicin.

In order to gain insight into the role of the *pefCD* genes in GAS physiology, we created a polar mutation in *pefC* by insertion inactivation (ZE4951 strain) in the background of the wild type strain, NZ131 (Table 6 and Figure 22A). For complementation of *pefCD* polar mutation, we cloned the *pefRCD* operon with its native promoter into a shuttle vector (pKSM201). *E. coli* cells harboring the plasmid carrying the GAS *pefRCD* operon (pANKITA5b) did not exhibit any growth phenotype. However, despite our multiple attempts, we failed to create a sub clone that expresses only the *pefCD* genes (under the *pef* promoter). We therefore used the entire *pefRCD* operon (carried by pANKITA5b) to complement the ZE4951 mutant. Analysis of ZE4951 growth in THYB media demonstrated that inactivation of the *pef* system resulted in a pronounced phenotype; the mutant cells grew slower and reached the stationary phase of growth at a lower cell density in comparison to the isogenic NZ131 wild type strain (Figure 22B). In addition, cell viability of the mutant strain was significantly reduced during overnight incubation in stationary phase (data not shown). The growth defect of the ZE4951 mutant was reversed in the presence the *pefRCD* genes expressed in trans (pANKITA5b) but not in the presence of an empty shuttle vector (pKSM201, Figure 22). This analysis suggests that the *pefCD* genes are required for optimal GAS growth in standard laboratory medium.

When tested for heme sensitivity, the ZE4951 mutant strain exhibited a larger zone of clearance around a heme-submerged disc compared with the wild type strain (Table 8). The mutant sensitivity to heme was restored to the wild type level when complemented in trans with the *pefRCD* genes, but not in the presence of the control plasmid. These observations supported the hypothesis that PefCD consists an efflux system that extrudes heme or heme-related toxic metabolites. While some exporters are selective for a given substrate, many are able to expel a range of structurally unrelated molecules (93, 252). Examining the growth of the mutant strain around discs containing the anthracyclic compound, doxorubicin, revealed increased sensitivity compared with the parent strain (Table 8). As with the sensitivity to heme, the doxorubicin hypersensitivity phenotype was reversed when the *pefRCD* genes were supplied in trans (Table 8). Heme and doxorubicin are structurally dissimilar; these data are consistent with the *in silico* analysis described above and imply that PefCD is an exporter with a broad substrate specificity.

5.3.3 Inactivation of the *pefCD* system is associated with elevated levels of heme-induced damage to cellular constituents

In order to uncover why the loss of the *pefCD* genes leads to reduced heme tolerance in GAS, we investigated the impact of heme on GAS cellular components in the wild type and mutant strains. In a recent study we demonstrated that exposure to low heme concentration was sufficient to damage the lipids in GAS envelope (50). Oxidized lipids react with a thiobarbituric acid (TBA) reagent to form adducts (named TBARS) that can be monitored by spectroscopic methods and quantify with a standard curve (50, 201). We

compared the time course of TBARS formation between the wild type and mutant strain after the addition of 1 μ M heme into the culture (Figure 23). Analysis of samples collected 30 minutes post exposure revealed that the ZE4951 mutant exhibited higher level of lipid damage than the wild type strain (3 versus 1.5 nmol/ml TBARS in the mutant and wild type strain respectively). Complementation of the *pefC* mutation with the *pefRCD* genes resulted in a significantly lower level of TBARS formation, in comparison to mutant cells harboring the negative control plasmid (0.97 and 2.49 nmol/ml respectively). Interestingly, the TBARS levels in the complemented mutant strain were reduced over time (from 0.98 to 0.38 nmol/ml in the 30 and 90 min samples respectively), while they remained approximately the same in the wild type, mutant, and the mutant cells harboring the control plasmid. Together these observations imply that the PefCD system defends GAS from heme-induced lipid damage and suggest that the expression of *pefRCD* genes under our experimental conditions may be limiting in the wild type strain.

Studies performed with eukaryotic systems showed that heme could harm nucleic acids (264). We asked if environmental heme can damage GAS genome and if the *pef* system offers protection from this harm. The repair of chemically altered bases (due to oxidation, deamination or alkylation) in the DNA is often mediated by repair mechanisms that involve the formation apurinic/apyrimidinic (AP) sites. Therefore, the amount of AP sites serves as a good indicator for DNA damage and repair. To quantitate the formation of AP sites in GAS chromosome, we used a reagent (ARP) that reacts specifically with the aldehyde group in the open ring form of the AP sites (265). Chromosomal DNA was

extracted from culture samples that were harvested at different time points and was allowed to react with ARP reagent. The formation of AP sites was detected by ELISA and quantified using a standard curve (Figure 24). Analysis of chromosomal DNA from culture samples of the wild type strain collected 30 minutes after the addition of heme revealed about 90% increase in the number of AP sites compared to the background level (11 and 5.8 AP sites per 10^5 bp respectively). The AP sites level was reduced over time, but remained 40% above the background (8 AP sites per 10^5 bp) in the samples collected 90 minutes after treatment. Interestingly, in *pefC* mutant the background level of AP sites was about twice as high compared with the wild type strain (11.5 AP sites per 10^5 bp). Heme exposures resulted in a transient 117% increase in the number of AP sites, which was reduced to background level within 60 minutes (25 and 11.5 AP sites per 10^5 bp in the 30 and 90 minutes respectively). The high AP levels observed in the mutant strain were complemented to those observed in the wild type strain by the *pefRCD* genes expressed from a plasmid in all samples. The levels of AP sites in the mutant strain carrying the empty vector were comparable to that of the mutant strain alone. These experiments indicate that environmental heme led to DNA damage in GAS and that the *pefCD* genes offered protection from DNA damage during growth in laboratory medium as well as in medium containing externally added heme. In addition, our data highlights the presence of DNA repair mechanisms in GAS.

5.3.4 The *pefCD* prevents cellular heme accumulation

One interpretation of the experiments described above is that following the addition of heme to the culture medium GAS cells absorb it in surplus amounts; in the absence of a

functional PefCD system, the bacterium accumulates heme or heme-related metabolites that damage the cell constituents. To directly test this hypothesis, we examined the cellular heme content by the acidified chloroform extraction method (251) described in the material and methods (Figure 25). Culture samples of equal cell density were collected 90 minutes after the addition of 3 μ M heme to the medium and the cells were washed extensively to remove surface bound heme prior to heme extraction. The presence of heme in the organic phase of the cell extracts was examined by spectroscopic analysis and the concentration of the extracted heme from each sample was extrapolated from a standard curve (Figure 25B and 25D). We extracted in these experiments about 30% more heme from the *pefC* mutant in comparison to the wild type strain. The heme concentration obtained from cells of the *pefC* mutant complemented with the *pefRCD* genes, was 7% lower than that extracted from the wild type cells. On the other hand, the presence of the empty vector did not have a significant impact on the heme concentration in the extract from the *pefC* mutant. Therefore, the PefC accumulates more heme than the wild type strain. This observation suggests that the PefCD system expels surplus heme from GAS cells.

5.4 Discussion

Heme is an important nutrient for the β -hemolytic GAS, which uses it in order to obtain iron within the host environment (131). Despite its nutritional value, heme is a harmful molecule, damaging to GAS envelope even in low concentrations (50). In the current study, we investigated how GAS manages the toxic challenges imposed by environmental

heme. We recently identified a 3-gene operon that was induced by heme and named it after the *pefRCD* system in GBS (50, 95). Following up on our initial observations, we carried out a functional characterization of the *pefCD* genes in the GAS strain, NZ131. We established that they play an important role in heme tolerance; defending GAS membrane and chromosome from the toxic effects of heme stress and prevents heme accumulation in the bacterial cells. This is the first heme tolerance pathway to be described in GAS.

To examine the role of the *pefCD* genes in GAS, we created a polar mutation in *pefC*, which we then supplemented with the *pefRCD* expressed from a plasmid. All of the observed phenotypes of the *pefC* mutant were effectively complemented, indicating that under our experimental conditions, the PefCD proteins were expressed in trans at sufficient levels despite the presence of the putative repressor, *pefR*, on the complementation plasmid. Our failed attempts to clone *pefCD* under the native *pef* promoter in the absence of *pefR* raises the possibility that the constitutive expression of the *pefCD* genes is detrimental to *E. coli*. Toxicity of membrane proteins when overexpressed or of proteins expressed in heterologous host is not uncommon. A similar problem was reported for the related SatAB system of *S. suis* (255).

Examining the phenotype of the *pefC* mutant and the complemented strain showed that the loss of the PefCD system led to increased sensitivity to heme and doxorubicin (Table 8). This observation is consistent with the bioinformatics analysis that revealed significant similarity among PefCD proteins and the confirmed MDR transporters SatAB,

PatAB, and LmrCD from *S. suis*, *S. pneumoniae* and *L. lactis* respectively (255, 257, 266). Together, these observations imply that the PefCD proteins consist of a MDR transporter that expels doxorubicin and heme or heme related metabolites. Our additional findings demonstrated that GAS accumulates heme in the absence of a functional PefCD transporter (Figure 25), strongly implicating heme as a substrate of the *pefCD* system. The *pefC* mutant exhibited growth attenuation in THYB (Figure 22B). THYB contains infusions of brain and heart tissues. Therefore, the mutant growth phenotype might have resulted from increased sensitivity to the heme that is already present in the medium. Alternatively or in addition, PefCD may help in the clearance of other toxic molecules that are generated during growth. Interestingly, a previous study performed in the JRS4 strain revealed that the *pefC* (*rscA*) gene is induced at low pH and by heat stress and that a *pefC* mutant could not grow at 40 °C. The growth phenotype at a high temperature raised the possibility that the *pefCD* proteins export molecules that harm the membrane structure and fluidity (254). Heme could be such a molecule, since it is known to penetrate membranes and undermine the membrane permeability (245, 267). Alternatively, other compounds exported by PefCD may be responsible for this phenotype.

We previously reported that the addition of 4 µM heme to the culture medium produced oxidative damage in the envelope of the invasive MGAS5005 strain (50). In this work, we made similar observations with the nephritogenic NZ131, and showed that exposure to 1 µM heme led to noticeable levels of lipid peroxidation (Figure 23B). Moreover, we showed for the first time that externally added heme (5 µM) is also damaging to GAS

chromosome (Figure 24B). Together, these observations highlight the destructive impact of environmental heme on GAS cellular components even at relatively low concentrations. A number of observations demonstrate the importance of the PefCD system in heme detoxification and suggest a positive correlation between the expression of *pefCD* system and detoxification capacity: 1) The *pefC* mutant experienced more lipid and DNA damage comparing with the wild type strain after heme treatment (Figure 23B and 24B). 2) The level of lipid peroxidation in the wild type strain remained constant for 30-90 minutes post treatment, while it was reduced over time in the complemented strain (Figure 23B). 3) More AP sites were detected in the chromosome of the *pefC* mutant comparing to the wild type strain even in the absence of externally added heme. 4) Heme begins to accumulate in the mutant cells after its addition to the growth medium (Figure 25D). The *pef* regulon in GBS is induced by levels of heme that are lower than those required to fully activate the putative HrtAB transporter; it was therefore suggested that the Pef exporters allow for adjustments in small variations in heme and PPIX concentrations under different physiological conditions while the Hrt exporter may be needed to defend GBS against higher heme concentrations (95). Here, we established that the PefCD system in GAS is responsive to low levels of environmental heme (1-5 μ M) and participate in the detoxification process. We did not identify HrtAB homologues in GAS, but it is possible that additional transporter(s) in GAS are recruited at higher heme concentrations.

GAS is a versatile pathogen that exhibits wide tissue tropism and adaptability that enables it to inhibit not only the epithelia of the skin and mucous membranes, but also to

flourish within soft tissues, the lymphatic system, and the blood (4). Therefore, depending on the nature and stages of infection, GAS is expected to confront a wide spectrum of heme concentrations, ranging from low amounts (e.g., during simple skin or mucosal infection) to very high concentrations (such as during invasive infections associated with significant erythrocyte lysis and tissue destruction). Furthermore, heme tolerance varies among GAS isolates with highly invasive strains such as MGAS5005 showing higher resistance (Heme MIC = 50 μ M) than strains that are typically associated with local infections such as NZ131 (MIC = 10 μ M) (50). We propose that the PefRCD represent a fundamental heme defense pathway that is shared by all GAS strains, safeguarding the organism against environmental heme. Highly invasive strains may carry additional pathway(s) that might confer increased resistance.

The role of active export in the management of heme (and other porphyrins) levels and toxicity in bacterial systems is not fully appreciated and only few systems have been described up to date. Two systems were identified in Gram-negative bacteria (MacAB/TolC and MtrCDE for *E. coli* and *N. gonorrhoeae*, respectively) (239, 242, 268). Both exporters consist of cytoplasmic transporters that connect via a membrane fusion protein to an outer membrane channel/tunnel protein. Both cytoplasmic transporters are MDR systems that export a number of compounds in addition to heme and/or porphyrins. However, MacAB is an ATP-type transporter while MtrC belongs to the Resistance/Nodulation/Division (RND) family of transporters, which uses the proton motive force for energy-dependent export. In Gram-positive bacteria, four types of energy dependent exporters used for heme and/or PPIX detoxification were described

(Figure 26). Intriguingly, HrtAB, which was first identified in *S. aureus* (244), belongs to the MacAB family of ABC-type efflux carriers. In this family of ABC transporters, the membrane permease (IM) and the ATPase (ABC) domains are encoded by separate polypeptides (Class 3) (252). HrtAB mediates heme tolerance in a number of Gram-positive bacteria. It was shown to pump heme directly out of the membrane compartment in *L. lactis* (245) and it is likely that it functions in a similar manner in the other Gram-positive species. In *L. monocytogenes*, a P-Type ATPase, that displays homology to bacterial heavy-metal transporting ATPases, confers resistance to heme and hemoglobin (247). The two other types of transporters were described first in GBS: PefAB (antiporter) belongs to the MFS family that relies on the proton motive force and PefCD, which is a Class I, ABC-type transporters (95). In this study, we showed that the GAS PefCD system contributes to tolerance against both heme and doxorubicin. The involvement of the other transporters from Gram-positive bacteria in resistance to compounds other than porphyrins was not examined. We established significant orthology between the GBS PefCD and the system encoded by GAS. Moreover, our *in silico* analysis suggests that the previously described SatAB transporter from *S. suis* is an orthologous system and that a *pefRCD*-like operon is also found in the members of the pyogenic streptococci. In GBS, the PefCD proteins export heme and PPIX (95). Our work here illustrates that this transporter in GAS exports heme and doxorubicin. The *S. suis*, SatAB, is a narrow-spectrum fluoroquinolone exporter (norfloxacin and ciprofloxacin) (255). It will be interesting to find out whether the PefCD system is a MDR transporter that has heme as one of its substrates or if it has evolved distinct

substrate specificities among various species reflecting differences in ecological niches and lifestyle.

REFERENCES

1. Carapetis JR, Steer AC, Mulholland EK, Weber M. The global burden of group A streptococcal diseases. *The Lancet Infectious diseases*. 2005;5(11):685-94.
2. Cunningham MW. Pathogenesis of group A streptococcal infections. *Clin Microbiol Rev*. 2000;13(3):470-511.
3. Carapetis JR, McDonald M, Wilson NJ. Acute rheumatic fever. *Lancet*. 2005;366(9480):155-68.
4. Cunningham MW. Pathogenesis of group A streptococcal infections and their sequelae. *Advances in experimental medicine and biology*. 2008;609:29-42.
5. Snider LA, Swedo SE. Post-streptococcal autoimmune disorders of the central nervous system. *Current opinion in neurology*. 2003;16(3):359-65.
6. Walker MJ, Barnett TC, McArthur JD, Cole JN, Gillen CM, Henningham A, et al. Disease manifestations and pathogenic mechanisms of group a Streptococcus. *Clinical microbiology reviews*. 2014;27(2):264-301.
7. Young MH, Aronoff DM, Engleberg NC. Necrotizing fasciitis: pathogenesis and treatment. *Expert review of anti-infective therapy*. 2005;3(2):279-94.
8. Cole JN, Henningham A, Gillen CM, Ramachandran V, Walker MJ. Human pathogenic streptococcal proteomics and vaccine development. *Proteomics Clinical applications*. 2008;2(3):387-410.
9. Gryllos I, Cywes C, Shearer MH, Cary M, Kennedy RC, Wessels MR. Regulation of capsule gene expression by group A Streptococcus during pharyngeal colonization and invasive infection. *Molecular microbiology*. 2001;42(1):61-74.
10. Dinkla K, Sastalla I, Godehardt AW, Janze N, Chhatwal GS, Rohde M, et al. Upregulation of capsule enables Streptococcus pyogenes to evade immune recognition by antigen-specific antibodies directed to the G-related alpha2-macroglobulin-binding protein GRAB located on the bacterial surface. *Microbes and infection / Institut Pasteur*. 2007;9(8):922-31.
11. Dale JB, Washburn RG, Marques MB, Wessels MR. Hyaluronate capsule and surface M protein in resistance to opsonization of group A streptococci. *Infect Immun*. 1996;64(5):1495-501.
12. Crater DL, van de Rijn I. Hyaluronic acid synthesis operon (has) expression in group A streptococci. *The Journal of biological chemistry*. 1995;270(31):18452-8.
13. DeAngelis PL, Papaconstantinou J, Weigel PH. Molecular cloning, identification, and sequence of the hyaluronan synthase gene from group A Streptococcus pyogenes. *The Journal of biological chemistry*. 1993;268(26):19181-4.
14. Bhakdi S, Trandum-Jensen J, Sziegoleit A. Mechanism of membrane damage by streptolysin-O. *Infect Immun*. 1985;47(1):52-60.
15. Timmer AM, Timmer JC, Pence MA, Hsu LC, Ghochani M, Frey TG, et al. Streptolysin O promotes group A Streptococcus immune evasion by accelerated macrophage apoptosis. *The Journal of biological chemistry*. 2009;284(2):862-71.
16. Nizet V, Beall B, Bast DJ, Datta V, Kilburn L, Low DE, et al. Genetic locus for streptolysin S production by group A streptococcus. *Infect Immun*. 2000;68(7):4245-54.

17. Miyoshi-Akiyama T, Takamatsu D, Koyanagi M, Zhao J, Imanishi K, Uchiyama T. Cytocidal effect of *Streptococcus pyogenes* on mouse neutrophils in vivo and the critical role of streptolysin S. *The Journal of infectious diseases*. 2005;192(1):107-16.
18. Hytonen J, Haataja S, Gerlach D, Podbielski A, Finne J. The SpeB virulence factor of *Streptococcus pyogenes*, a multifunctional secreted and cell surface molecule with streptadhesin, laminin-binding and cysteine protease activity. *Molecular microbiology*. 2001;39(2):512-9.
19. Chaussee MS, Phillips ER, Ferretti JJ. Temporal production of streptococcal erythrogenic toxin B (streptococcal cysteine proteinase) in response to nutrient depletion. *Infect Immun*. 1997;65(5):1956-9.
20. Svensson MD, Scaramuzzino DA, Sjobring U, Olsen A, Frank C, Bessen DE. Role for a secreted cysteine proteinase in the establishment of host tissue tropism by group A streptococci. *Molecular microbiology*. 2000;38(2):242-53.
21. Shelburne SA, 3rd, Granville C, Tokuyama M, Sitkiewicz I, Patel P, Musser JM. Growth characteristics of and virulence factor production by group A *Streptococcus* during cultivation in human saliva. *Infect Immun*. 2005;73(8):4723-31.
22. Collin M, Olsen A. Effect of SpeB and EndoS from *Streptococcus pyogenes* on human immunoglobulins. *Infect Immun*. 2001;69(11):7187-9.
23. Shet A, Kaplan EL, Johnson DR, Cleary PP. Immune response to group A streptococcal C5a peptidase in children: implications for vaccine development. *The Journal of infectious diseases*. 2003;188(6):809-17.
24. O'Connor SP, Cleary PP. Localization of the streptococcal C5a peptidase to the surface of group A streptococci. *Infect Immun*. 1986;53(2):432-4.
25. Edwards RJ, Taylor GW, Ferguson M, Murray S, Rendell N, Wrigley A, et al. Specific C-terminal cleavage and inactivation of interleukin-8 by invasive disease isolates of *Streptococcus pyogenes*. *The Journal of infectious diseases*. 2005;192(5):783-90.
26. Uchiyama S, Andreoni F, Schuepbach RA, Nizet V, Zinkernagel AS. DNase Sda1 allows invasive M1T1 Group A *Streptococcus* to prevent TLR9-dependent recognition. *PLoS Pathog*. 2012;8(6):e1002736.
27. Brinkmann V, Reichard U, Goosmann C, Fauler B, Uhlemann Y, Weiss DS, et al. Neutrophil extracellular traps kill bacteria. *Science*. 2004;303(5663):1532-5.
28. McArthur JD, McKay FC, Ramachandran V, Shyam P, Cork AJ, Sanderson-Smith ML, et al. Allelic variants of streptokinase from *Streptococcus pyogenes* display functional differences in plasminogen activation. *FASEB journal : official publication of the Federation of American Societies for Experimental Biology*. 2008;22(9):3146-53.
29. Janulczyk R, Ricci S, Bjorck L. MtsABC is important for manganese and iron transport, oxidative stress resistance, and virulence of *Streptococcus pyogenes*. *Infect Immun*. 2003;71(5):2656-64.
30. Montañez GE, Neely MN, Eichenbaum Z. The streptococcal iron uptake (Siu) transporter is required for iron uptake and virulence in a zebrafish infection model. *Microbiology*. 2005;151(Pt 11):3749-57.

31. Fisher M, Huang YS, Li X, McIver KS, Toukoki C, Eichenbaum Z. Shr is a broad-spectrum surface receptor that contributes to adherence and virulence in group A streptococcus. *Infection and immunity*. 2008;76(11):5006-15.
32. Bates CS, Montañez GE, Woods CR, Vincent RM, Eichenbaum Z. Identification and characterization of a *Streptococcus pyogenes* operon involved in binding of hemoproteins and acquisition of iron. *Infection and immunity*. 2003;71(3):1042-55.
33. Zhu H, Liu M, Lei B. The surface protein Shr of *Streptococcus pyogenes* binds heme and transfers it to the streptococcal heme-binding protein Shp. *BMC microbiology*. 2008;8:15.
34. Voyich JM, Musser JM, DeLeo FR. *Streptococcus pyogenes* and human neutrophils: a paradigm for evasion of innate host defense by bacterial pathogens. *Microbes and infection / Institut Pasteur*. 2004;6(12):1117-23.
35. Musumeci M, Maccari S, Massimi A, Stati T, Sestili P, Corritore E, et al. Iron excretion in iron dextran-overloaded mice. *Blood transfusion = Trasfusione del sangue*. 2014;12(4):485-90.
36. Doherty CP. Host-pathogen interactions: the role of iron. *The Journal of nutrition*. 2007;137(5):1341-4.
37. Bullen JJ, Rogers HJ, Spalding PB, Ward CG. Natural resistance, iron and infection: a challenge for clinical medicine. *Journal of medical microbiology*. 2006;55(Pt 3):251-8.
38. Tong Y, Guo M. Bacterial heme-transport proteins and their heme-coordination modes. *Archives of Biochemistry and Biophysics*. 2009;481(1):1-15.
39. Skaar EP. The battle for iron between bacterial pathogens and their vertebrate hosts. *PLoS Pathog*. 2010;6(8):e1000949.
40. Stojiljkovic I, Evavold BD, Kumar V. Antimicrobial properties of porphyrins. *Expert opinion on investigational drugs*. 2001;10(2):309-20.
41. Nobles CL, Maresso AW. The theft of host heme by Gram-positive pathogenic bacteria. *Metallomics : integrated biometal science*. 2011;3(8):788-96.
42. Drakesmith H, Prentice AM. Hepcidin and the iron-infection axis. *Science*. 2012;338(6108):768-72.
43. Drakesmith H, Nemeth E, Ganz T. Ironing out Ferroportin. *Cell metabolism*. 2015.
44. Johnson EE, Wessling-Resnick M. Iron metabolism and the innate immune response to infection. *Microbes and infection / Institut Pasteur*. 2012;14(3):207-16.
45. Goldoni A. Porphyrin: fascinating molecules with biological significance 2000; (Atomic, Molecular, and Supramolecular Studies). Available from: <http://oldweb.elettra.trieste.it/science/highlights/2001-2002/index.html>.
46. Falk JE. Chromatography of porphyrins and metalloporphyrins. *Journal of chromatography*. 1961;5:277-99.
47. Biesaga M, Pyrzynska K, Trojanowicz M. Porphyrins in analytical chemistry. A review. *Talanta*. 2000;51(2):209-24.
48. Li C, Stocker R. Heme oxygenase and iron: from bacteria to humans. *Redox report : communications in free radical research*. 2009;14(3):95-101.
49. Milgrom RL. *The Colour of Life: An Introduction to the Chemistry of Porphyrins and Related Compounds*. Oxford, UK: Oxford University Press; 1997.

50. Sachla AJ, Le Breton Y, Akhter F, McIver KS, Eichenbaum Z. The crimson conundrum: heme toxicity and tolerance in GAS. *Front Cell Infect Microbiol.* 2014;4:159.
51. Cescau S, Cwerman H, Letoffe S, Delepelaire P, Wandersman C, Biville F. Heme acquisition by hemophores. *Biometals : an international journal on the role of metal ions in biology, biochemistry, and medicine.* 2007;20(3-4):603-13.
52. Wandersman C, Delepelaire P. Bacterial iron sources: from siderophores to hemophores. *Annu Rev Microbiol.* 2004;58:611-47.
53. Letoffe S, Redeker V, Wandersman C. Isolation and characterization of an extracellular haem-binding protein from *Pseudomonas aeruginosa* that shares function and sequence similarities with the *Serratia marcescens* HasA haemophore. *Molecular microbiology.* 1998;28(6):1223-34.
54. Rossi M-S, Fetherston JD, Létoffé S, Carniel E, Perry RD, Ghigo J-M. Identification and Characterization of the Hemophore-Dependent Heme Acquisition System of *Yersinia pestis*. *Infection and Immunity.* 2001;69(11):6707-17.
55. Cope LD, Thomas SE, Latimer JL, Slaughter CA, Muller-Eberhard U, Hansen EJ. The 100 kDa haem:haemopexin-binding protein of *Haemophilus influenzae*: structure and localization. *Molecular microbiology.* 1994;13(5):863-73.
56. Stojiljkovic I, Larson J, Hwa V, Anic S, So M. HmbR outer membrane receptors of pathogenic *Neisseria* spp.: iron-regulated, hemoglobin-binding proteins with a high level of primary structure conservation. *Journal of bacteriology.* 1996;178(15):4670-8.
57. Henderson DP, Payne SM. Characterization of the *Vibrio cholerae* outer membrane heme transport protein HutA: sequence of the gene, regulation of expression, and homology to the family of TonB-dependent proteins. *Journal of bacteriology.* 1994;176(11):3269-77.
58. Lewis LA, Gray E, Wang YP, Roe BA, Dyer DW. Molecular characterization of hpuAB, the haemoglobin-haptoglobin-utilization operon of *Neisseria meningitidis*. *Molecular microbiology.* 1997;23(4):737-49.
59. Haley KP, Skaar EP. A battle for iron: host sequestration and *Staphylococcus aureus* acquisition. *Microbes and infection / Institut Pasteur.* 2012;14(3):217-27.
60. Hammer ND, Skaar EP. Molecular mechanisms of *Staphylococcus aureus* iron acquisition. *Annu Rev Microbiol.* 2011;65:129-47.
61. Fabian M, Solomaha E, Olson JS, Maresso AW. Heme transfer to the bacterial cell envelope occurs via a secreted hemophore in the Gram-positive pathogen *Bacillus anthracis*. *The Journal of biological chemistry.* 2009;284(46):32138-46.
62. Maresso AW, Garufi G, Schneewind O. *Bacillus anthracis* secretes proteins that mediate heme acquisition from hemoglobin. *PLoS Pathog.* 2008;4(8):e1000132.
63. Allen CE, Schmitt MP. Novel hemin binding domains in the *Corynebacterium diphtheriae* HtaA protein interact with hemoglobin and are critical for heme iron utilization by HtaA. *Journal of bacteriology.* 2011;193(19):5374-85.
64. Bates CS, Toukoki C, Neely MN, Eichenbaum Z. Characterization of MtsR, a new metal regulator in group A streptococcus, involved in iron acquisition and virulence. *Infect Immun.* 2005;73(9):5743-53.

65. Toukoki C, Gold KM, McIver KS, Eichenbaum Z. MtsR is a dual regulator that controls virulence genes and metabolic functions in addition to metal homeostasis in the group A streptococcus. *Molecular microbiology*. 2010;76(4):971-89.
66. Lei B, Smoot LM, Menning HM, Voyich JM, Kala SV, Deleo FR, et al. Identification and characterization of a novel heme-associated cell surface protein made by *Streptococcus pyogenes*. *Infect Immun*. 2002;70(8):4494-500.
67. Frankenberg-Dinkel N. Bacterial heme oxygenases. *Antioxidants & redox signaling*. 2004;6(5):825-34.
68. Reed JR, Huber WJ, 3rd, Backes WL. Human heme oxygenase-1 efficiently catabolizes heme in the absence of biliverdin reductase. *Drug metabolism and disposition: the biological fate of chemicals*. 2010;38(11):2060-6.
69. Tomaro ML, Batlle AM. Bilirubin: its role in cytoprotection against oxidative stress. *The international journal of biochemistry & cell biology*. 2002;34(3):216-20.
70. Ollinger R, Wang H, Yamashita K, Wegiel B, Thomas M, Margreiter R, et al. Therapeutic applications of bilirubin and biliverdin in transplantation. *Antioxidants & redox signaling*. 2007;9(12):2175-85.
71. Schluchter WM, Glazer AN. Characterization of Cyanobacterial Biliverdin Reductase: CONVERSION OF BILIVERDIN TO BILIRUBIN IS IMPORTANT FOR NORMAL PHYCOBILIPROTEIN BIOSYNTHESIS. *Journal of Biological Chemistry*. 1997;272(21):13562-9.
72. Iyanagi T, Xia C, Kim JJ. NADPH-cytochrome P450 oxidoreductase: prototypic member of the diflavin reductase family. *Archives of biochemistry and biophysics*. 2012;528(1):72-89.
73. Wang A, Zeng Y, Han H, Weeratunga S, Morgan BN, Moenne-Loccoz P, et al. Biochemical and structural characterization of *Pseudomonas aeruginosa* Bfd and FPR: ferredoxin NADP+ reductase and not ferredoxin is the redox partner of heme oxygenase under iron-starvation conditions. *Biochemistry*. 2007;46(43):12198-211.
74. Skaar EP, Gaspar AH, Schneewind O. IsdG and IsdI, heme-degrading enzymes in the cytoplasm of *Staphylococcus aureus*. *The Journal of biological chemistry*. 2004;279(1):436-43.
75. Skaar EP, Gaspar AH, Schneewind O. *Bacillus anthracis* IsdG, a heme-degrading monooxygenase. *Journal of bacteriology*. 2006;188(3):1071-80.
76. Reniere ML, Haley KP, Skaar EP. The flexible loop of *Staphylococcus aureus* IsdG is required for its degradation in the absence of heme. *Biochemistry*. 2011;50(31):6730-7.
77. Nambu S, Matsui T, Goulding CW, Takahashi S, Ikeda-Saito M. A new way to degrade heme: the *Mycobacterium tuberculosis* enzyme MhuD catalyzes heme degradation without generating CO. *The Journal of biological chemistry*. 2013;288(14):10101-9.
78. Zhang R, Zhang J, Guo G, Mao X, Tong W, Zhang Y, et al. Crystal structure of *Campylobacter jejuni* ChuZ: a split-barrel family heme oxygenase with a novel heme-binding mode. *Biochemical and biophysical research communications*. 2011;415(1):82-7.
79. Uchida T, Sekine Y, Matsui T, Ikeda-Saito M, Ishimori K. A heme degradation enzyme, HutZ, from *Vibrio cholerae*. *Chemical communications (Cambridge, England)*. 2012;48(53):6741-3.

80. Guo Y, Guo G, Mao X, Zhang W, Xiao J, Tong W, et al. Functional identification of HugZ, a heme oxygenase from *Helicobacter pylori*. *BMC microbiology*. 2008;8:226.
81. Chiabrando D, Vinchi F, Fiorito V, Mercurio S, Tolosano E. Heme in pathophysiology: a matter of scavenging, metabolism and trafficking across cell membranes. *Frontiers in pharmacology*. 2014;5:61.
82. Winterbourn CC. Toxicity of iron and hydrogen peroxide: the Fenton reaction. *Toxicology letters*. 1995;82-83:969-74.
83. Mense SM, Zhang L. Heme: a versatile signaling molecule controlling the activities of diverse regulators ranging from transcription factors to MAP kinases. *Cell research*. 2006;16(8):681-92.
84. Nisenbaum EJ, Novikov DS, Lui YW. The presence and role of iron in mild traumatic brain injury: an imaging perspective. *Journal of neurotrauma*. 2014;31(4):301-7.
85. Anzaldi LL, Skaar EP. Overcoming the heme paradox: heme toxicity and tolerance in bacterial pathogens. *Infect Immun*. 2010;78(12):4977-89.
86. Jani D, Nagarkatti R, Beatty W, Angel R, Slebodnick C, Andersen J, et al. HDP—A Novel Heme Detoxification Protein from the Malaria Parasite. *PLoS Pathogens*. 2008;4(4):e1000053.
87. Stojiljkovic I, Hantke K. Transport of haemin across the cytoplasmic membrane through a haemin-specific periplasmic binding-protein-dependent transport system in *Yersinia enterocolitica*. *Molecular microbiology*. 1994;13(4):719-32.
88. Wyckoff EE, Lopreato GF, Tipton KA, Payne SM. *Shigella dysenteriae* ShuS promotes utilization of heme as an iron source and protects against heme toxicity. *Journal of bacteriology*. 2005;187(16):5658-64.
89. Kaur AP, Lansky IB, Wilks A. The Role of the Cytoplasmic Heme-binding Protein (PhuS) of *Pseudomonas aeruginosa* in Intracellular Heme Trafficking and Iron Homeostasis. *The Journal of biological chemistry*. 2009;284(1):56-66.
90. Li W, Sharma M, Kaur P. The DrrAB efflux system of *Streptomyces peucetius* is a multidrug transporter of broad substrate specificity. *The Journal of biological chemistry*. 2014;289(18):12633-46.
91. Quigley JG, Yang Z, Worthington MT, Phillips JD, Sabo KM, Sabath DE, et al. Identification of a human heme exporter that is essential for erythropoiesis. *Cell*. 2004;118(6):757-66.
92. Korolnek T, Zhang J, Beardsley S, Scheffer GL, Hamza I. Control of metazoan heme homeostasis by a conserved multidrug resistance protein. *Cell metabolism*. 2014;19(6):1008-19.
93. Lubelski J, Konings WN, Driessen AJ. Distribution and physiology of ABC-type transporters contributing to multidrug resistance in bacteria. *Microbiology and molecular biology reviews : MMBR*. 2007;71(3):463-76.
94. Stauff DL, Skaar EP. *Bacillus anthracis* HssRS signalling to HrtAB regulates haem resistance during infection. *Molecular microbiology*. 2009;72(3):763-78.
95. Fernandez A, Lechardeur D, Derre-Bobillot A, Couve E, Gaudu P, Gruss A. Two coregulated efflux transporters modulate intracellular heme and protoporphyrin IX availability in *Streptococcus agalactiae*. *PLoS Pathog*. 2010;6(4):e1000860.

96. Lechardeur D, Cesselin B, Liebl U, Vos MH, Fernandez A, Brun C, et al. Discovery of Intracellular Heme-binding Protein HrtR, Which Controls Heme Efflux by the Conserved HrtB-HrtA Transporter in *Lactococcus lactis*. *The Journal of biological chemistry*. 2012;287(7):4752-8.
97. Haley KP, Skaar EP. A battle for iron: host sequestration and *Staphylococcus aureus* acquisition. *Microbes and infection / Institut Pasteur*. 2012;14(3):217-27.
98. Mayfield JA, Dehner CA, DuBois JL. Recent advances in bacterial heme protein biochemistry. *Curr Opin Chem Biol*. 2011;15(2):260-6.
99. Pishchany G, Skaar EP. Taste for blood: hemoglobin as a nutrient source for pathogens. *PLoS Pathog*. 2012;8(3):e1002535.
100. Benson DR, Rivera M. Heme uptake and metabolism in bacteria. *Metal ions in life sciences*. 2013;12:279-332.
101. Letoffe S, Heuck G, Delepelaire P, Lange N, Wandersman C. Bacteria capture iron from heme by keeping tetrapyrrol skeleton intact. *Proc Natl Acad Sci U S A*. 2009;106(28):11719-24.
102. Turlin E, Debarbouille M, Augustyniak K, Gilles AM, Wandersman C. *Staphylococcus aureus* FepA and FepB proteins drive heme iron utilization in *Escherichia coli*. *PloS one*. 2013;8(2):e56529.
103. Wilks A, Ikeda-Saito M. Heme utilization by pathogenic bacteria: not all pathways lead to biliverdin. *Accounts of chemical research*. 2014;47(8):2291-8.
104. Wilks A, Heinzl G. Heme oxygenation and the widening paradigm of heme degradation. *Archives of biochemistry and biophysics*. 2014;544:87-95.
105. Unno M, Matsui T, Ikeda-Saito M. Crystallographic studies of heme oxygenase complexed with an unstable reaction intermediate, verdoheme. *Journal of inorganic biochemistry*. 2012;113:102-9.
106. Schmitt MP. Utilization of host iron sources by *Corynebacterium diphtheriae*: identification of a gene whose product is homologous to eukaryotic heme oxygenases and is required for acquisition of iron from heme and hemoglobin. *Journal of bacteriology*. 1997;179(3):838-45.
107. Wilks A, Schmitt MP. Expression and characterization of a heme oxygenase (Hmu O) from *Corynebacterium diphtheriae*. Iron acquisition requires oxidative cleavage of the heme macrocycle. *The Journal of biological chemistry*. 1998;273(2):837-41.
108. Zhu W, Hunt DJ, Richardson AR, Stojiljkovic I. Use of heme compounds as iron sources by pathogenic neisseriae requires the product of the hemO gene. *Journal of bacteriology*. 2000;182(2):439-47.
109. Zhu W, Wilks A, Stojiljkovic I. Degradation of heme in gram-negative bacteria: the product of the hemO gene of Neisseriae is a heme oxygenase. *Journal of bacteriology*. 2000;182(23):6783-90.
110. Bruggemann H, Bauer R, Raffestin S, Gottschalk G. Characterization of a heme oxygenase of *Clostridium tetani* and its possible role in oxygen tolerance. *Archives of microbiology*. 2004;182(2-3):259-63.
111. Hassan S, Ohtani K, Wang R, Yuan Y, Wang Y, Yamaguchi Y, et al. Transcriptional regulation of hemO encoding heme oxygenase in *Clostridium perfringens*. *Journal of microbiology (Seoul, Korea)*. 2010;48(1):96-101.

112. Ratliff M, Zhu W, Deshmukh R, Wilks A, Stojiljkovic I. Homologues of neisserial heme oxygenase in gram-negative bacteria: degradation of heme by the product of the *pigA* gene of *Pseudomonas aeruginosa*. *Journal of bacteriology*. 2001;183(21):6394-403.
113. Wegele R, Tasler R, Zeng Y, Rivera M, Frankenberg-Dinkel N. The heme oxygenase(s)-phytochrome system of *Pseudomonas aeruginosa*. *The Journal of biological chemistry*. 2004;279(44):45791-802.
114. Gisk B, Wiethaus J, Aras M, Frankenberg-Dinkel N. Variable composition of heme oxygenases with different regiospecificities in *Pseudomonas* species. *Archives of microbiology*. 2012;194(7):597-606.
115. Barker KD, Barkovits K, Wilks A. Metabolic flux of extracellular heme uptake in *Pseudomonas aeruginosa* is driven by the iron-regulated heme oxygenase (HemO). *Journal of Biological Chemistry*. 2012;287(33):27447.
116. Tong Y, Guo M. Bacterial heme-transport proteins and their heme-coordination modes. *Archives of biochemistry and biophysics*. 2009;481(1):1-15.
117. Suits MD, Pal GP, Nakatsu K, Matte A, Cygler M, Jia Z. Identification of an *Escherichia coli* O157:H7 heme oxygenase with tandem functional repeats. *Proceedings of the National Academy of Sciences of the United States of America*. 2005;102(47):16955-60.
118. Schneider S, Paoli M. Crystallization and preliminary X-ray diffraction analysis of the haem-binding protein HemS from *Yersinia enterocolitica*. *Acta crystallographica Section F, Structural biology and crystallization communications*. 2005;61(Pt 8):802-5.
119. Liu M, Boulouis HJ, Biville F. Heme degrading protein HemS is involved in oxidative stress response of *Bartonella henselae*. *PloS one*. 2012;7(5):e37630.
120. Lansky IB, Lukat-Rodgers GS, Block D, Rodgers KR, Ratliff M, Wilks A. The cytoplasmic heme-binding protein (PhuS) from the heme uptake system of *Pseudomonas aeruginosa* is an intracellular heme-trafficking protein to the delta-regioselective heme oxygenase. *The Journal of biological chemistry*. 2006;281(19):13652-62.
121. O'Neill MJ, Bhakta MN, Fleming KG, Wilks A. Induced fit on heme binding to the *Pseudomonas aeruginosa* cytoplasmic protein (PhuS) drives interaction with heme oxygenase (HemO). *Proceedings of the National Academy of Sciences of the United States of America*. 2012;109(15):5639-44.
122. Wu R, Skaar EP, Zhang R, Joachimiak G, Gornicki P, Schneewind O, et al. *Staphylococcus aureus* IsdG and IsdI, heme-degrading enzymes with structural similarity to monooxygenases. *The Journal of biological chemistry*. 2005;280(4):2840-6.
123. Matsui T, Nambu S, Ono Y, Goulding CW, Tsumoto K, Ikeda-Saito M. Heme degradation by *Staphylococcus aureus* IsdG and IsdI liberates formaldehyde rather than carbon monoxide. *Biochemistry*. 2013;52(18):3025-7.
124. Reniere ML, Ukpabi GN, Harry SR, Stec DF, Krull R, Wright DW, et al. The IsdG-family of haem oxygenases degrades haem to a novel chromophore. *Molecular microbiology*. 2010;75(6):1529-38.

125. Puri S, O'Brian MR. The hmuQ and hmuD genes from *Bradyrhizobium japonicum* encode heme-degrading enzymes. *Journal of bacteriology*. 2006;188(18):6476-82.
126. Haley KP, Janson EM, Heilbronner S, Foster TJ, Skaar EP. *Staphylococcus lugdunensis* IsdG liberates iron from host heme. *Journal of bacteriology*. 2011;193(18):4749-57.
127. Chim N, Iniguez A, Nguyen TQ, Goulding CW. Unusual diheme conformation of the heme-degrading protein from *Mycobacterium tuberculosis*. *Journal of molecular biology*. 2010;395(3):595-608.
128. Hu Y, Jiang F, Guo Y, Shen X, Zhang Y, Zhang R, et al. Crystal structure of HugZ, a novel heme oxygenase from *Helicobacter pylori*. *The Journal of biological chemistry*. 2011;286(2):1537-44.
129. Liu X, Gong J, Wei T, Wang Z, Du Q, Zhu D, et al. Crystal structure of HutZ, a heme storage protein from *Vibrio cholerae*: A structural mismatch observed in the region of high sequence conservation. *BMC structural biology*. 2012;12:23.
130. Lynskey NN, Lawrenson RA, Sriskandan S. New understandings in *Streptococcus pyogenes*. *Current opinion in infectious diseases*. 2011;24(3):196-202.
131. Eichenbaum Z, Muller E, Morse SA, Scott JR. Acquisition of iron from host proteins by the group A streptococcus. *Infection and immunity*. 1996;64(12):5428-9.
132. Nygaard TK, Blouin GC, Liu M, Fukumura M, Olson JS, Fabian M, et al. The mechanism of direct heme transfer from the streptococcal cell surface protein Shp to HtsA of the HtsABC transporter. *The Journal of biological chemistry*. 2006;281(30):20761-71.
133. Sook BR, Block DR, Sumithran S, Montanez GE, Rodgers KR, Dawson JH, et al. Characterization of SiaA, a streptococcal heme-binding protein associated with a heme ABC transport system. *Biochemistry*. 2008;47(8):2678-88.
134. Ouattara M, Cunha EB, Li X, Huang YS, Dixon D, Eichenbaum Z. Shr of group A streptococcus is a new type of composite NEAT protein involved in sequestering haem from methaemoglobin. *Molecular microbiology*. 2010;78(3):739-56.
135. Ouattara M, Pennati A, Devlin DJ, Huang YS, Gadda G, Eichenbaum Z. Kinetics of heme transfer by the Shr NEAT domains of Group A Streptococcus. *Archives of biochemistry and biophysics*. 2013;538(2):71-9.
136. Dahesh S, Nizet V, Cole JN. Study of streptococcal hemoprotein receptor (Shr) in iron acquisition and virulence of M1T1 group A streptococcus. *Virulence*. 2012;3(7):566-75.
137. Otwinowski Z, Minor W. Processing of X-ray diffraction data collected in oscillation mode. *Method Enzymol*. 1997;276:307-26.
138. McCoy AJ, Grosse-Kunstleve RW, Storoni LC, Read RJ. Likelihood-enhanced fast translation functions. *Acta crystallographica Section D, Biological crystallography*. 2005;61(Pt 4):458-64.
139. Storoni LC, McCoy AJ, Read RJ. Likelihood-enhanced fast rotation functions. *Acta crystallographica Section D, Biological crystallography*. 2004;60(Pt 3):432-8.
140. Perrakis A, Harkiolaki M, Wilson KS, Lamzin VS. ARP/wARP and molecular replacement. *Acta Crystallogr D Biol Crystallogr*. 2001;57(Pt 10):1445-50.

141. Perrakis A, Morris R, Lamzin VS. Automated protein model building combined with iterative structure refinement. *Nat Struct Biol.* 1999;6(5):458-63.
142. Murshudov GN, Vagin AA, Dodson EJ. Refinement of macromolecular structures by the maximum-likelihood method. *Acta crystallographica Section D, Biological crystallography.* 1997;53(Pt 3):240-55.
143. Emsley P, Cowtan K. Coot: model-building tools for molecular graphics. *Acta Crystallographica Section D.* 2004;60(12-1):2126-32.
144. Krissinel E, Henrick K. Secondary-structure matching (SSM), a new tool for fast protein structure alignment in three dimensions. *Acta Crystallogr D Biol Crystallogr.* 2004;60(Pt 12 Pt 1):2256-68.
145. Asakura T, Minakami S, Yoneyama Y, Yoshikawa H. Combination of globin and its derivatives with hemins and porphyrins. *J Biochem.* 1964;56:594-600.
146. Docherty JC, Firneisz GD, Schacter BA. Methene bridge carbon atom elimination in oxidative heme degradation catalyzed by heme oxygenase and NADPH-cytochrome P-450 reductase. *Archives of biochemistry and biophysics.* 1984;235(2):657-64.
147. Gisk B, Yasui Y, Kohchi T, Frankenberg-Dinkel N. Characterization of the haem oxygenase protein family in *Arabidopsis thaliana* reveals a diversity of functions. *The Biochemical journal.* 2010;425(2):425-34.
148. Collman JP, Brauman JI, Halbert TR, Suslick KS. Nature of O₂ and CO binding to metalloporphyrins and heme proteins. *Proceedings of the National Academy of Sciences of the United States of America.* 1976;73(10):3333-7.
149. Stookey LL. Ferrozine-A New Spectrophotometric Reagent for Iron ANALYTICAL CHEMISTRY. 1970;42(7):779-81.
150. Liu Y, Ortiz de Montellano PR. Reaction intermediates and single turnover rate constants for the oxidation of heme by human heme oxygenase-1. *The Journal of biological chemistry.* 2000;275(8):5297-307.
151. Loutet SA, Kobylarz MJ, Chau CH, Murphy ME. IruO is a reductase for heme degradation by IsdI and IsdG proteins in *Staphylococcus aureus*. *The Journal of biological chemistry.* 2013;288(36):25749-59.
152. Ridley KA, Rock JD, Li Y, Ketley JM. Heme utilization in *Campylobacter jejuni*. *J Bacteriol.* 2006;188(22):7862-75.
153. Heinemann IU, Jahn M, Jahn D. The biochemistry of heme biosynthesis. *Archives of biochemistry and biophysics.* 2008;474(2):238-51.
154. Hogle SL, Barbeau KA, Gledhill M. Heme in the marine environment: from cells to the iron cycle. *Metallomics : integrated biometal science.* 2014.
155. Brown JS, Holden DW. Iron acquisition by Gram-positive bacterial pathogens. *Microbes Infect.* 2002;4(11):1149-56.
156. Caza M, Kronstad JW. Shared and distinct mechanisms of iron acquisition by bacterial and fungal pathogens of humans. *Frontiers in cellular and infection microbiology.* 2013;3:80.
157. Kozarov E. Bacterial invasion of vascular cell types: vascular infectology and atherogenesis. *Future cardiology.* 2012;8(1):123-38.
158. Maines MD, Kappas A. The degradative effects of porphyrins and heme compounds on components of the microsomal mixed function oxidase system. *The Journal of biological chemistry.* 1975;250(6):2363-9.

159. Solar I, Dulitzky J, Shaklai N. Hemin-promoted peroxidation of red cell cytoskeletal proteins. *Archives of biochemistry and biophysics*. 1990;283(1):81-9.
160. Solar I, Muller-Eberhard U, Shaklai N. Serum proteins as mediators of hemin efflux from red cell membranes: specificity of hemopexin. *FEBS letters*. 1989;256(1-2):225-9.
161. Krishnamurthy P, Xie T, Schuetz JD. The role of transporters in cellular heme and porphyrin homeostasis. *Pharmacology & therapeutics*. 2007;114(3):345-58.
162. Khan AA, Quigley JG. Control of intracellular heme levels: heme transporters and heme oxygenases. *Biochimica et biophysica acta*. 2011;1813(5):668-82.
163. Wakeman CA, Stauff DL, Zhang Y, Skaar EP. Differential activation of *Staphylococcus aureus* heme detoxification machinery by heme analogues. *Journal of bacteriology*. 2014;196(7):1335-42.
164. Wakeman CA, Skaar EP. Metalloregulation of Gram-positive pathogen physiology. *Curr Opin Microbiol*. 2012;15(2):169-74.
165. Stauff DL, Skaar EP. *Bacillus anthracis* HssRS signalling to HrtAB regulates haem resistance during infection. *Mol Microbiol*. 2009;72(3):763-78.
166. Torres VJ, Stauff DL, Pishchany G, Bezbradica JS, Gordy LE, Iturregui J, et al. A *Staphylococcus aureus* regulatory system that responds to host heme and modulates virulence. *Cell Host Microbe*. 2007;1(2):109-19.
167. Heyer A, Gatgens C, Hentschel E, Kalinowski J, Bott M, Frunzke J. The two-component system ChrSA is crucial for haem tolerance and interferes with HrrSA in haem-dependent gene regulation in *Corynebacterium glutamicum*. *Microbiol-Sgm*. 2012;158:3020-31.
168. Ito Y, Nakagawa S, Komagata A, Ikeda-Saito M, Shiro Y, Nakamura H. Heme-dependent autophosphorylation of a heme sensor kinase, ChrS, from *Corynebacterium diphtheriae* reconstituted in proteoliposomes. *FEBS letters*. 2009;583(13):2244-8.
169. Bibb LA, Kunkle CA, Schmitt MP. The ChrA-ChrS and HrrA-HrrS signal transduction systems are required for activation of the hmuO promoter and repression of the hema promoter in *Corynebacterium diphtheriae*. *Infection and immunity*. 2007;75(5):2421-31.
170. Bibb LA, King ND, Kunkle CA, Schmitt MP. Analysis of a heme-dependent signal transduction system in *Corynebacterium diphtheriae*: Deletion of the chrA/S genes results in heme sensitivity and diminished heme-dependent activation of the hmuO promoter. *Infection and immunity*. 2005;73(11):7406-12.
171. Bozja J, Yi K, Shafer WM, Stojiljkovic I. Porphyrin-based compounds exert antibacterial action against the sexually transmitted pathogens *Neisseria gonorrhoeae* and *Haemophilus ducreyi*. *Int J Antimicrob Ag*. 2004;24(6):578-84.
172. Hagman KE, Pan WB, Spratt BG, Balthazar JT, Judd RC, Shafer WM. Resistance of *Neisseria-Gonorrhoeae* to Antimicrobial Hydrophobic Agents Is Modulated by the Mtrrcde Efflux System. *Microbiol-Uk*. 1995;141:611-22.
173. Pedersen MB, Garrigues C, Tuphile K, Brun C, Vido K, Bennedsen M, et al. Impact of aeration and heme-activated respiration on *Lactococcus lactis* gene expression: identification of a heme-responsive operon. *Journal of bacteriology*. 2008;190(14):4903-11.

174. Lechardeur D, Fernandez A, Robert B, Gaudu P, Trieu-Cuot P, Lamberet G, et al. The 2-Cys Peroxiredoxin Alkyl Hydroperoxide Reductase C Binds Heme and Participates in Its Intracellular Availability in *Streptococcus agalactiae*. *Journal of Biological Chemistry*. 2010;285(21):16032-41.
175. Thompson JM, Jones HA, Perry RD. Molecular characterization of the hemin uptake locus (*hmu*) from *Yersinia pestis* and analysis of *hmu* mutants for hemin and hemoprotein utilization. *Infection and immunity*. 1999;67(8):3879-92.
176. Wilks A. The ShuS protein of *Shigella dysenteriae* is a heme-sequestering protein that also binds DNA. *Archives of biochemistry and biophysics*. 2001;387(1):137-42.
177. Wyckoff EE, Lopreato GF, Tipton KA, Payne SA. *Shigella dysenteriae* ShuS promotes utilization of heme as an iron source and protects against heme toxicity. *Journal of bacteriology*. 2005;187(16):5658-64.
178. Negari S, Sulpher J, Pacello F, Ingrey K, Battistoni A, Lee BC. A role for *Haemophilus ducreyi* Cu,ZnSOD in resistance to heme toxicity. *Biometals : an international journal on the role of metal ions in biology, biochemistry, and medicine*. 2008;21(3):249-58.
179. Nambu S, Matsui T, Goulding CW, Takahashi S, Ikeda-Saito M. A New Way to Degrade Heme THE MYCOBACTERIUM TUBERCULOSIS ENZYME MhuD CATALYZES HEME DEGRADATION WITHOUT GENERATING CO. *Journal of Biological Chemistry*. 2013;288(14):10101-9.
180. Uchida T, Sekine Y, Matsui T, Ikeda-Saito M, Ishimori K. A heme degradation enzyme, HutZ, from *Vibrio cholerae*. *Chem Commun*. 2012;48(53):6741-3.
181. Zhang R, Zhang JY, Guo G, Mao XH, Tong WD, Zhang Y, et al. Crystal structure of *Campylobacter jejuni* ChuZ: A split-barrel family heme oxygenase with a novel heme-binding mode. *Biochem Bioph Res Co*. 2011;415(1):82-7.
182. Cunningham MW. Pathogenesis of group A streptococcal infections and their sequelae. *Adv Exp Med Biol*. 2008;609:29-42.
183. Cole JN, Barnett TC, Nizet V, Walker MJ. Molecular insight into invasive group A streptococcal disease. *Nat Rev Microbiol*. 2011;9(10):724-36.
184. Nizet V. Streptococcal beta-hemolysins: genetics and role in disease pathogenesis. *Trends Microbiol*. 2002;10(12):575-80.
185. Ouattara M, Cunha EB, Li XR, Huang YS, Dixon D, Eichenbaum Z. Shr of group A streptococcus is a new type of composite NEAT protein involved in sequestering haem from methaemoglobin. *Mol Microbiol*. 2010;78(3):739-56.
186. Liu M, Lei B. Heme transfer from streptococcal cell surface protein Shp to HtsA of transporter HtsABC. *Infect Immun*. 2005;73(8):5086-92.
187. Lyon WR, Gibson CM, Caparon MG. A role for trigger factor and an rgg-like regulator in the transcription, secretion and processing of the cysteine proteinase of *Streptococcus pyogenes*. *The EMBO journal*. 1998;17(21):6263-75.
188. Wiegand I, Hilpert K, Hancock RE. Agar and broth dilution methods to determine the minimal inhibitory concentration (MIC) of antimicrobial substances. *Nature protocols*. 2008;3(2):163-75.
189. Drew WL, Barry AL, O'Toole R, Sherris JC. Reliability of the Kirby-Bauer disc diffusion method for detecting methicillin-resistant strains of *Staphylococcus aureus*. *Applied microbiology*. 1972;24(2):240-7.

190. Ribardo DA, McIver KS. Defining the Mga regulon: comparative transcriptome analysis reveals both direct and indirect regulation by Mga in the group A streptococcus. *Mol Microbiol.* 2006;62(2):491-508.
191. Jiang N, Leach LJ, Hu X, Potokina E, Jia T, Druka A, et al. Methods for evaluating gene expression from Affymetrix microarray datasets. *BMC bioinformatics.* 2008;9:284.
192. Bailey TL, Williams N, Misleh C, Li WW. MEME: discovering and analyzing DNA and protein sequence motifs. *Nucleic acids research.* 2006;34(Web Server issue):W369-73.
193. Kanehisa M. The KEGG database. *Novartis Foundation symposium.* 2002;247:91-101; discussion -3, 19-28, 244-52.
194. Thompson JD, Gibson TJ, Higgins DG. Multiple sequence alignment using ClustalW and ClustalX. *Current protocols in bioinformatics / editorial board, Andreas D Baxevanis [et al].* 2002;Chapter 2:Unit 2 3.
195. Asakura T, Minakami S, Yoneyama Y, Yoshikawa H. Combination of Globin and Its Derivatives with Hemins and Porphyrins. *Journal of biochemistry.* 1964;56:594-600.
196. Mike LA, Choby JE, Brinkman PR, Olive LQ, Dutter BF, Ivan SJ, et al. Two-component system cross-regulation integrates *Bacillus anthracis* response to heme and cell envelope stress. *PLoS pathogens.* 2014;10(3):e1004044.
197. McShan WM, Ferretti JJ, Karasawa T, Suvorov AN, Lin S, Qin B, et al. Genome sequence of a nephritogenic and highly transformable M49 strain of *Streptococcus pyogenes*. *Journal of bacteriology.* 2008;190(23):7773-85.
198. Simon D, Ferretti JJ. Electrotransformation of *Streptococcus pyogenes* with plasmid and linear DNA. *FEMS microbiology letters.* 1991;66(2):219-24.
199. Sumbly P, Porcella SF, Madrigal AG, Barbian KD, Virtaneva K, Ricklefs SM, et al. Evolutionary origin and emergence of a highly successful clone of serotype M1 group a *Streptococcus* involved multiple horizontal gene transfer events. *The Journal of infectious diseases.* 2005;192(5):771-82.
200. Chang EF, Wong RJ, Vreman HJ, Igarashi T, Galo E, Sharp FR, et al. Heme oxygenase-2 protects against lipid peroxidation-mediated cell loss and impaired motor recovery after traumatic brain injury. *The Journal of neuroscience : the official journal of the Society for Neuroscience.* 2003;23(9):3689-96.
201. Hong R, Kang TY, Michels CA, Gadura N. Membrane lipid peroxidation in copper alloy-mediated contact killing of *Escherichia coli*. *Applied and environmental microbiology.* 2012;78(6):1776-84.
202. van Kuijk FJGM, Sevanian A, Handelman GJ, Dratz EA. A new role for phospholipase A2: protection of membranes from lipid peroxidation damage. *Trends in Biochemical Sciences.* 12:31-4.
203. Thomas JP, Maiorino M, Ursini F, Girotti AW. Protective action of phospholipid hydroperoxide glutathione peroxidase against membrane-damaging lipid peroxidation. In situ reduction of phospholipid and cholesterol hydroperoxides. *The Journal of biological chemistry.* 1990;265(1):454-61.
204. Dalle-Donne I, Rossi R, Giustarini D, Milzani A, Colombo R. Protein carbonyl groups as biomarkers of oxidative stress. *Clin Chim Acta.* 2003;329(1-2):23-38.

205. Lechardeur D, Cesselin B, Liebl U, Vos MH, Fernandez A, Brun C, et al. Discovery of Intracellular Heme-binding Protein HrtR, Which Controls Heme Efflux by the Conserved HrtB-HrtA Transporter in *Lactococcus lactis*. *Journal of Biological Chemistry*. 2012;287(7):4752-8.
206. Leday TV, Gold KM, Kinkel TL, Roberts SA, Scott JR, McIver KS. TrxR, a new CovR-repressed response regulator that activates the Mga virulence regulon in group A streptococcus. *Infection and immunity*. 2008;76(10):4659-68.
207. Baruch M, Belotserkovsky I, Hertzog BB, Ravins M, Dov E, McIver KS, et al. An Extracellular Bacterial Pathogen Modulates Host Metabolism to Regulate Its Own Sensing and Proliferation (vol 156, pg 97, 2014). *Cell*. 2014;156(3):617-.
208. Lund PA. Microbial molecular chaperones. *Advances in Microbial Physiology*, Vol 44. 2001;44:93-140.
209. Alexopoulos JA, Guarne A, Ortega J. ClpP: A structurally dynamic protease regulated by AAA+ proteins. *J Struct Biol*. 2012;179(2):202-10.
210. Elsholz AKW, Gerth U, Hecker M. Regulation of CtsR Activity in Low GC, Gram plus Bacteria. *Adv Microb Physiol*. 2010;57:119-+.
211. Antelmann H, Helmann JD. Thiol-Based Redox Switches and Gene Regulation. *Antioxid Redox Sign*. 2011;14(6):1049-63.
212. Ahn SJ, Wen ZT, Burne RA. Multilevel control of competence development and stress tolerance in *Streptococcus mutans* UA159. *Infection and immunity*. 2006;74(3):1631-42.
213. Han H, Liu C, Wang Q, Xuan C, Zheng B, Tang J, et al. The two-component system Ihk/Irr contributes to the virulence of *Streptococcus suis* serotype 2 strain 05ZYH33 through alteration of the bacterial cell metabolism. *Microbiology*. 2012;158(Pt 7):1852-66.
214. Zhu WM, Wilks A, Stojiljkovic I. Degradation of heme in gram-negative bacteria: the product of the hemO gene of *Neisseriae* is a heme oxygenase. *Journal of bacteriology*. 2000;182(23):6783-90.
215. Goutelle S, Maurin M, Rougier F, Barbaut X, Bourguignon L, Ducher M, et al. The Hill equation: a review of its capabilities in pharmacological modelling. *Fundamental & clinical pharmacology*. 2008;22(6):633-48.
216. Yifrach O. Hill coefficient for estimating the magnitude of cooperativity in gating transitions of voltage-dependent ion channels. *Biophys J*. 2004;87(2):822-30.
217. Arruda MA, Rossi AG, de Freitas MS, Barja-Fidalgo C, Graca-Souza AV. Heme inhibits human neutrophil apoptosis: involvement of phosphoinositide 3-kinase, MAPK, and NF-kappaB. *J Immunol*. 2004;173(3):2023-30.
218. Kumar S, Bandyopadhyay U. Free heme toxicity and its detoxification systems in human. *Toxicol Lett*. 2005;157(3):175-88.
219. Wakeman CA, Hammer ND, Stauff DL, Attia AS, Anzaldi LL, Dikalov SI, et al. Menquinone biosynthesis potentiates haem toxicity in *Staphylococcus aureus*. *Mol Microbiol*. 2012;86(6):1376-92.
220. Toukoki C, Gold KM, McIver KS, Eichenbaum Z. MtsR is a dual regulator that controls virulence genes and metabolic functions in addition to metal homeostasis in the group A streptococcus. *Mol Microbiol*. 2010;76(4):971-89.
221. Skaar EP, Humayun M, Bae T, DeBord KL, Schneewind O. Iron-source preference of *Staphylococcus aureus* infections. *Science*. 2004;305(5690):1626-8.

222. Nakano S, Kuster-Schock E, Grossman AD, Zuber P. Spx-dependent global transcriptional control is induced by thiol-specific oxidative stress in *Bacillus subtilis*. *P Natl Acad Sci USA*. 2003;100(23):13603-8.
223. Voyich JM, Braughton KR, Sturdevant DE, Vuong C, Kobayashi SD, Porcella SF, et al. Engagement of the pathogen survival response used by group A streptococcus to avert destruction by innate host defense. *J Immunol*. 2004;173(2):1194-201.
224. Elsholz AKW, Hempel K, Pother DC, Becher D, Hecker M, Gerth U. CtsR inactivation during thiol-specific stress in low GC, Gram plus bacteria. *Mol Microbiol*. 2011;79(3):772-85.
225. Narberhaus F. Negative regulation of bacterial heat shock genes. *Mol Microbiol*. 1999;31(1):1-8.
226. Kietzman CC, Caparon MG. CcpA and LacD.1 affect temporal regulation of *Streptococcus pyogenes* virulence genes. *Infection and immunity*. 2010;78(1):241-52.
227. Seki M, Iida K, Saito M, Nakayama H, Yoshida S. Hydrogen peroxide production in *Streptococcus pyogenes*: involvement of lactate oxidase and coupling with aerobic utilization of lactate. *Journal of bacteriology*. 2004;186(7):2046-51.
228. Le Breton Y, Mistry P, Valdes KM, Quigley J, Kumar N, Tettelin H, et al. Genome-wide identification of genes required for fitness of group A *Streptococcus* in human blood. *Infection and immunity*. 2013;81(3):862-75.
229. Wilkinson SP, Grove A. Ligand-responsive transcriptional regulation by members of the MarR family of winged helix proteins. *Curr Issues Mol Biol*. 2006;8:51-62.
230. Cole JN, Barnett TC, Nizet V, Walker MJ. Molecular insight into invasive group A streptococcal disease. *Nat Rev Micro*. 2011;9(10):724-36.
231. Cohen-Poradosu R, Kasper DL. Group A streptococcus epidemiology and vaccine implications. *Clin Infect Dis*. 2007;45(7):863-5.
232. Ralph AP, Carapetis JR. Group a streptococcal diseases and their global burden. *Current topics in microbiology and immunology*. 2013;368:1-27.
233. Wong SSY, Yuen K-Y. *Streptococcus pyogenes* and re-emergence of scarlet fever as a public health problem. *Emerging Microbes & Infections*. 2012;1(7):e2.
234. Everse J, Hsia N. The Toxicities of Native and Modified Hemoglobins. *Free Radical Biology and Medicine*. 1997;22(6):1075-99.
235. Perrone S, Tataranno ML, Stazzoni G, Del Vecchio A, Buonocore G. Oxidative injury in neonatal erythrocytes. *J Matern Fetal Neonatal Med*. 2012;25(Suppl 5):104-8.
236. Kumar S, Bandyopadhyay U. Free heme toxicity and its detoxification systems in human. *Toxicology letters*. 2005;157(3):175-88.
237. Dutra FF, Bozza MT. Heme on innate immunity and inflammation. *Frontiers in pharmacology*. 2014;5:115.
238. Hagman KE, Pan W, Spratt BG, Balthazar JT, Judd RC, Shafer WM. Resistance of *Neisseria gonorrhoeae* to antimicrobial hydrophobic agents is modulated by the mtrRCDE efflux system. *Microbiology (Reading, England)*. 1995;141 (Pt 3):611-22.
239. Bozja J, Yi K, Shafer WM, Stojiljkovic I. Porphyrin-based compounds exert antibacterial action against the sexually transmitted pathogens *Neisseria*

gonorrhoeae and *Haemophilus ducreyi*. *International Journal of Antimicrobial Agents*. 2004;24(6):578-84.

240. Yamanaka H, Kobayashi H, Takahashi E, Okamoto K. MacAB is involved in the secretion of *Escherichia coli* heat-stable enterotoxin II. *Journal of bacteriology*. 2008;190(23):7693-8.

241. Kobayashi N, Nishino K, Yamaguchi A. Novel macrolide-specific ABC-type efflux transporter in *Escherichia coli*. *Journal of bacteriology*. 2001;183(19):5639-44.

242. Turlin E, Heuck G, Simões Brandão MI, Szili N, Mellin JR, Lange N, et al. Protoporphyrin (PPIX) efflux by the MacAB-TolC pump in *Escherichia coli*. *MicrobiologyOpen*. 2014;3(6):849-59.

243. Stauff DL, Bagaley D, Torres VJ, Joyce R, Anderson KL, Kuechenmeister L, et al. *Staphylococcus aureus* HrtA is an ATPase required for protection against heme toxicity and prevention of a transcriptional heme stress response. *Journal of bacteriology*. 2008;190(10):3588-96.

244. Friedman DB, Stauff DL, Pishchany G, Whitwell CW, Torres VJ, Skaar EP. *Staphylococcus aureus* redirects central metabolism to increase iron availability. *PLoS Pathog*. 2006;2(8):e87.

245. Joubert L, Derre-Bobillot A, Gaudu P, Gruss A, Lechardeur D. HrtBA and menaquinones control haem homeostasis in *Lactococcus lactis*. *Molecular microbiology*. 2014;93(4):823-33.

246. Torres VJ, Stauff DL, Pishchany G, Bezbradica JS, Gordy LE, Iturregui J, et al. A *Staphylococcus aureus* regulatory system that responds to host heme and modulates virulence. *Cell Host Microbe*. 2007;1(2):109-19.

247. McLaughlin HP, Xiao Q, Rea RB, Pi H, Casey PG, Darby T, et al. A putative P-type ATPase required for virulence and resistance to haem toxicity in *Listeria monocytogenes*. *PloS one*. 2012;7(2):e30928.

248. Le Breton Y, McIver KS. Genetic Manipulation of *Streptococcus pyogenes* (The Group A *Streptococcus*, GAS). *Curr Protoc Microbiol*. 30:9d.3.1-9d.3.29.

249. Husmann LK, Yung DL, Hollingshead SK, Scott JR. Role of putative virulence factors of *Streptococcus pyogenes* in mouse models of long-term throat colonization and pneumonia. *Infect Immun*. 1997;65(4):1422-30.

250. Kinkel TL, McIver KS. CcpA-mediated repression of streptolysin S expression and virulence in the group A streptococcus. *Infect Immun*. 2008;76(8):3451-63.

251. Lombardo ME, Araujo LS, Ciccarelli AB, Battle A. A spectrophotometric method for estimating heme in biological systems. *Anal Biochem*. 2005;341(2):199-203.

252. Davidson AL, Dassa E, Orelle C, Chen J. Structure, function, and evolution of bacterial ATP-binding cassette systems. *Microbiology and molecular biology reviews* : MMBR. 2008;72(2):317-64, table of contents.

253. Saier MH, Jr., Tran CV, Barabote RD. TCDB: the Transporter Classification Database for membrane transport protein analyses and information. *Nucleic acids research*. 2006;34(Database issue):D181-6.

254. Dalton TL, Collins JT, Barnett TC, Scott JR. RscA, a member of the MDR1 family of transporters, is repressed by CovR and required for growth of

- Streptococcus pyogenes under heat stress. Journal of bacteriology. 2006;188(1):77-85.
255. Escudero JA, San Millan A, Gutierrez B, Hidalgo L, La Ragione RM, AbuOun M, et al. Fluoroquinolone efflux in Streptococcus suis is mediated by SatAB and not by SmrA. Antimicrobial agents and chemotherapy. 2011;55(12):5850-60.
256. Garvey MI, Baylay AJ, Wong RL, Piddock LJ. Overexpression of patA and patB, which encode ABC transporters, is associated with fluoroquinolone resistance in clinical isolates of Streptococcus pneumoniae. Antimicrobial agents and chemotherapy. 2011;55(1):190-6.
257. Lubelski J, de Jong A, van Merkerk R, Agustiandari H, Kuipers OP, Kok J, et al. LmrCD is a major multidrug resistance transporter in Lactococcus lactis. Molecular microbiology. 2006;61(3):771-81.
258. Holden MT, Heather Z, Paillot R, Steward KF, Webb K, Ainslie F, et al. Genomic evidence for the evolution of Streptococcus equi: host restriction, increased virulence, and genetic exchange with human pathogens. PLoS Pathog. 2009;5(3):e1000346.
259. Tettelin H, Nelson KE, Paulsen IT, Eisen JA, Read TD, Peterson S, et al. Complete genome sequence of a virulent isolate of Streptococcus pneumoniae. Science. 2001;293(5529):498-506.
260. Ward PN, Holden MT, Leigh JA, Lennard N, Bignell A, Barron A, et al. Evidence for niche adaptation in the genome of the bovine pathogen Streptococcus uberis. BMC genomics. 2009;10:54.
261. Hu P, Yang M, Zhang A, Wu J, Chen B, Hua Y, et al. Complete genome sequence of Streptococcus suis serotype 3 strain ST3. Journal of bacteriology. 2011;193(13):3428-9.
262. Pridgeon JW, Zhang D, Zhang L. Complete Genome Sequence of a Virulent Strain, Streptococcus iniae ISET0901, Isolated from Diseased Tilapia. Genome Announcements. 2014;2(3):e00553-14.
263. Thompson JD, Gibson TJ, Higgins DG. Multiple sequence alignment using ClustalW and ClustalX. Current protocols in bioinformatics / editorial board, Andreas D Baxevanis [et al]. 2002;Chapter 2:Unit 2.3.
264. Ishikawa S-i, Tamaki S, Ohata M, Arihara K, Itoh M. Heme induces DNA damage and hyperproliferation of colonic epithelial cells via hydrogen peroxide produced by heme oxygenase: A possible mechanism of heme-induced colon cancer. Molecular Nutrition & Food Research. 2010;54(8):1182-91.
265. Kow YW, Dare A. Detection of Abasic Sites and Oxidative DNA Base Damage Using an ELISA-like Assay. Methods. 2000;22(2):164-9.
266. Robertson GT, Doyle TB, Lynch AS. Use of an efflux-deficient streptococcus pneumoniae strain panel to identify ABC-class multidrug transporters involved in intrinsic resistance to antimicrobial agents. Antimicrobial agents and chemotherapy. 2005;49(11):4781-3.
267. Schmitt TH, Frezzatti WA, Jr., Schreier S. Hemin-induced lipid membrane disorder and increased permeability: a molecular model for the mechanism of cell lysis. Arch Biochem Biophys. 1993;307(1):96-103.
268. Tatsumi R, Wachi M. TolC-dependent exclusion of porphyrins in Escherichia coli. Journal of bacteriology. 2008;190(18):6228-33.

269. Gill SR, Fouts DE, Archer GL, Mongodin EF, Deboy RT, Ravel J, et al. Insights on evolution of virulence and resistance from the complete genome analysis of an early methicillin-resistant *Staphylococcus aureus* strain and a biofilm-producing methicillin-resistant *Staphylococcus epidermidis* strain. *Journal of bacteriology*. 2005;187(7):2426-38.
270. Hanahan D, Meselson M. Plasmid screening at high colony density. *Methods Enzymol*. 1983;100:333-42.
271. Abbaspour N, Hurrell R, Kelishadi R. Review on iron and its importance for human health. *Journal of Research in Medical Sciences : The Official Journal of Isfahan University of Medical Sciences*. 2014;19(2):164-74.
272. Huber WJ, 3rd, Marohnic CC, Peters M, Alam J, Reed JR, Masters BS, et al. Measurement of membrane-bound human heme oxygenase-1 activity using a chemically defined assay system. *Drug metabolism and disposition: the biological fate of chemicals*. 2009;37(4):857-64.
273. Larkin MA, Blackshields G, Brown NP, Chenna R, McGettigan PA, McWilliam H, et al. Clustal W and Clustal X version 2.0. *Bioinformatics*. 2007;23(21):2947-8.
274. Tamura K, Peterson D, Peterson N, Stecher G, Nei M, Kumar S. MEGA5: molecular evolutionary genetics analysis using maximum likelihood, evolutionary distance, and maximum parsimony methods. *Molecular biology and evolution*. 2011;28(10):2731-9.
275. Edgar RC. MUSCLE: multiple sequence alignment with high accuracy and high throughput. *Nucleic acids research*. 2004;32(5):1792-7.

APPENDIX

Appendix A: Tables

Table 1: Strains and plasmids used in chapter 2

Name	Description	Reference
Strains		
<i>E.coli</i> Top10	Host for pZZ2 propagation	Invitrogen
<i>E.coli</i> BL21 Star	Host for pZZ2 expression	Invitrogen
Plasmids		
pET101/D-TOPO	Directional TOPO® TA cloning	Invitrogen
pOM101	vector	(135)
pZZ2	Expresses Shp-His tag from P _{T7} Expresses HupZ-His tag from P _{T7}	This study

Table 2: Crystallographic data collection and refinement statistics

PDB Code	4NU4
Space group	P1
Cell Dimensions	

a (Å)	41.82
b (Å)	61.18
c (Å)	61.35
α (°)	78.59
β (°)	86.76
γ (°)	80.07
Molecules/asymmetric unit	4
Resolution range	50.0 – 2.0
Total observations	142558
Unique reflections	39089
Completeness	98.2 (97.7) ^a
$\langle I/\sigma(I) \rangle$	13.6 (7.7)
R _{sym} (%)	9.9 (37.7)
Refinement resolution range	50 – 2.0
R _{cryst} (%)	17.0
R _{free} (%)	21.7
Number of solvent	270
Mean B-factor (Å ²)	24.7
RMS deviations from ideality	
Bond length (Å)	0.03
Angles (°)	2.2

^aValues in parentheses are given for the highest resolution shell (2.00-2.03 Å)

Table 3: Strains used in chapter 3

Name	Description	References
Strains		
MGAS5005	GAS (M1), isolated from cerebrospinal fluid	(199)
NZ131	GAS (M49) isolated from acute post-glomerulonephritis infection	(197)
GA01398	GAS (M11).	GA-EIP*
GA06439	GAS (M114)	GA-EIP*
GA02581	GAS (M1)	GA-EIP*
GA02582	GAS (M1)	GA-EIP*
GA10156	GAS (M75)	GA-EIP*
COL (MRSA)	<i>S. aureus</i> , clinical specimen isolated from operating theater in England	(269)
<i>E. cloni</i> ® 10G	Host for pAJS11 propagation and expression	Lucigen
Plasmids		
pRham™ N-His	Protein expression vector, Kan ^R , expressed from rhaP _{BAD}	Lucigen

pAJS11	Expresses N-Terminal His-tag PefR, KanR	This study
--------	---	------------

*Georgia Emerging Infections Program (GA-EIP)

Table 4: Primers used in chapter 3

Target	PCR primers	Sequence (5'-3')
<i>pefR</i> ORF	ZE515	CATCATCACCACCATCACTCACAAGTG ATAGGTGATTTACG
	ZE516	GTGGCGGCCGCTCTATTAAGCATCGTTG TCTCCTTTATAA
P_{pef}	ZE561	AAGGCGTTCCCAAGAGAGCTAG
	ZE562	CCTTGAGGACCTGCTAGATGCTCTAC
<i>pefR</i>	ZE569	CAATGTGATGCCTTCCCAAG
	ZE570	CGCTGTCAGCAACTCTTC
<i>pefC</i>	ZE571	CCTCATCATGGGTTTGGTG
	ZE572	ACGCCACGGAGATTTTCC
<i>rpsL</i>	ZE581	CAGATTCACCAGCTTTGAAC
	ZE582	CAACACGAGTAGCAACG
prsA	prsA-M1-RT-L	GGGCAGACTTTGCAGCTATTG

	prsA-M1-RT-R	TCGCCTGAGTCAAACGTATAGG
<i>clpL</i>	clpL-M1-RT-L	TGGCTTGAGCTAAACCTTCA
	clpL-M1-RT-R	CTTGGCACGACGAACTAAAA
<i>opuAA</i>	opuAA-M1-RT-L	TGATTTGCAAGACAGCATGA
	opuAA-M1-RT-L	CATCAAAGCAATCCGATCAC
<i>endoS</i>	endoS-M1-RT-L	CTCGGTCAATAGCGTAGGAGAAG
	endoS-M1-RT-L	GCGTGCCGAACGGTATG
<i>ptsA</i>	ptsA-M1-RT-L	TTTTTTAAAACCAGGCGAAGC
	ptsA-M1-RT-L	TTGTCTCAGGGACCAAATCC
<i>sagA</i>	sagA-M1-RT-L	GCTACTAGTGTAGCTGAAACAACCTCAA
	sagA-M1-RT-L	AGCAACAAGTAGTACAGCAGCAA
<i>spt7R</i>	spt7R-M1-RT-L	TCATTTGCGGCTGAAATAATAATG
	spt7R-M1-RT-L	GCAATGGGATTCAATTTTTGGA
<i>slo</i>	slo-M1-RT-L	TTGTTGAGGATAATGTAAGAATGTTTA
		G
	slo-M1-RT-R	TCCTGGCTTGCAACTGATTG
<i>fasC</i>	fasC-M1-RT-L	TGCGCACAAATTATGAAATATCTTC
	fasC-M1-RT-R	GAGCTTCAAGCAATTTGGAATTC
<i>mtsA</i>	mtsA-M1-RT-L	TGAGGGTCTTGACCGATTG
	mtsA-M1-RT-R	AAGTCGTGGCAACCAATTC

Table 5: Bacteriostatic effect of heme

Strain^a	Agar dilution (μM)	Broth dilution (μM)	Disc diffusion (mm)
NZ131 (M49)	10	10	9
GA01398 (M11)	20	30	1.25
GA06439 (M114)	20	30	6.75
GA02581 (M1)	20	50	6
GA02582 (M1)	15	50	4.75
GA10156 (M75)	20	30	4.5
MGAS5005 (M1)	20	50	5.5
<i>S. aureus</i> (control)	260	80	4.25

The minimal heme concentration that inhibits bacterial growth (MIC) was determined by the methods of agar dilution and broth macrodilution. The growth inhibitory effect of heme is also expressed as the clearance zone around heme impregnate discs (10 mM). See material and methods for details. Data are representative of two independent replicates.

^a GAS M type (if available) is indicated in parentheses

Table 6: List of bacterial strains and plasmids used in chapter 4.

Strain name	Characteristics	References
<i>S. pyogenes</i>		
NZ131	M49 serotype isolated from acute post-glomerulonephritis infection	(197)
ZE4951	NZ131 derivative with <i>pefC::pMZ1</i> mutation	This study
ZE4951/pANKITA5b	ZEM4951 strain complemented with <i>pefRCD</i> locus expressed from plasmid pANKITA5b	This study
ZE4951/pKSM201	ZEM4951 strain harboring the pKSM201 vector	This study
<i>E. coli</i>		
DH5 α	<i>hsdR17 ecA gyrA endA1 relA1</i>	(270)
Plasmids		
pMZ1	pUC-Spec derivative containing <i>pefC</i> internal fragment and the spec	This study

	resistance gene <i>aad9</i>	
pKSM201	Shuttle vector containing the kanamycin resistance gene <i>aphA3</i>	(250)
pANKITA5b	pKSM201 derivative carrying the <i>pefRCD</i> genes	This study

Table 7: List of primers used in chapter 4.

Primers name (Target)	Restriction site	Sequence (5'-3')	Source
ZE565 (<i>pefC</i>)	EcoR1	GGGGAATTCTTATGGTGGGTCATTGTTG	This study
ZE566 (<i>pefC</i>)	EcoR1	AATGAATTCTAAGCGAGGGATGAGCTGT G	This study
ZE634 (<i>pefRCD</i>)	SpeI	AAGGACTAGTGGTCTTGGCTAATAAGGC G	This study
ZE635 (<i>pefRCD</i>)	SpeI	AGGGACTAGTTTGGGATTCATGTTAGCG AG	This study

Table 8: Determination of heme and doxorubicin sensitivity by disc diffusion assay

Strain Name	Zone of clearance (mm)	
	Heme	Doxorubicin
WT (NZ131)	11.8±1.37	16
Mutant (ZE4951)	15.8±1.53 ^a	23±1.25 ^c
Complement (ZE4951/pANKITA5b)	9±0.23	17±0.19
Control (ZE4951/pKSM201)	13±0.31 ^b	22±1.27 ^d

The letters a, b, c, and d represent *P values* of statistical significance at 0.05 levels of significance calculated using student t-test (of equal variance). The statistical significance was evaluated by comparing WT with Mutant & Complement with Control data set.

Appendix B: Figures

FIGURE 1.

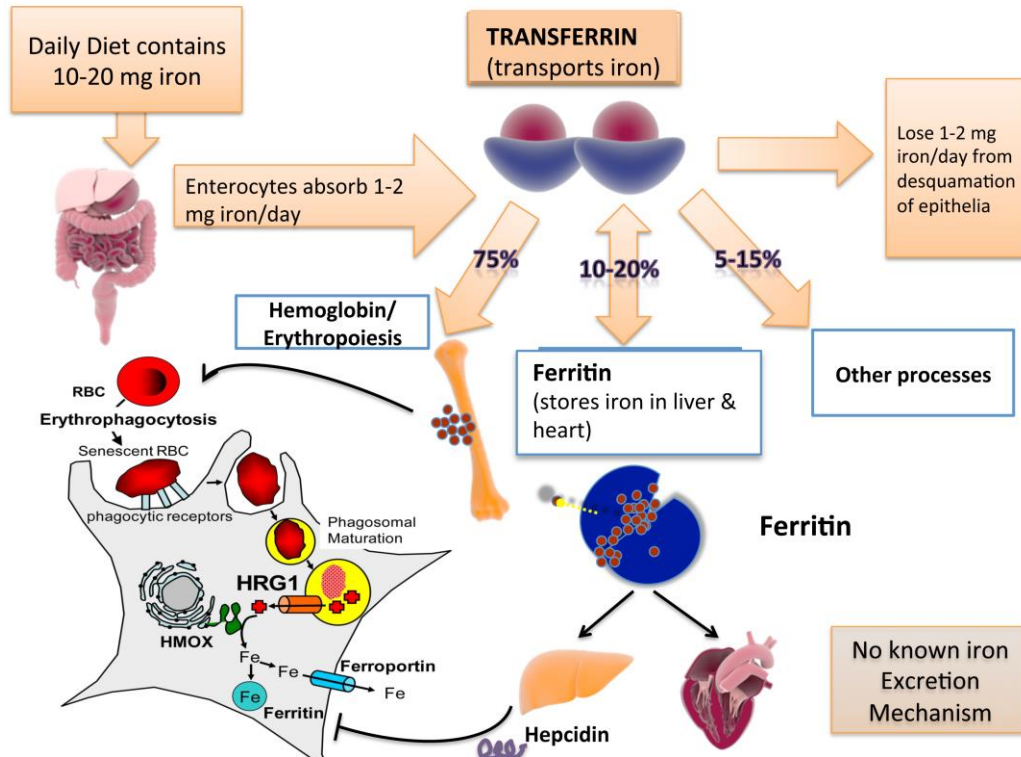


Figure 1: Iron homeostasis. The fate of the acquired iron in the human body depends upon the physiological needs and stimuli resulting in transfer or storage of the metal (see text for details). This figure is adapted from (271).

FIGURE 2.

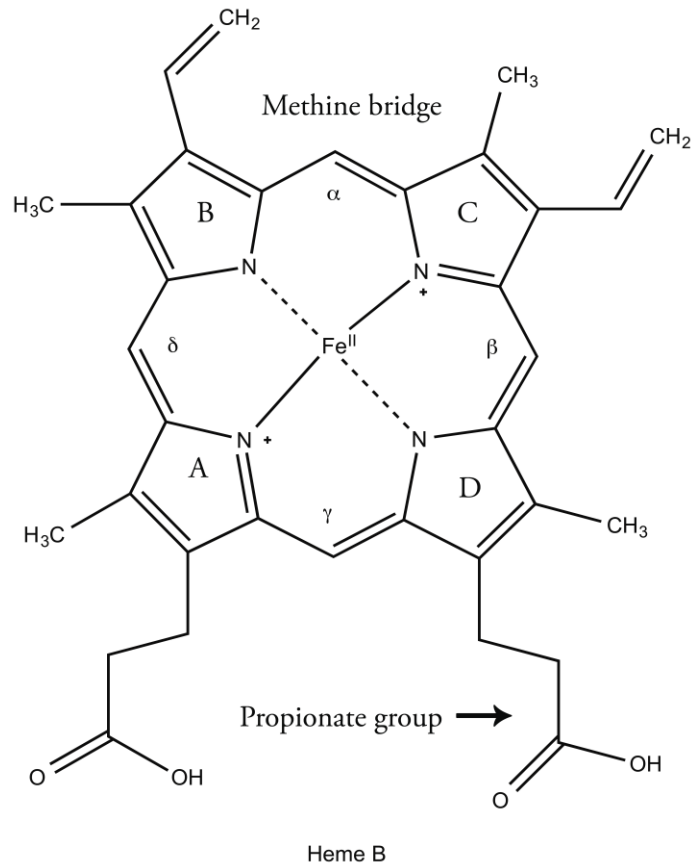


Figure 2: The structure of porphyrin-heme. The B form of heme (Fe⁺²-PPIX) or hemin (Fe⁺³-PPIX) is a macrocyclic compound that consists of four tetrapyrrole rings (depicted as A, B, C, and D) held together by four methine bridges (α, β, γ, and δ). The nitrogen atoms of tetrapyrrole can coordinate metal iron that can take part in various biochemical reactions.

FIGURE 3.

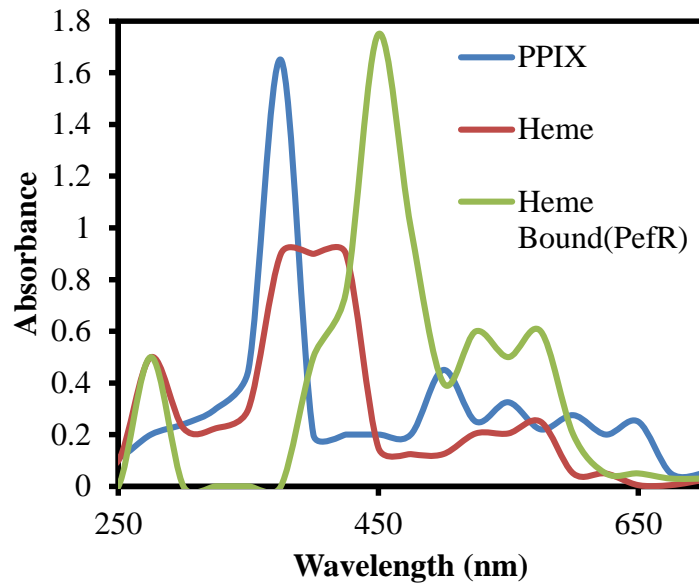


Figure 3: Spectral features of heme-porphyrin. A typical UV-visible spectra for PPIX, free heme, and heme bound protein (PefR, from GAS).

FIGURE 4.

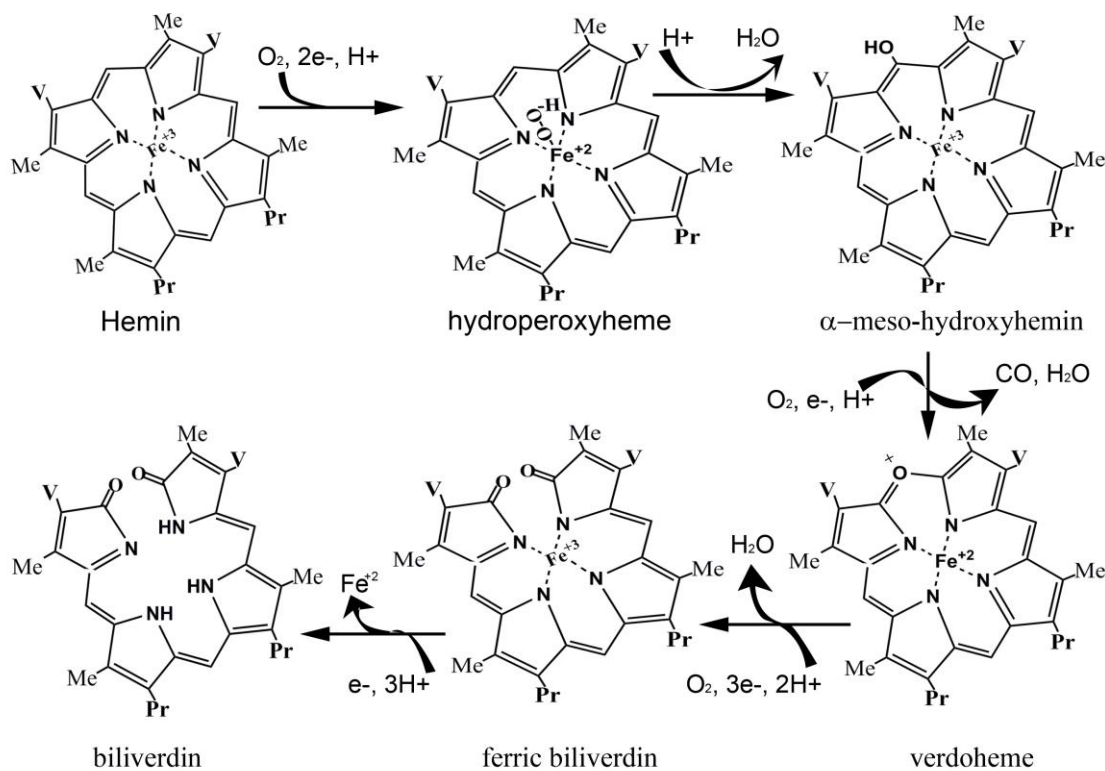


Figure 4: Catalytic intermediates of heme degradation by HO-1 The regiospecific degradation of ferric heme (which absorbs at the Soret region) involves oxygenation leading to formation of transient and highly unstable ferrous-hydroperoxyheme, which self-stabilizes by hydroxylation reaction on the edge of a tetrapyrrole. The hydroxylated ferric heme after undergoing second oxygenation reaction leads to release of CO and formation of ferrous-verdoheme. The verdoheme upon final oxygenation yields ferric biliverdin with the opening of macrocyclic structure. Ferric biliverdin through gain of protons releases iron and produces a chromophore biliverdin (which absorbs between 640 to 680 nm).

FIGURE 5.

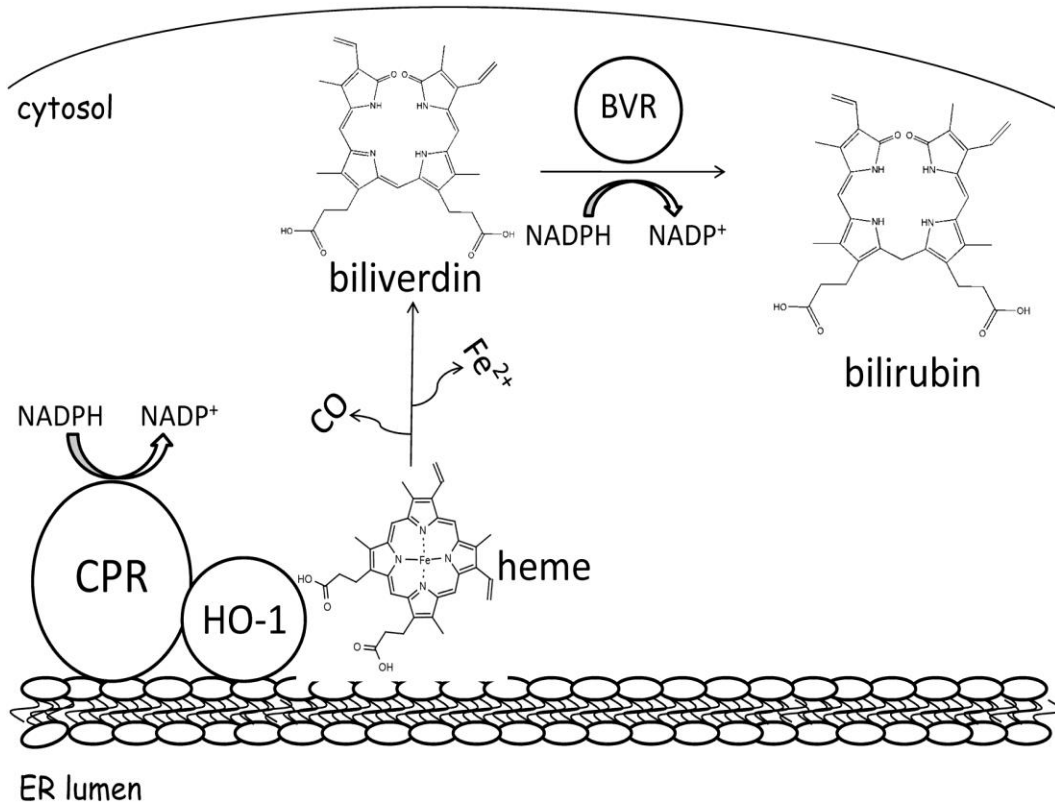


Figure 5: Heme degradation pathway catalyzed by HO-1 (272).

FIGURE 6.

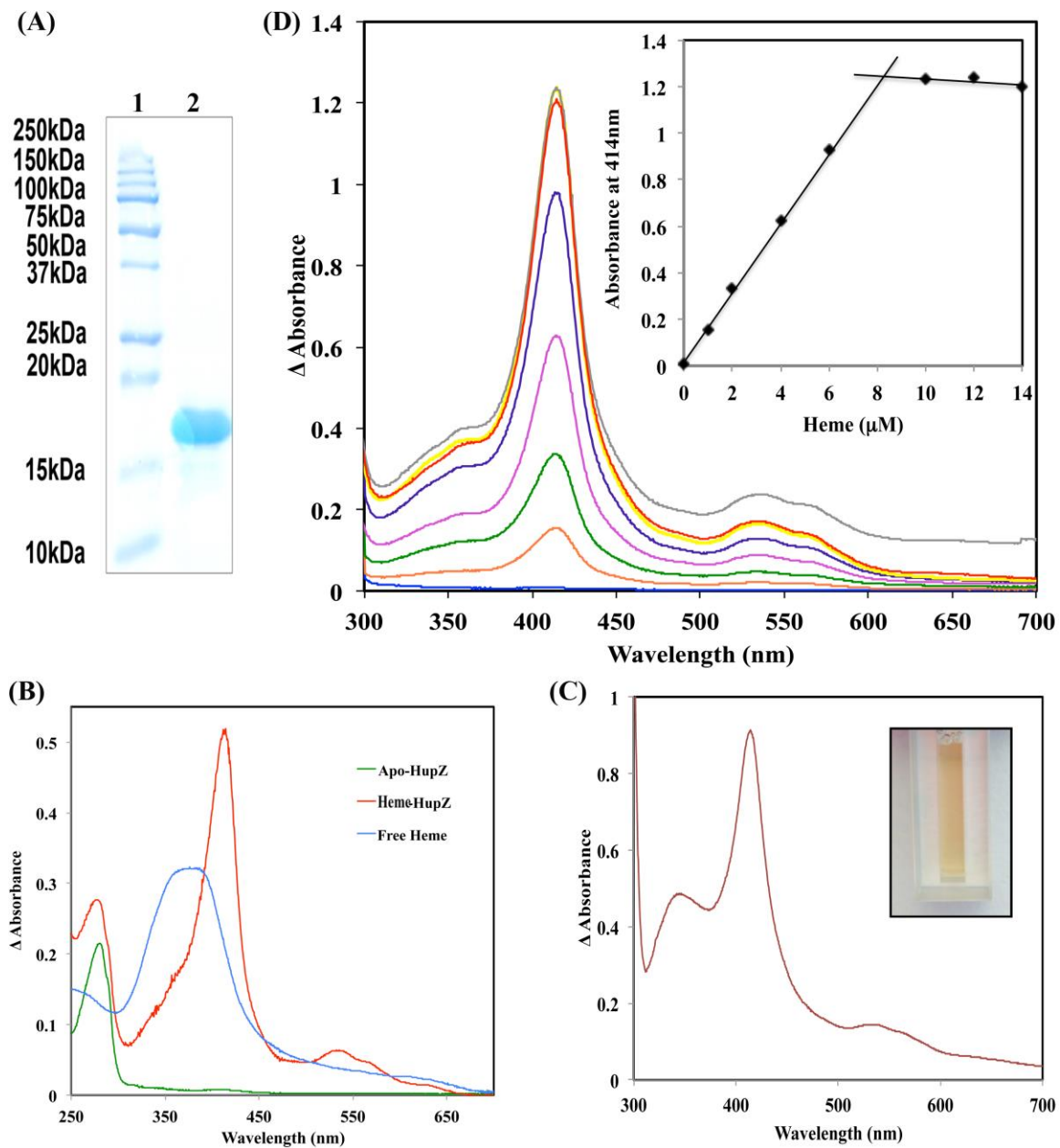


Figure 6: HupZ is a heme binding protein. Counter-clockwise: **A.** SDS-PAGE showing purified recombinant HupZ next to molecular markers. **B.** UV-visible absorption spectrum of 10 μM HupZ as purified from *E. coli* and the heme-bound form (heme-

HupZ) in SPB. The UV-visible absorption spectrum of 5 μM heme is included. A sample containing only SPB was used as a blank. **C.** UV-visible absorption spectrum of HupZ as purified (in SPB) from *E. coli* grown in the presence of 5-aminolevulinic acid. The FPLC purified fraction is documented in inset. **D.** Differential absorption spectroscopy of heme-HupZ complex. Increasing amounts of heme were added at final concentrations of 1, 2, 4, 6, 10, 12, and 14 μM to both the blank and apo-HupZ (10 μM). The insert shows the stoichiometry of heme binding to HupZ. The changes in absorbance at 414 nm were plotted against heme concentration, defining a 1:1 stoichiometry with tight binding. The data are representative of at least two independent spectroscopic analyses.

FIGURE 7

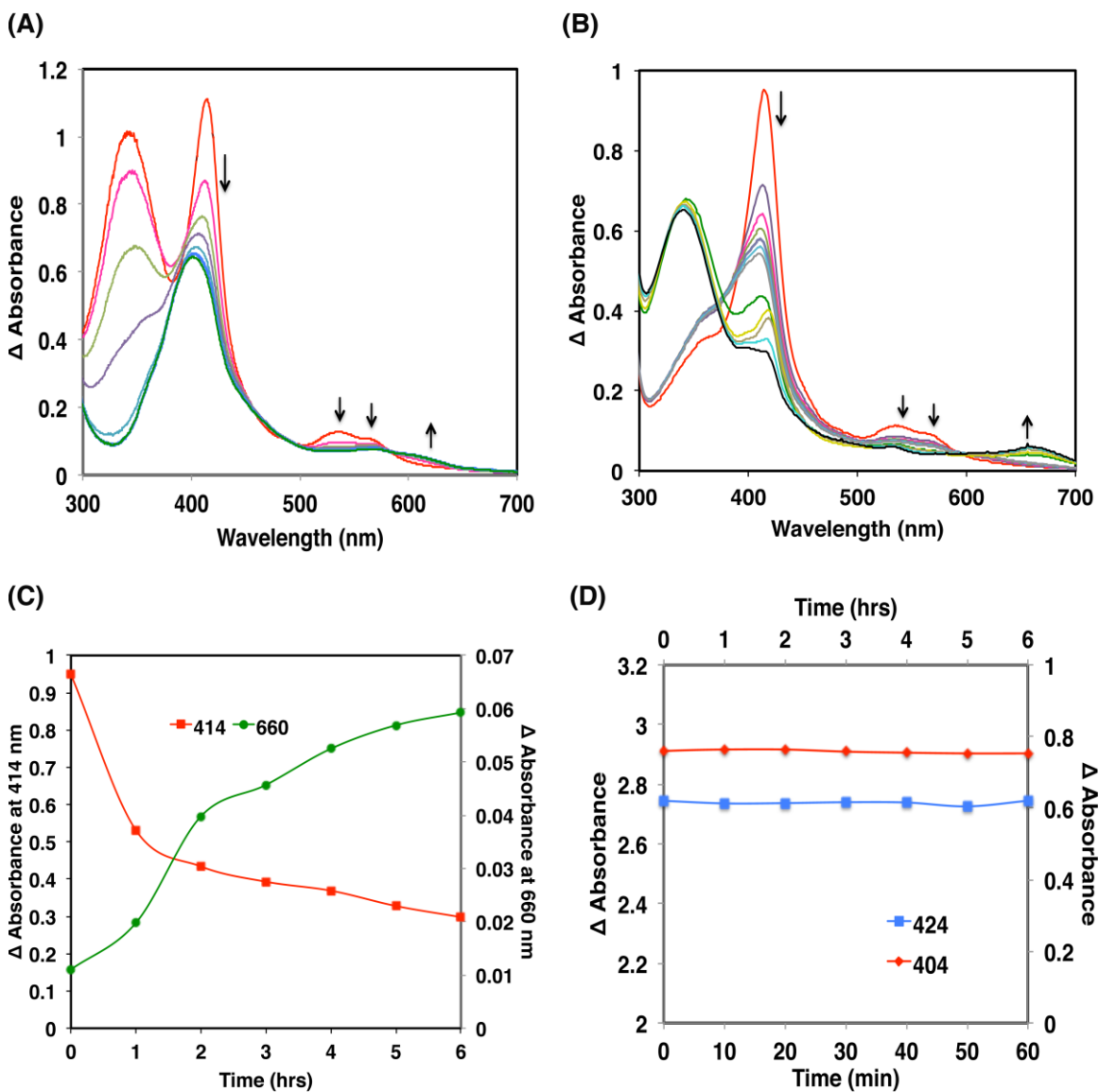


Figure 7: Heme degradation by HupZ. **A.** Heme degradation in the presence of CPR and NADPH. UV-Visible absorption spectra were recorded before and at 10, 20, 30, 40, 50 and 60 min after the addition of 250 μ M NADPH to 10 μ M Holo-HupZ and 0.4 μ M CPR in SPB. SPB containing all reaction components other than HupZ and NADPH was used as a blank. **B.** Heme degradation in the presence of CPR and NADPH regeneration

system. The same as in A, except that the reaction contained 100 μM NADPH, 6.5 mM glucose-6-phosphate, and 1 unit of glucose-6-phosphate dehydrogenase as NADPH regeneration system. UV-Visible absorption spectra were recorded before and after the addition of NADPH, at 10 min intervals for 1 h, and then every 60 min for additional 5 h.

C. The spectral changes insert demonstrates the changes in absorbance at 414 and at 660 nm over time for every hour. Catalase (2 μM) was included in all of the reactions. The data are representative of at least two independent spectroscopic analyses.

D. Control reactions for HupZ heme degradation. For Shp control, 20 μM holoShp was incubated with 0.4 μM CPR, 500 μM NADPH and 2 μM catalase in SPB (pH 7.4). Spectral changes were recorded at 25 $^{\circ}\text{C}$ for 60 min. For free heme control: 10 μM of hemin chloride was incubated with 0.4 μM CPR, 2 μM catalase and 100 μM of NADPH with regeneration system in SPB (pH 7.4). Spectral changes were monitored every 60 min for 6 h at 25 $^{\circ}\text{C}$.

FIGURE 8.

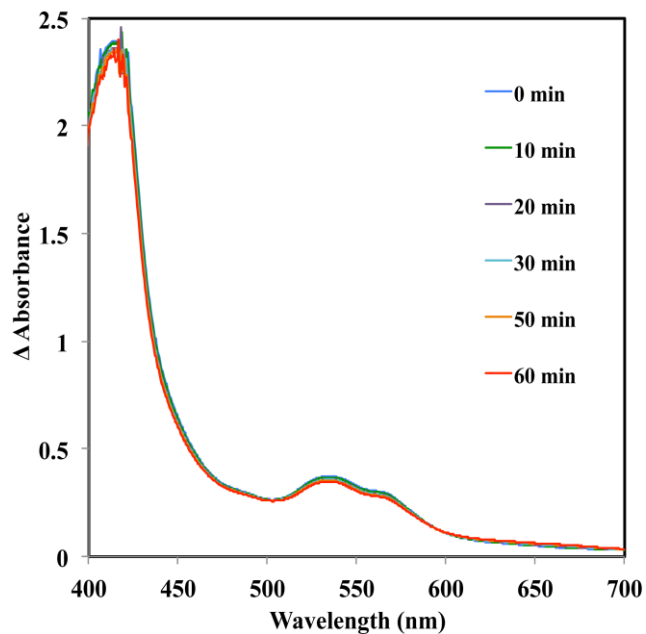


Figure 8: Evaluation of heme degradation by HupZ using FNR-Fdx as reducing equivalent. UV-visible absorption spectra were recorded before and at 10, 20, 30, 50 and 60 min after the addition of 500 μ M NADPH to 20 μ M Holo-HupZ, 10 μ M spinach Fdx, 0.1 unit/mL spinach FNR and 2 μ M catalase, in 1 mL SPB. The reaction spectra were recorded using SPB as blank.

FIGURE 9.

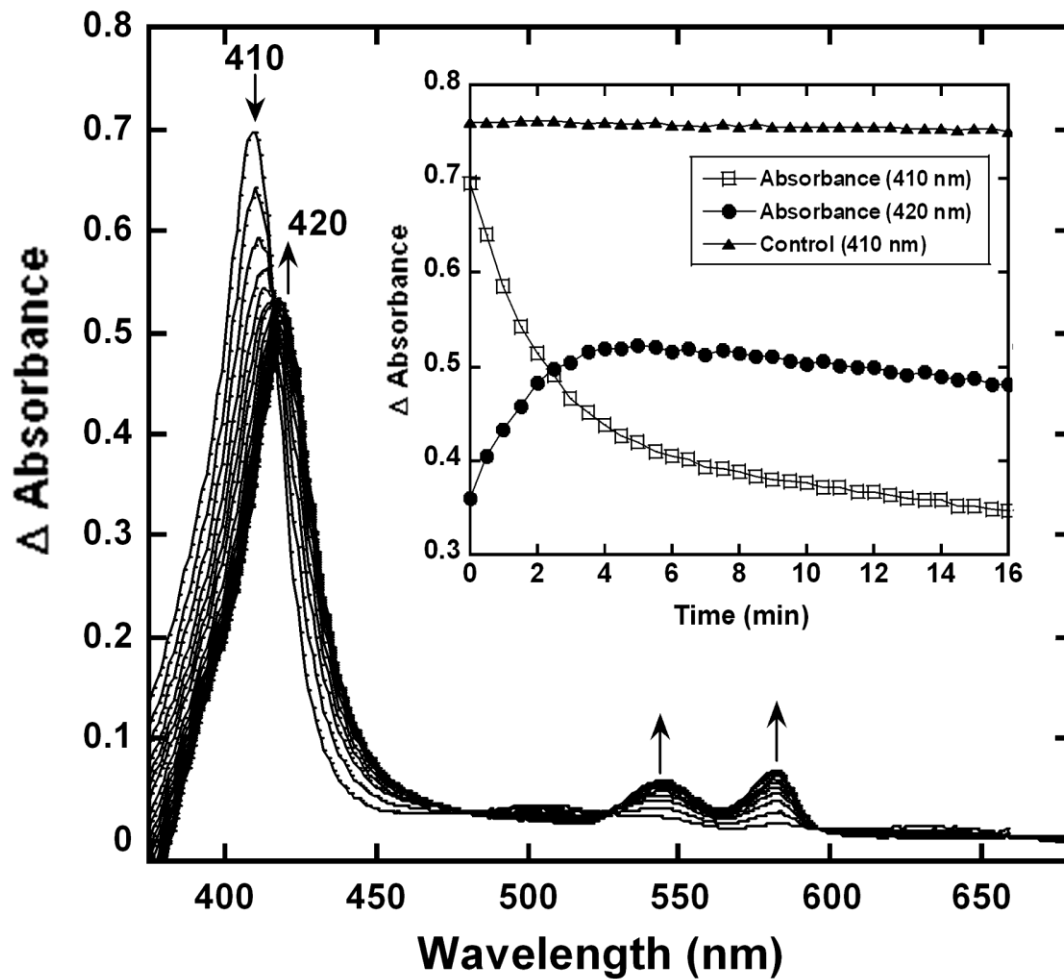


Figure 9: Differential absorption spectra of holoHupZ reaction in the presence of myoglobin. Myoglobin ($4 \mu\text{M}$) was added to a sample containing holoHupZ ($5 \mu\text{M}$), $0.4 \mu\text{M}$ CPR and $2 \mu\text{M}$ catalase in SPB. The spectra were recorded before and after the addition of $500 \mu\text{M}$ NADPH at 30 s intervals for 16 min. SPB containing all reaction components other than myoglobin and NADPH was used as a blank. The control reaction was carried out in a similar manner, except without HupZ. The insert shows the

absorption changes at 410 (experiment and control) and 420 (experiment) nm over time.
The data are representative of at least two independent spectroscopic analyses.

FIGURE 10.

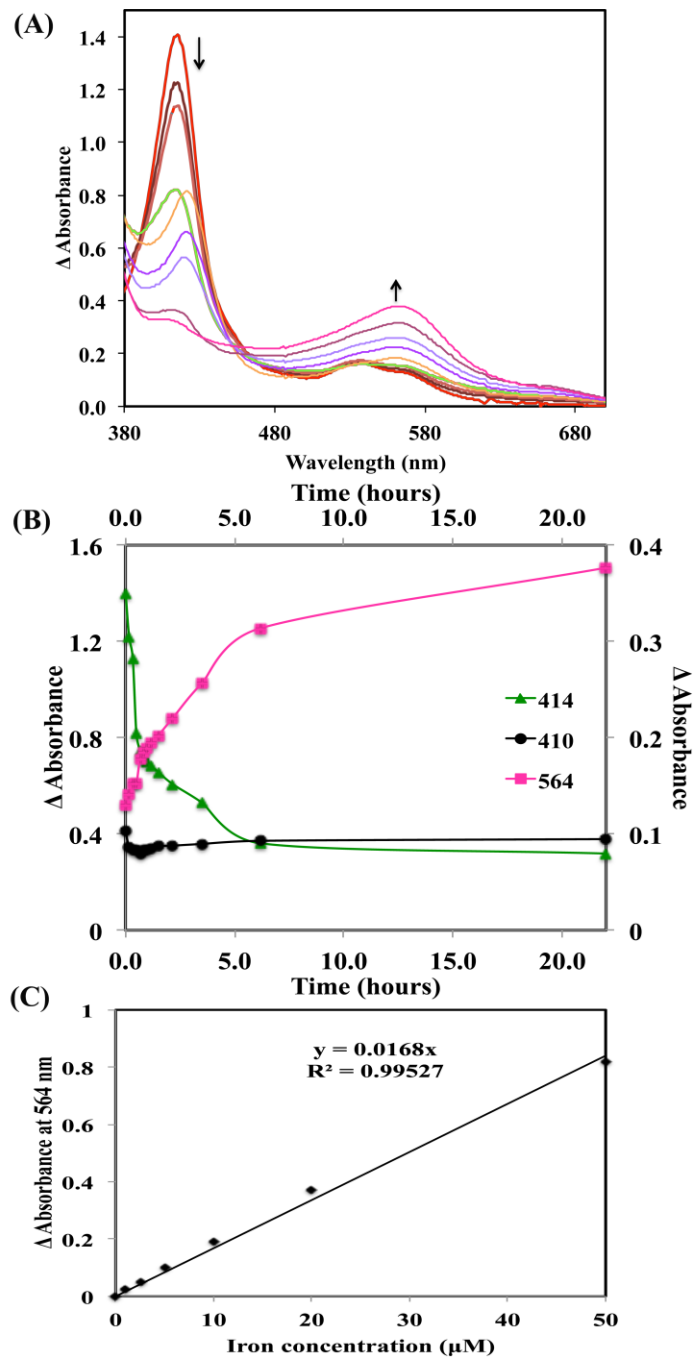


Figure 10: Differential absorption spectra of holoHupZ reaction in the presence of ferrozine. A. Heme degradation by holoHupZ (20 μ M) was carried out in SPB containing CPR (0.4 μ M), 200 μ M NADPH with regeneration system, ferrozine (1 mM),

and catalase (2 μM). UV-visible absorption spectra were recorded before and 12, 18, 30, 42, 48, 60 min after the addition of NADPH and then every 60 min for 5 h, and an additional time point was taken after 22 h. SPB containing all the reaction components other than holoHupZ and NADPH was used as a blank. As a control, heme (20 μM) was incubated in sample buffer with ferrozine and catalase. **B.** The absorbance changes over time at 414 (heme degradation) and 564 (iron-ferrozine complex) nm in the sample and control reactions (for free hemin) at 410 nm were recorded. The data are representative of at least two independent spectroscopic analyses. **C. Titration of ferrozine with ferrous iron.** 250 μM of ferrozine was incubated with an increasing concentration of FeSO_4 (0.1, 0.5, 1, 5, 10, 20, and 50 μM) solution in SPB in a 1 mL final volume and spectral changes were recorded. The standard curve was obtained from plotting the increase in absorbance at 564 nm against the ferrous iron concentration.

FIGURE 11.

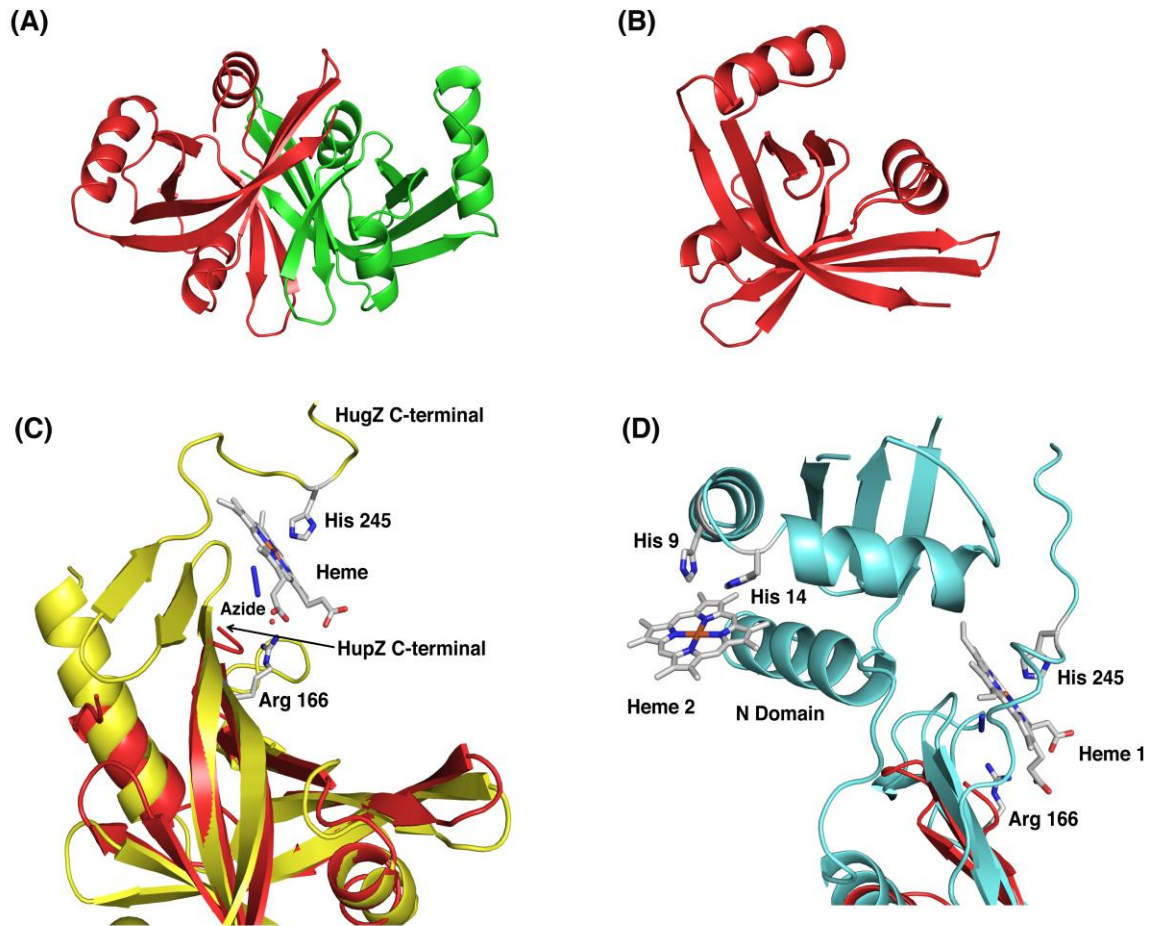


Figure 11: Crystal structure of HupZ. A. Structure of HupZ homodimer. The two monomers are colored in red and green. **B. The split barrel fold of HupZ monomer with the three α -helices and six β -strands labeled.** **C. Superposition of HupZ (red) with HugZ (yellow).** The heme binds to the extended C-terminal end of HugZ, which appears to be truncated in HupZ. His245 near the C-terminal end is involved in heme-Fe coordination and conserved across other split barrel heme oxygenases. The Arg166 important for enzymatic activity of HugZ is substituted by glycine on secondary structure

matching. Heme, Arg166, His245 and azide from the HugZ structure are shown in stick representation and colored by element type in C and D. **D. Superimposed structures of HupZ (red) and ChuZ (cyan).** ChuZ binds two heme moieties. The first heme binds at the flexible C-terminal end of the split barrel domain similar to HugZ with similar coordination, while the second heme binds at the N-terminal domain, which is absent in HupZ.

FIGURE 12.

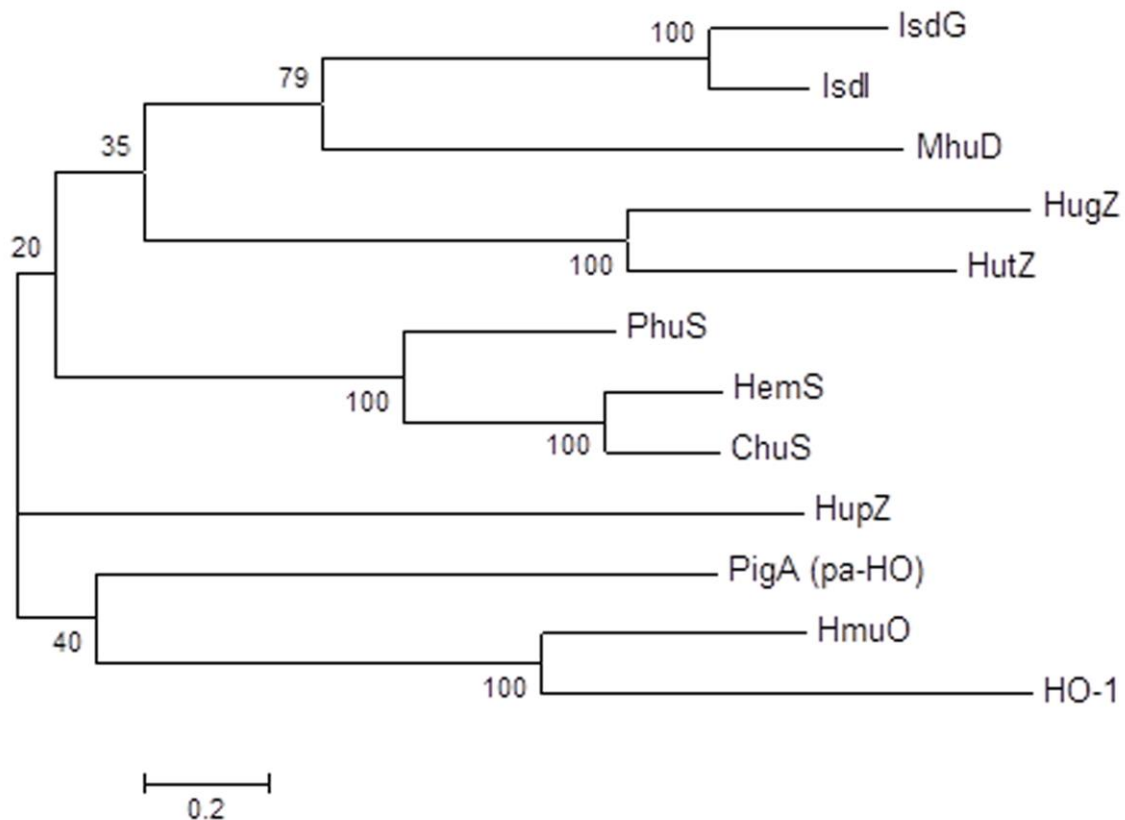


Figure 12: Phylogenetic tree of HupZ with other heme degrading enzymes. The tree was obtained from multiple sequence alignment in ClustalW (273). We used neighbor-joining method for tree construction and bootstrap analysis (parameter set at 1000 resampling) performed using MEGA win-5.21 software (274). The locus tag or the accession number for each protein used in the sequence alignment is as follows: HupZ locus tag: Spy_0844 [*S. pyogenes* M1 GAS]; IsdG locus tag: NWMN_1047 [*S. aureus* subsp. aureus str. Newman]; IsdI locus tag: NWMN_0111 [*S. aureus* subsp. aureus str. Newman]; HugZ locus tag: HP0318 [*H. pylori* 26695]; HutZ locus tag: VCA0907 [*V.*

cholerae O1 biovar El Tor str. N16961]; PigA (Pa-HO) locus tag: PA0672 [*P. aeruginosa* PAO1]; HmuO locus tag: CDC7B_1652 [*C. diphtheriae* C7(beta)]; HO-1 locus tag: CTA-286B10.6 [*Homo sapiens*]; MhuD locus tag: Rv3592 [*M. tuberculosis* H37Rv]; HemS accession number: **P31517** [*Y. enterocolitica*]; ChuS locus tag: E2348C_3742 [*E. coli* O127:H6 str. E2348/69]; PhuS accession number: AF055999 [*P. aeruginosa* PAO1]. Bootstrap units were obtained from 500 repeats of neighbor joining using the MEGA win-5.21 software.

FIGURE 13

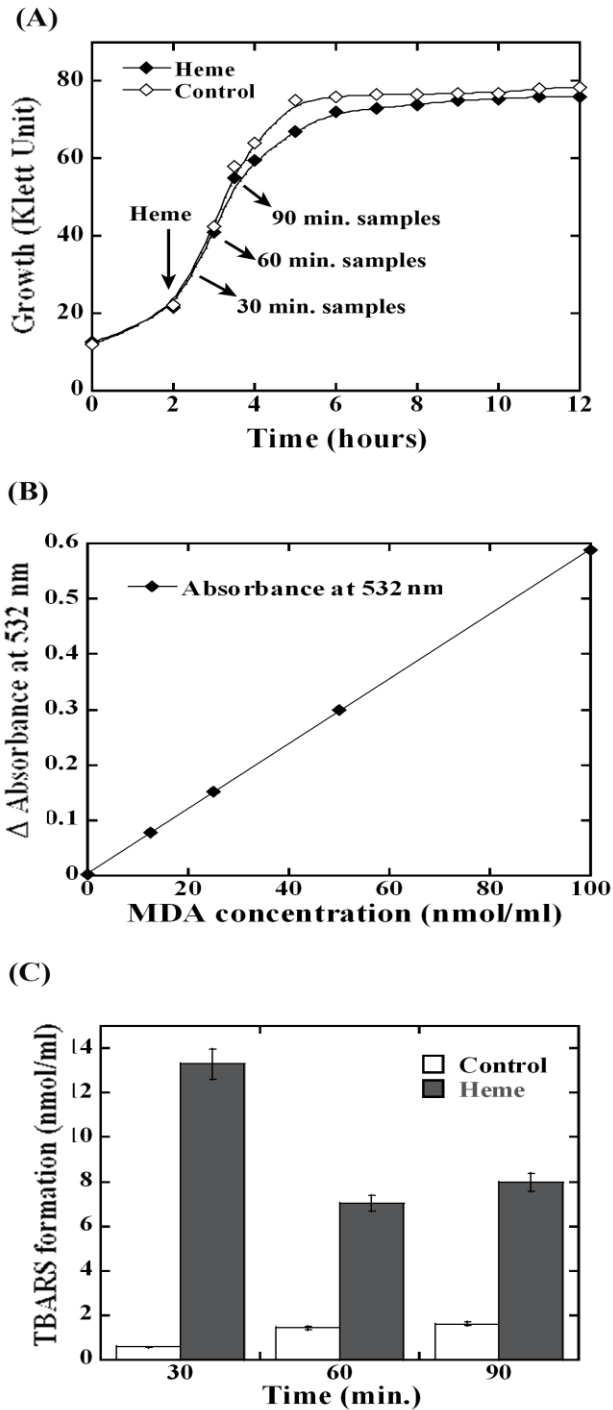


Figure 13: Heme exposure leads to lipid peroxidation in GAS. A. Cell growth.

MGAS5005 cells growing in C-medium were treated with 4 μ M heme in 0.035% DMSO

(Heme) or with mock treatment (0.035% DMSO, Control) at the early logarithmic growth phase. Culture samples were harvested 30, 60 and 90 min post exposure and processed.

B. Malondialdehyde (MDA) standard curve. 100 μ l samples of MDA at a concentration of 0, 12.5, 25, 50, and 100 nmol/ml were allowed to react with thiobarbituric acid (TBA, see material and methods). The absorption at 532 nm of the supernatants from processed samples was determined and plotted as a function of MDA concentration exposure. The linear equation obtained for the standard curve was $y = 0.0059x$ with R^2 value of 0.9997.

C. Lipid peroxidation following heme exposure. Cell lysates were prepared and allowed to react with TBA. The sample absorption at 532 nm was determined and the formation of TBA-reactive-substances (TBARS) was calculated using the standard curve shown in B. All samples were standardized with respect to the cell number in the corresponding culture. Data are representative of biological triplicates.

FIGURE 14.

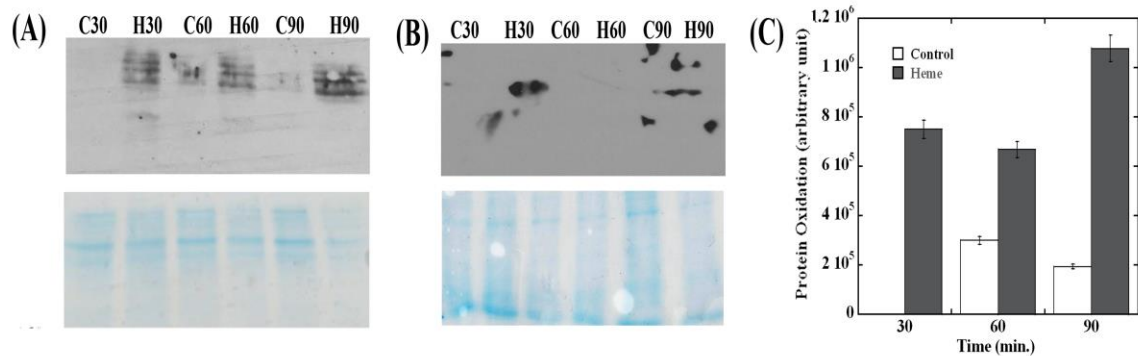


Figure 14: Protein oxidation following heme exposure.

The membrane (A) and cytoplasmic proteins (B) extracted from cells harvested at different time points post treatment were allowed to react with DNPH (see material and methods) before fractionation by SDS-PAGE. Sample identity (H for heme treated cells and C for controls) and collection times (30, 60 and 90 min) are indicated [top panel]. Western blot with anti-DNP antibodies (OxyBlot) developed by chemiluminescence [bottom panel]. Coomassie blue-stained gel. All samples were standardized with respect to the cell number in the corresponding culture. C. Quantification of protein oxidation. The reaction with anti-DNP antibody in each membrane sample was quantified by densitometry. Arbitrary values for the heme treated samples (Heme) and mock treated (Control) after background subtraction are plotted. Error bars are shown. Data are representative of biological triplicates. Note that the western blot showing larger spots in an area outside of the lane is a technical artifact associated with the film development and it's not a true reaction (prominent in Figure 9B, top panel).

FIGURE 15.

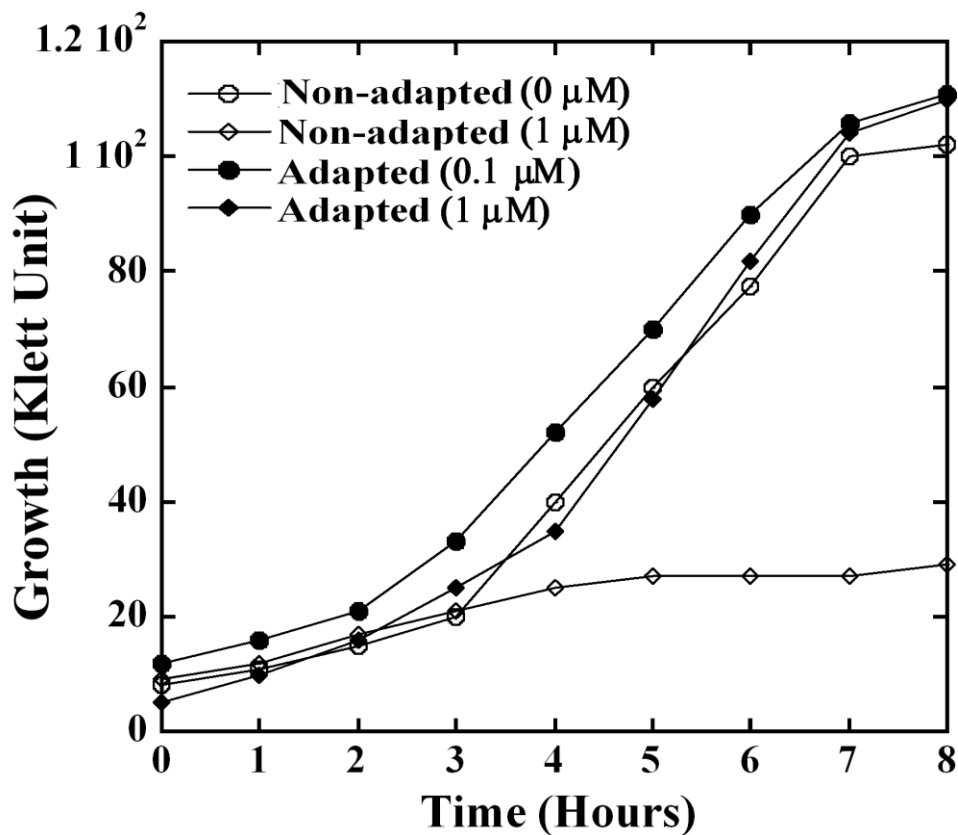


Figure 15: GAS employs an adaptation strategy to avert growth phenotypes associated with heme stress. NZ131 cells were grown overnight in C-medium supplemented with 0.1 μM (adapted culture) and without heme (non-adapted culture). The overnight cultures were used as an inoculum to monitor growth in presence and absence of heme. Briefly, non-adapted culture was grown in C-media supplemented with 0 and 1 μM heme, whereas adapted culture was sub-cultured into C-media containing 0.1 and 1 μM heme. The growth was monitored colorimetrically for 8 hours at 37 $^{\circ}\text{C}$.

FIGURE 16A

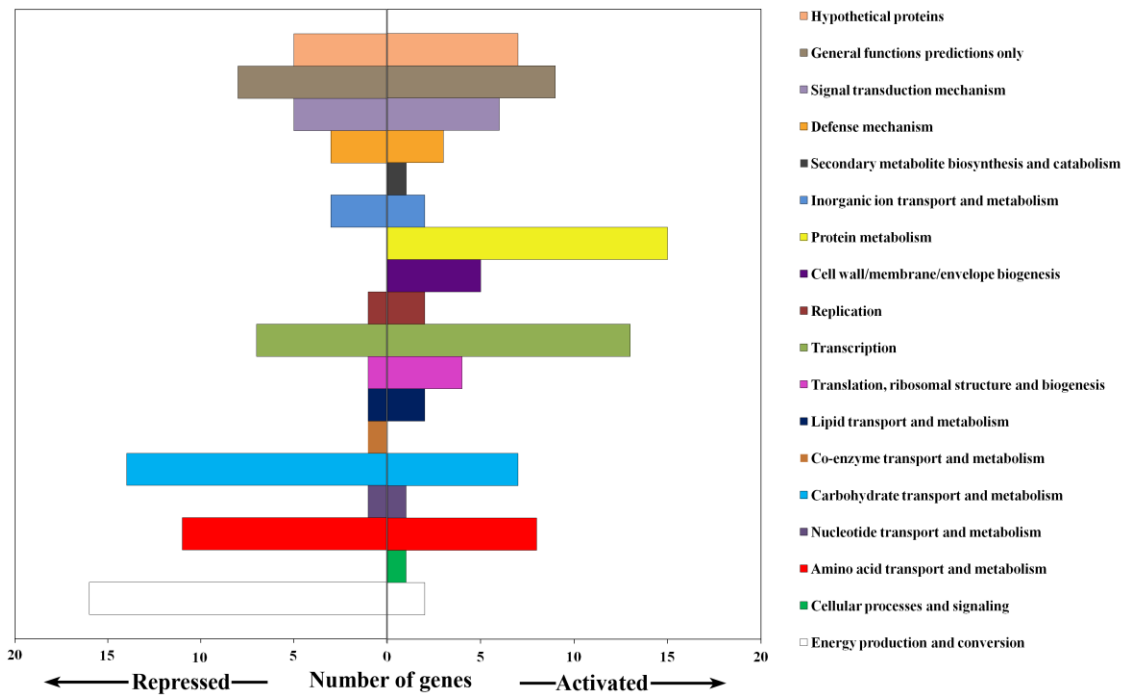


Figure 16 A: Genes responding to heme stress in MIT1 GAS strain MGAS5005.

FIGURE 16 B

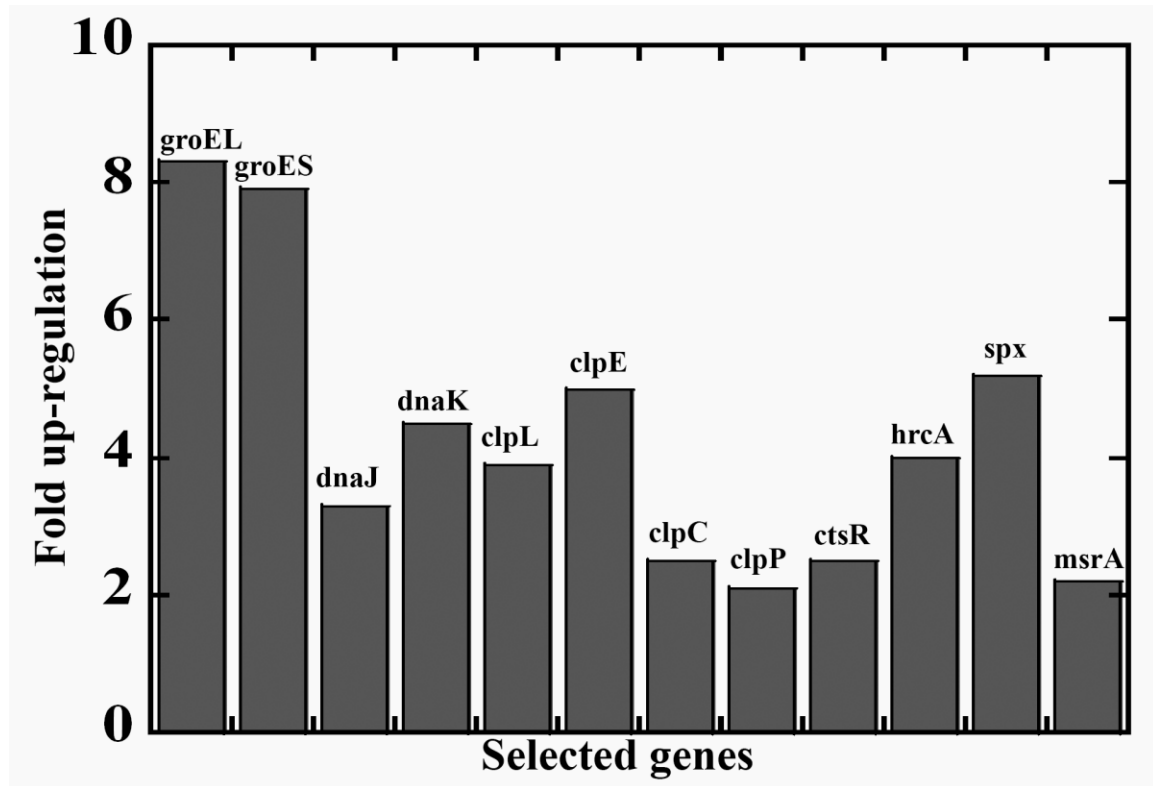


Figure 11 B Genes responding to heme stress in M1T1 GAS strain MGAS5005.

Total RNA was extracted 90 min post treatment and analyzed by microarray. **A.** Genes repressed or activated following exposure to 4 μ M heme (in 0.035% DMSO) compared with mock treatment (0.035% DMSO). Data for genes whose expression was significantly different between cells exposed to heme and those subjected to mock treatment were combined and assigned to categories. **B.** Selected heme-activated genes revealing protein and redox stress response. Values represent relative expression levels (fold-change) in heme treated bacteria compare with mock treatment.

FIGURE 17.

```
GAS PefR MSQVIGDLRELIHQIEQISDEIAKKYDVEHLAGPQGYVLVFLAKHQNEIFVKDIEKQLR 60
GBS PefR MENPLQKARILVNQLEKYLDRYAKEYDVEHLAGPQGHLVMHLYKHPDKDMSIKDAEEILH 60
      *.: : . * *::*:*: * . **:*****:.....* ** :::: :** *: *:

GAS PefR ISKSVASHLVKRMVKNGFINVMPQSVDKRYKQVVLAAQVGRDKLPLLRECRKDIEHYFLKE 120
GBS PefR ISKSVASNLVKRMEKNGFIAIVPSKTDKRVKYLTLHLGKQKATQFEIFLEKLHSTMLAG 120
      *****:***** ***** :*:*.*** * : *::*:*:* . :. :... :*

GAS PefR ITKEELLTAKKVIEQLKQNMLTYKGDNDA 149
GBS PefR ITKEEIRTTKKVIRTLAKNMAMEDFD--- 146
      *****: *:*****. * :** . *
```

Figure 17: Multiple sequence alignment of PefR amino acid sequence from GBS and GAS. The degree of homology between GAS PefR (encoded by MGAS5005 *spy_0195*) and GBS PefR (encoded by *gbs1402*) is depicted in pair-wise sequence alignment performed using ClustalW. The amino acids are represented by single letter code. The symbols: (*) indicate identical residues; (:) indicate strongly similar residues; (.) designate weakly similar residues. An accuracy of alignment was also confirmed using MUSCLE tool (275) that showed identical alignment output as well.

FIGURE 18.

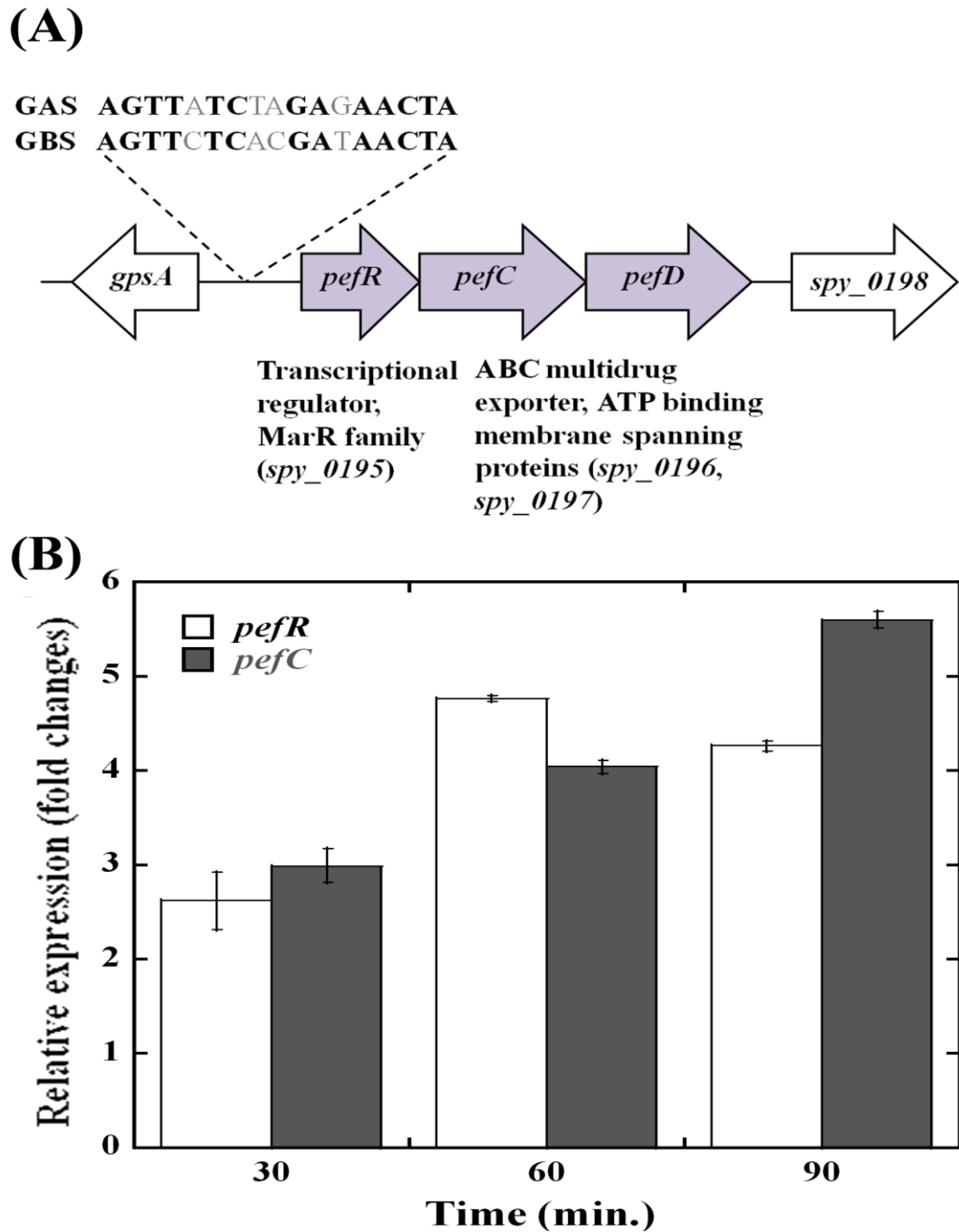


Figure 18: The streptococcal *pefRCD* locus. A. Genetic organization of the *pefRCD* gene cluster in GAS. The putative PefR binding identified *in silico* and its homology to

the PefR binding motif from GBS (95) are shown. **B.** Time course of *pefRC* expression in response to heme stress. Total RNA was extracted at different time points following heme or mock treatment and the relative expression of the *pefR* and *pefC* genes was evaluated by Real-time quantitative RT-PCR.

FIGURE 19.

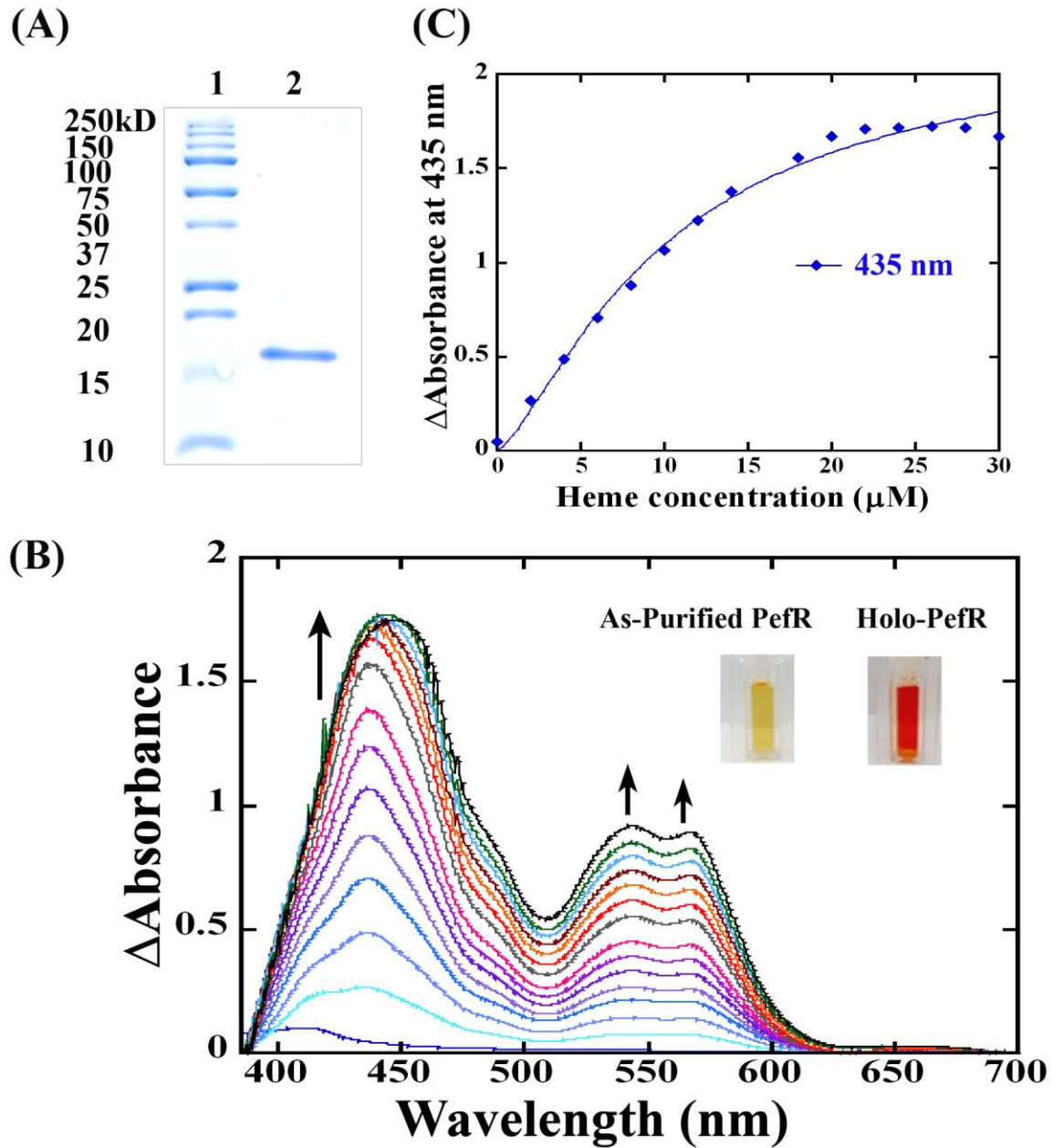


Figure 19: The PefR from GAS is a heme binding protein. **A.** A Coomassie blue-stained gel showing purified recombinant PefR from GAS next to a molecular marker. **B.** Heme titration of PefR. UV-visible spectrum of 10 μM PefR (in SPB) following incubation with an increasing concentration of hemin chloride (2-30 μM) in 2 μM

increments. SBP with the corresponding heme concentration was used as blank and subtracted from the sample spectrum. Heme binding by PefR is indicated by the increased absorption at 435, 530 and 560 nm. The arrow indicates the direction of the absorption changes. The images are of PefR as-purified from *E. coli* and of holo-PefR (after heme reconstitution and removal of heme excess by gel filtration and dialysis). This data represents three independent heme-titration experiments. **C.** Stoichiometry of heme binding to PefR. The changes in absorbance at 435 nm were plotted against heme concentration. The K_d was determined by fitting the data into modified hills equation for multiple binding sites (215). The K_d equals 10 μM and nH (hill's coefficient) is 1.37 μM .

FIGURE 20.

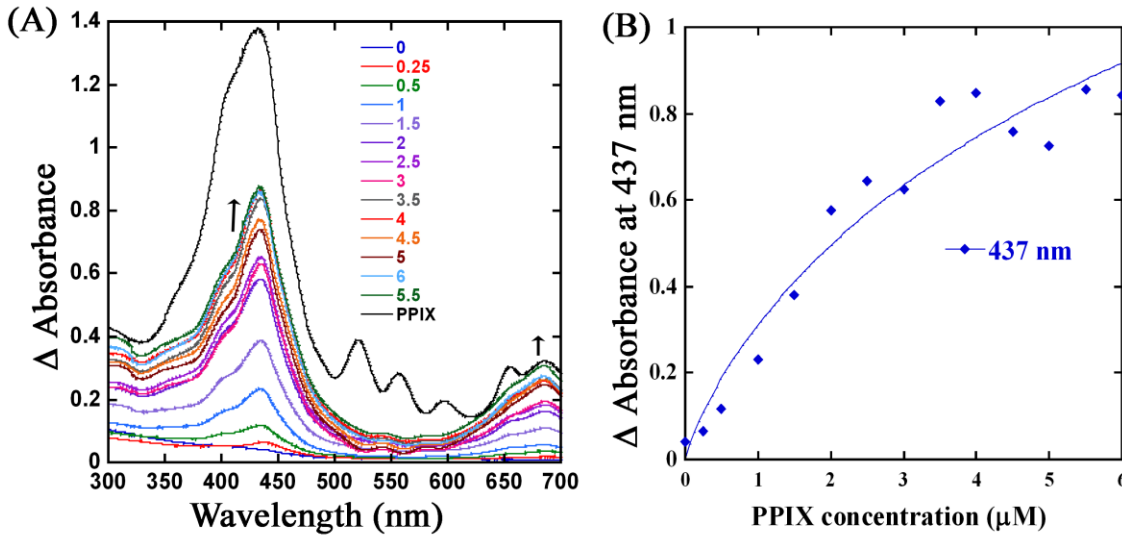
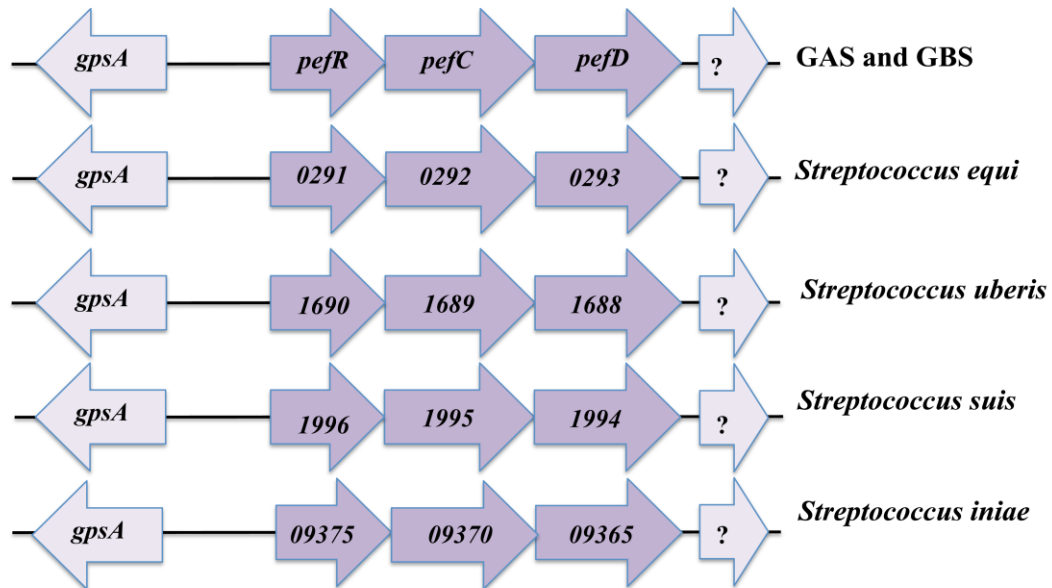


Figure 20: The PefR is capable of PPIX binding. A. PPIX titration of PefR. Change in the UV-visible spectral profile of 5 μ M of PefR (in SPB) when titrated with an increasing concentration of PPIX (0.25-6 μ M) in 0.5 μ M increments was monitored across wavelength (300 – 700 nm). Free PPIX spectrum (shown in black) showed absorbance peaks in 432, 521, 556, 596, 655 and 685 nm regions. The PefR bound PPIX demonstrated maximum absorbance at 437 and 686 nm; absorbance at these wavelengths showed increase with PPIX concentrations (0.25 - 6 μ M; shown in different colors). The arrow indicates the direction of the absorption changes. **B.** Stoichiometry of PPIX binding to PefR. The spectral changes at 437 nm were plotted against PPIX concentration. The K_d was determined by fitting the data into linear equation.

FIGURE 21.

(A)



(B)

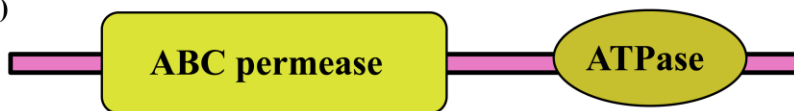


Figure 21: The prevalence of the *pefRCD* operon in human and zoonotic streptococci. A. The genomic arrangement and occurrence of the *pefRCD* genes in GAS (MGAS5005 strain) and GBS (NEM316 strain) is also conserved among members of the pyogenic cluster namely, *S. equi* (4047 strain), *S. uberis* (0140J strain), and *S. iniae* (ISET0901). Additionally, this system is found in *S. suis* (JS14 strain). These PefCD homologs are referred to as SatAB in the literature (255). The *pef* operon consists of a MarR-like transcriptional regulator (locus tag for strains tested: *Spy_0195*, *gbs1402*, *SEQ_0290*, *SUB_1690*, *SSUJS14_1996*, and *DQ08_09375*) controlling an adjacent ABC-type efflux system (*Spy_0196-97*, *gbs1401-00*, *SEQ_0292-93*, *SUB_1689-88*, *SSUJS14_1995-94*, and *DQ08_09370-65*). The neighboring genes upstream and

downstream from the *pef* operon consist of lipid metabolism (*gpsA*) and unknown functions, respectively. **B.** The efflux system, PefCD belongs to the class-1 type of ABC transporters. PefC and PefD both contain a membrane permease domain fused to an ATPase domain on the same polypeptide chain.

FIGURE 22.

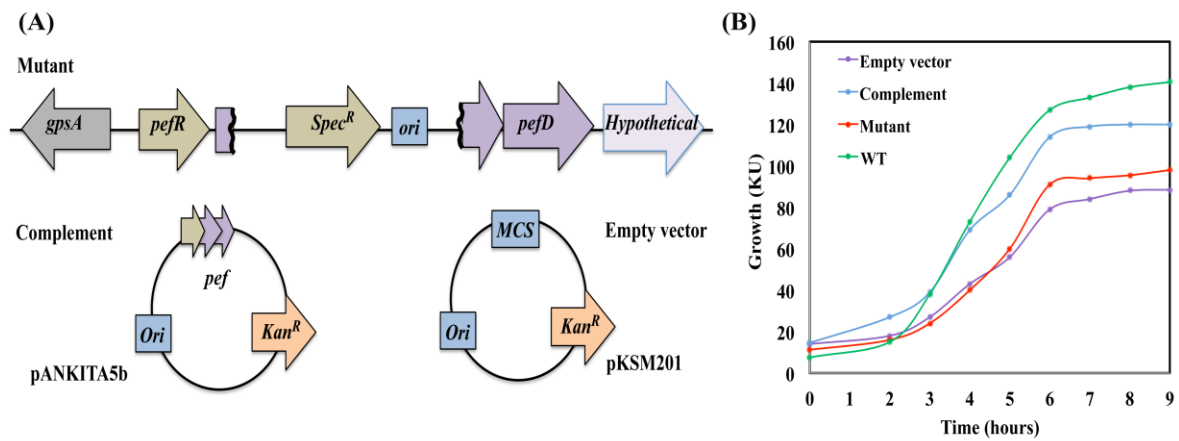


Figure 22: Insertional inactivation of *pefC* in GAS leads to impaired growth phenotype. A. A schematic representation of the *pefC::pMZ1* mutation in the ZE4951 strain and the plasmids used for complementation analysis. The *aad9* and *aphA3* genes confer the resistance to spectinomycin ($Spec^R$) and kanamycin (Kan^R), respectively. MCS is a multiple cloning site. The *Ori* (pSH71 derivative) enabled replication of plasmids in multiple hosts (*E. coli* and GAS). Plasmid pANKITA5b carries the *pefRCD* cluster cloned into the MCS in pKSM201. **B.** Growth of the NZ131 (WT), ZE4951 (Mutant), ZE4951/pANKITA5b (Complement), and ZE4951/pKSM201 (Empty vector) strains. Fresh THYB media were inoculated with GAS cells ($OD_{600\text{ nm}} = 0.05$) and the cultures were grown statically at 37 °C. Cell growth was monitored colorimetrically and expressed in Klett units. The data are representative of two independent experiments.

FIGURE 23.

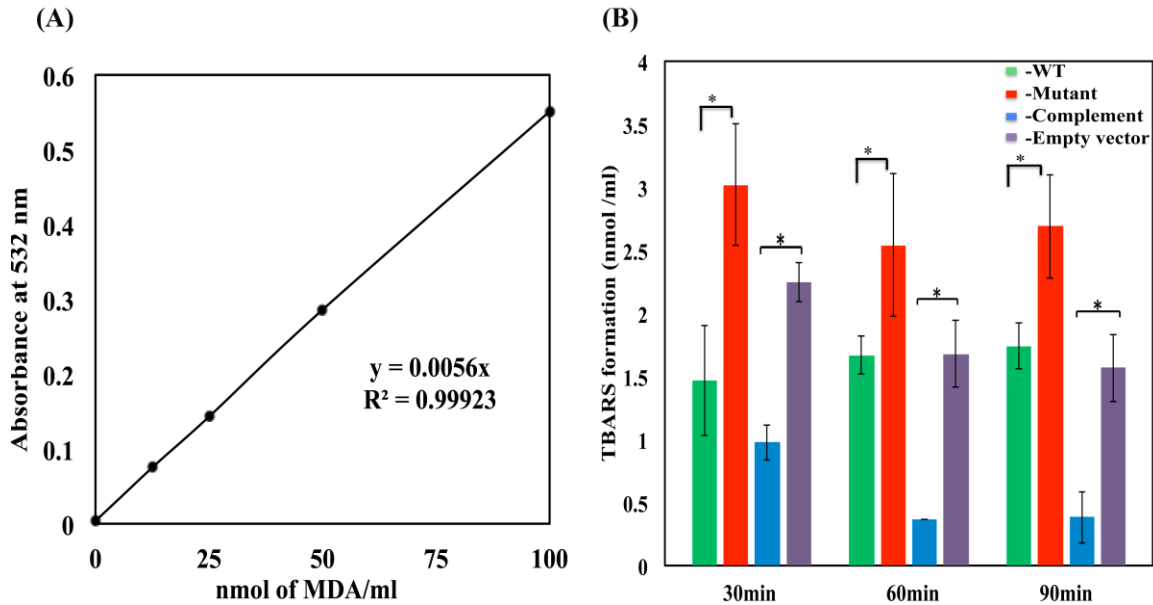


Figure 23: The PefCD transporter protects GAS from heme-mediated lipid oxidation. **A.** Lipid peroxidation standard curve. The curve was generated by plotting the absorbance monitored at 532 nm and formed as a result of reactivity between a series of malondialdehyde solutions (0, 12.5, 25, 50, and 100 nmol/ml) with the TBA reagent. **B.** **Lipid peroxidation following heme exposure.** Cultures of NZ131 (WT), ZE4951 (Mutant), ZE4951/pANKITA5b (Complement), and ZE4951/pKSM201 (Empty vector) strains were treated with 1 μ M heme during the mid logarithmic phase of growth (60-70 Klett units). Culture samples were then collected at 30, 60, and 90 min post-heme exposure and allowed to react with TBA. The sample absorption at 532 nm was determined, and the formation of TBA-reactive-substances (TBARS) was calculated using the standard curve shown in A. All samples were standardized with respect to cell number. The data are derived from two independent experiments, each performed in

triplicates. The asterisk (*) denotes that the observed P value is statistically significant ($P < 0.05$) calculated using student t-test (equal variance) at 0.05 levels of significance.

FIGURE 24.

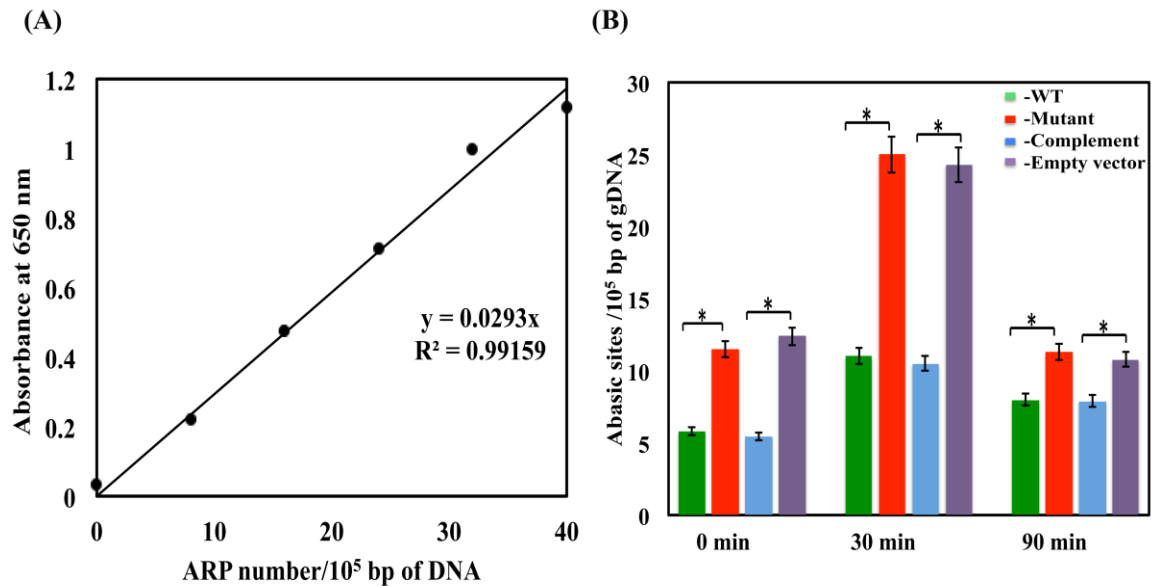


Figure 24: The PefCD transporter protects GAS chromosome from heme-mediated GAS damage. A. AP sites standard curve. The curve was generated by plotting absorbance at 650 nm from a genomic DNA series with 0, 8, 16, 24, 32, and 40 AP sites / 10⁵ bp after reaction with the ARP probe. **B.** AP site formation in GAS chromosome following heme exposure. Cultures of NZ131 (WT), ZE4951 (Mutant), ZE4951/pANKITA5b (Complement), and ZE4951/pKSM201 (Empty vector) strains were treated with 5 μ M heme during the mid logarithmic phase of growth (60-70 Klett units). Genomic DNA was extracted from samples collected at 0, 30 and 90 min post exposure was allowed to react with ARP-biotin and analyzed. The sample absorption at 650 nm was determined and AP site formation was calculated using the standard curve shown in A. All samples were standardized with respect to cell number. The data are derived from two independent experiments each done in triplicates. The asterisk (*)

denotes that the observed P value is statistically significant ($P < 0.05$) and is calculated using student t-test (equal variance) at 0.05 levels of significance.

FIGURE 25.

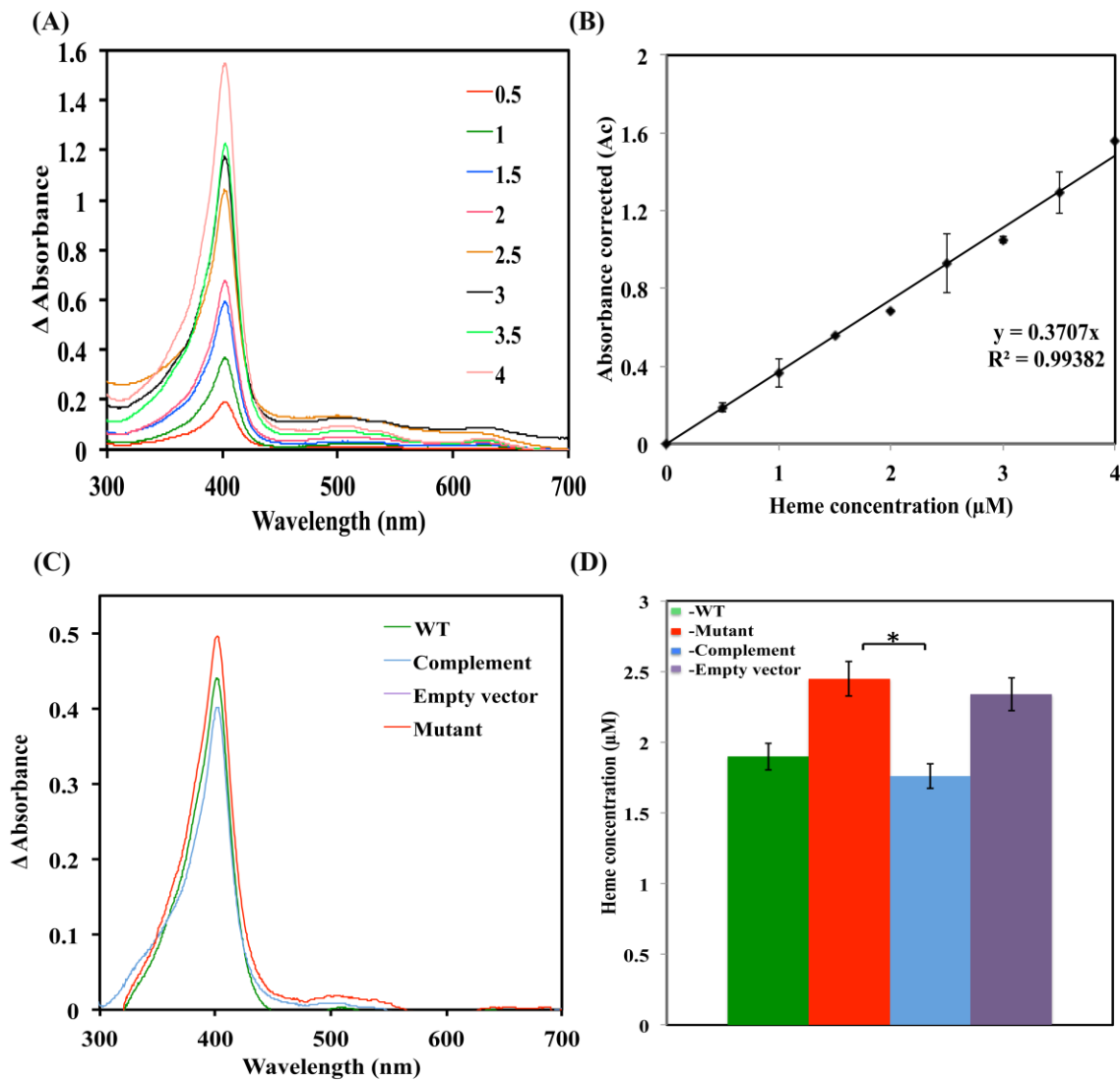


Figure 25: Inactivation of the *pefCD* transporter leads to cellular accumulation of heme in cells grown in the presence of heme. A. UV-visible spectra across wavelengths (250-700 nm) were recorded for organic fractions recovered after acidified chloroform extraction performed on a range of heme standards. **B.** The observed absorbance at 388, 450, and 330 nm from UV scans (of organic fractions) were plugged into $A_c = 2A_{388} - (A_{450} + A_{330})$ equation. The A_c values for standards extracted using

chloroform for a range of hemin concentrations (0-4 μM , with 0.5 μM increments) were plotted against its hemin concentrations to generate a standard plot. The line equation of a standard plot was used to extrapolate hemin concentrations in the experimental samples. Cultures of NZ131 (WT), ZE4951 (Mutant), ZE4951/pANKITA5b (Complement), and ZE4951/pKSM201 (Empty vector) strains were treated with 3 μM heme during the mid logarithmic phase of growth (60-70 Klett units). Cells were harvested, washed, and were subjected to chloroform extraction. **C.** UV-visible spectra across different wavelengths (250-700 nm) of the collected organic phases from tests samples were recorded. **D.** Heme concentration in the test samples. The concentrations of heme in the test samples were calculated using the standard curve shown in B. The data are derived from two independent experiments each performed in triplicates. The asterisk (*) denotes that the observed P value is statistically significant ($P < 0.05$) calculated using student t-test (equal variance) at 0.05 levels of significance.

FIGURE 26.

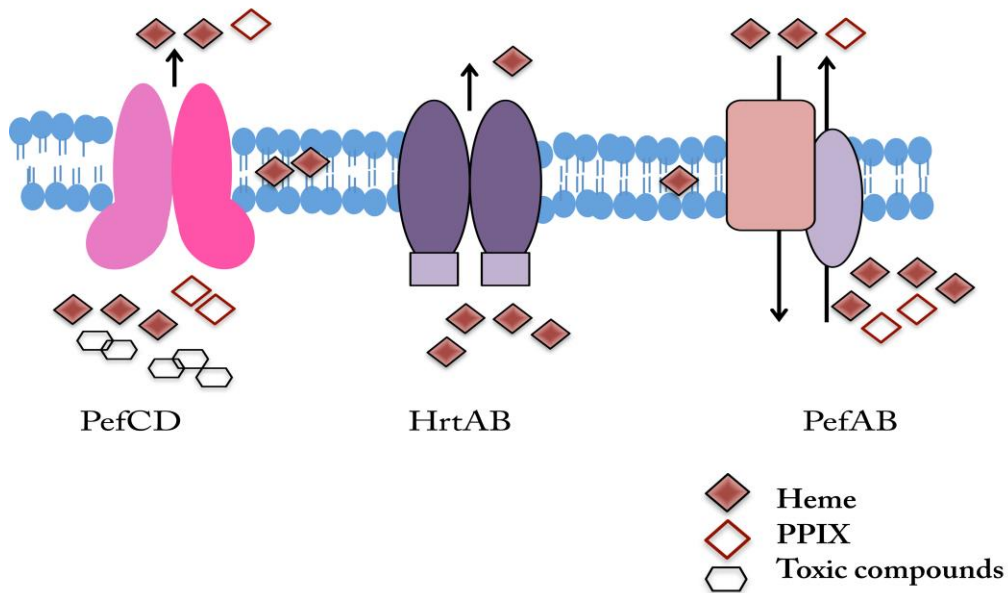


Figure 26: A schematic depiction of heme-tolerance transporters described in streptococci.

Putative homologs of the HrtAB (Class-3 ABC-type transporter) were identified in GBS, and were shown to be induced by heme. The PefAB and PefCD are heme and PPIX efflux machineries used by GBS. PefAB is related to the drug/proton antiporter family, while PefCD consists of Class-1 ABC type transporter. Our data show that GAS employs PefCD to efflux heme and provide cyto-protective function to various biomolecules.

Appendix C: Supplementary Tables

Table 1: The *S. pyogenes* MGAS5005 Heme stimulon.

<u>Locus^a</u>	<u>Gene^b</u>	<u>Expression^c</u>	<u>Putative function^d</u>
<i>Activated in the presence of Heme</i>			
		2.182 ±	
Spy0013	<i>ftsH</i>	0.033	Cell division protein - COG0465 [O] Phosphoribosylaminoimidazole carboxylase
Spy0031	<i>purK</i>	2.01 ± 0.095	ATPase subunit - COG0026 [F]
		2.638 ±	GB transport ATP-binding protein -
Spy0157	<i>opuAA</i>	0.162	COG4175 [E]
		2.127 ±	GB-binding protein/GB transport system
Spy0158	<i>opuABC</i>	0.147	permease protein - COG2113/4176 [E]
		2.552 ±	
Spy0186		0.086	Transcriptional regulator - COG1846 [K]
		2.778 ±	Transcriptional regulator, MarR family -
Spy0195	<i>pefR</i>	0.101*	COG1846 [K]
		2.001 ±	MDR ABC transporter ATP-binding and
Spy0196	<i>pefC</i>	0.104	permease protein - COG1132 [V]
		2.112 ±	MDR ABC transporter ATP-binding and
Spy0197	<i>pefD</i>	0.086	permease protein - COG1132 [V]
		2.673 ±	Serine/threonine sodium symporter -
Spy0275		0.112	COG3633 [E]

		3.594 ±	
Spy0300		0.091	Hydrolase, HAD superfamily - COG1418 [R]
Spy0301		4.24 ± 0.103	Integral membrane protein - COG0670 [R]
		2.191 ±	ATP-dependent Clp protease proteolytic
Spy0328	<i>clpP</i>	0.061	subunit - COG0740 [O]
		2.036 ±	
Spy0329		0.127	Hypothetical cytosolic protein
		2.202 ±	Peptide methionine sulfoxide reductase -
Spy0382	<i>msrA.2</i>	0.108	COG0225 [O]
		2.539 ±	
Spy0383		0.109	D-alanyl-D-alanine carboxypeptidase
		2.609 ±	67 kDa Myosin-crossreactive antigen -
Spy0385		0.088	COG0493 [E]
		2.162 ±	
Spy0423	<i>pepQ</i>	0.074	Xaa-Pro dipeptidase - COG0006 [E]
Spy0425		2.235 ± 0.07	Glycosyltransferase - COG0438 [M]
		2.519 ±	Plasmid stabilization system antitoxin protein
Spy0456		0.122	- COG3077 [L]
		2.185 ±	Plasmid stabilization system protein -
Spy0457		0.101	COG2026 [J/D]
		2.406 ±	Transcription antiterminator, BglG family -
Spy0474	<i>licT</i>	0.099	COG3711 [K]
Spy0477		2.195 ±	Hypothetical membrane spanning protein -

		0.061	COG3689 [S]
		2.804 ±	Hypothetical membrane spanning protein -
Spy0479		0.078	COG0785 [O]
		4.014 ±	Stress-responsive transcriptional regulator -
Spy0483		0.105	COG1983 [K/T]
		3.168 ±	
Spy0509	<i>tpi</i>	0.075	Triosephosphate isomerase - COG0149 [G]
		2.219 ±	(R,R)-butanediol dehydrogenase/acetoin
Spy0534		0.102	dehydrogenase - COG1028 [I/Q/R]
		3.791 ±	
Spy0660	<i>fruR</i>	0.165	Fructose repressor - COG1349 [K/G]
		4.285 ±	
Spy0661	<i>fruB</i>	0.163	1-phosphofructokinase - COG1105 [G]
		2.774 ±	PTS system, fructose-specific IIABC
Spy0662	<i>fruA</i>	0.153	component - COG1299/1445/1762 [G/T]
		2.111 ±	
Spy0677	<i>fms</i>	0.073	Peptide deformylase - COG0242 [J]
		3.928 ±	Putative ATP-dependent Clp proteinase
Spy0694	<i>clpL</i>	0.141	(ATP-binding subunit) - COG0542 [O]
		3.181 ±	ABC transporter substrate-binding protein -
Spy0743		0.139	COG2984 [R]
		2.488 ±	
Spy0744		0.113	Hypothetical protein

		2.051 ±	ABC transporter permease protein -
Spy0745		0.147	COG4120 [R]
		2.511 ±	
Spy0877		0.082	Hypothetical protein
		2.527 ±	
Spy0878		0.104	Hypothetical protein
		2.092 ±	
Spy0880	<i>hlyIII</i>	0.123	Putative hemolysin III - COG1272 [R]
		2.009 ±	(Citrate [pro-3S]-lyase)-ligase - COG3053
Spy0910	<i>citC</i>	0.058	[C]
		2.105 ±	
Spy0924		0.131	Transcriptional regulator, GntR family
		2.353 ±	
Spy0947	<i>ciaH</i>	0.055	TCS histidine kinase - COG1167 [K/E]
		2.094 ±	
Spy0948	<i>ciaR</i>	0.057	TCS response regulator - COG074 [T/K]
		2.188 ±	
Spy0982		0.089	Histidine-binding protein - COG0834 [E/T]
			Putative competence protein/transcription
Spy1137	<i>coiA</i>	2.296 ± 0.12	factor
			Ribosomal small subunit pseudouridine
Spy1138	<i>rsuA</i>	2.823 ± 0.136	synthase A - COG1187 [J]
Spy1139	<i>nagB</i>	3.114 ±	Glucosamine-6-phosphate isomerase -

		0.132	COG0363 [G]
		2.074 ±	
Spy1203		0.027	Phage protein
Spy1222	<i>int.2</i>	1.94 ± 0.143	Phi5005.2 integrase - COG0582 [L]
		5.047 ±	ATP-dependent clp protease ATP-binding
Spy1240	<i>clpE</i>	0.174	subunit - COG0542 [O]
		2.115 ±	Acetate CoA-transferase alpha subunit -
Spy1345	<i>atoD.1</i>	0.122	COG1788 [I]
		2.109 ±	CopAB ATPases metal-fist type repressor -
Spy1406	<i>copY</i>	0.102	COG3682 [K]
			Guanine-hypoxanthine permease - COG2252
Spy1477		2.34 ± 0.117	[R]
		3.327 ±	
Spy1497	<i>dnaJ</i>	0.103	Chaperone protein - COG0484 [O]
Spy1498	<i>dnaK</i>	4.58 ± 0.09	Chaperone protein - COG0443 [O]
		3.876 ±	
Spy1499	<i>grpE</i>	0.112	Hypothetical protein - COG0576 [O]
		4.081 ±	Heat-inducible transcription repressor -
Spy1500	<i>hrcA</i>	0.142	COG1420 [K]
		2.491 ±	
Spy1559	<i>trx</i>	0.125	Thioredoxin - COG0526 [O/C]
		2.127 ±	PTS system, lactose-specific IIBC component
Spy1633	<i>lacE</i>	0.066	- COG1455 [G]

		1.991 ±	
Spy1669	<i>def</i>	0.091	Peptide deformylase - COG0242 [J]
		2.936 ±	
Spy1670		0.101	Oxidoreductase - COG0431 [R]
Spy1709		2.961 ± 0.17	Hypothetical protein - COG3237 [S]
		2.448 ±	Hypothetical protein (Mga-associated) -
Spy1722		0.082	COG0477 [G/E/P/R]
		2.585 ±	Immunogenic secreted protein - COG0810
Spy1723	<i>isp</i>	0.131	[M]
		2.554 ±	
Spy1724	<i>ihk</i>	0.136	TCS histidine kinase - COG0642 [T]
		2.719 ±	
Spy1725	<i>irr</i>	0.164	TCS response regulator - COG0745 [T/K]
		3.699 ±	ABC transporter ATP-binding protein -
Spy1727		0.118	COG1136 [V]
		2.458 ±	Periplasmic component of efflux system -
Spy1728		0.127	COG0845 [M]
		3.357 ±	
Spy1729		0.148	Hypothetical protein
		2.691 ±	
Spy1730		0.078	Hypothetical protein
			Protein export protein PrsA precursor -
Spy1732	<i>prsA</i>	8.63 ± 0.043	COG0760 [O]

		2.173 ±	Multimodular transpeptidase-transglycosylase
Spy1753	<i>pbp2A</i>	0.036	- COG074 [M]
		8.351 ±	
Spy1761	<i>groEL</i>	0.134	60 kDa chaperonin - COG0459 [O]
		7.951 ±	
Spy1762	<i>groES</i>	0.134	10 kDa chaperonin - COG0234 [O]
		2.576 ±	Negative regulator of genetic competence -
Spy1763	<i>clpC</i>	0.075	COG0542 [O]
		2.567 ±	
Spy1764	<i>ctsR</i>	0.124	Transcriptional regulator
		5.238 ±	suppressor of clpP & clpX, spxA2 allele -
Spy1798	<i>spxA2</i>	0.093	COG1393 [P]
		2.204 ±	UTP--glucose-1-phosphate uridylyltransferase
Spy1853	<i>hasC</i>	0.078	- COG1210 [M]
Spy1865	<i>htrA</i>	3.539 ± 0.12	Protease Do - COG0265 [O]

Repressed in the presence of Heme

Spy0015		0.43 ± 0.158	Hypothetical protein
		0.368 ±	
Spy0040	<i>adhA</i>	0.112	Alcohol dehydrogenase - COG1064 [R]
		0.333 ±	Transcriptional regulator, LysR family -
Spy0117		0.088	COG0583 [K]
			Transcriptional regulator, LysR family -
Spy0118		0.374 ± 0.09	COG0583 [K]

		0.246 ±	V-type sodium ATP synthase subunit K -
Spy0127	<i>ntpK</i>	0.275	COG0636 [C]
		0.219 ±	V-type ATP synthase subunit C - COG1527
Spy0129	<i>ntpC</i>	0.274	[C]
		0.219 ±	V-type sodium ATP synthase subunit F -
Spy0130	<i>ntpF</i>	0.258	COG1436 [C]
		0.118 ±	V-type sodium ATP synthase subunit A -
Spy0131	<i>ntpA</i>	0.306	COG1155 [C]
			V-type sodium ATP synthase subunit B -
Spy0132	<i>ntpB</i>	0.092 ± 0.35	COG1156 [C]
		0.138 ±	V-type sodium ATP synthase subunit D -
Spy0133	<i>ntpD</i>	0.328	COG1394 [C]
		0.249 ±	
Spy0340	<i>lctO</i>	0.124	L-lactate oxidase - COG1304 [C]
		0.458 ±	Phosphoglycerate transporter protein -
Spy0361		0.107	COG2271 [G]
Spy0562	<i>sagA</i>	0.31 ± 0.19	Streptolysin S biosynthesis protein
		0.325 ±	Streptolysin S biosynthesis protein -
Spy0563	<i>sagB</i>	0.124	COG0778 [C]
		0.334 ±	
Spy0564	<i>sagC</i>	0.116	Streptolysin S biosynthesis protein
		0.286 ±	
Spy0565	<i>sagD</i>	0.129	Streptolysin S biosynthesis protein

		0.329 ±	Streptolysin S putative self-immunity protein
Spy0566	<i>sagE</i>	0.105	- COG1266 [R]
		0.273 ±	Streptolysin S biosynthesis protein -
Spy0567	<i>sagF</i>	0.135	COG0477 [G/E/P/R]
		0.282 ±	Streptolysin S export ATP-binding protein -
Spy0568	<i>sagG</i>	0.127	COG1131 [V]
		0.304 ±	Streptolysin S export transmembrane protein -
Spy0569	<i>sagH</i>	0.146	COG0842 [V]
		0.354 ±	Streptolysin S export transmembrane protein -
Spy0570	<i>sagI</i>	0.113	COG0842 [V]
		0.312 ±	Endonuclease/exonuclease/phosphatase
Spy0571		0.086	family protein - COG2374 [R]
		0.069 ±	PTS system, mannose/fructose family IIA
Spy0780	<i>ptsA</i>	0.312	component - COG2893 [G]
		0.073 ±	PTS system, mannose/fructose family IIB
Spy0781	<i>ptsB</i>	0.298	component - COG3444 [G]
		0.093 ±	PTS system, mannose/fructose family IIC
Spy0782	<i>ptsC</i>	0.262	component - COG3715 [G]
		0.369 ±	PTS system, mannose/fructose family IID
Spy0783	<i>ptsD</i>	0.202	component - COG3716 [G]
		0.467 ±	
Spy0784	<i>spt5S</i>	0.112	TCS histidine kinase - COG2972 [T]
Spy0830	<i>dpiA</i>	0.419 ±	Transcriptional regulatory protein - COG4565

		0.129	[K/T]
		0.273 ±	
Spy0901		0.174	Hypothetical protein
		0.306 ±	Citrate lyase acyl carrier protein - COG3052
Spy0905	<i>citD</i>	0.183	[C]
		0.291 ±	Citrate lyase beta chain/citryl-CoA lyase
Spy0906	<i>citE</i>	0.169	subunit - COG2301 [G]
			Citrate lyase alpha chain/citrate CoA-
Spy0907	<i>citF</i>	0.33 ± 0.129	transferase - COG3051 [C]
		0.315 ±	Apo-citrate lyase phosphoribosyl-dephospho-
Spy0908	<i>citX</i>	0.107	CoA transferase - COG3697 [H/I]
		0.479 ±	
Spy0929		0.089	SIR2 family protein - COG0846 [K/E]
		0.428 ±	ATPase associated with chromosome
Spy0930		0.103	architecture/replication - COG2110 [R]
			Glycine cleavage system H protein -
Spy0931		0.411 ± 0.1	COG0509 [E]
		0.416 ±	Luciferase-like monooxygenase - COG2141
Spy0932		0.102	[C]
		0.428 ±	Probable NADH-dependent flavin
Spy0933		0.085	oxidoreductase - COG1902 [C]
			Nucleoside transport system permease protein
Spy0940		0.48 ± 0.059	- COG4603 [R]

		0.417 ±	Nucleoside transport ATP-binding protein -
Spy0941		0.067	COG3845 [R]
		0.459 ±	
Spy0942		0.079	Nucleoside-binding protein - COG1744 [R]
		0.443 ±	16S rRNA m(2)G 1207 methyltransferase -
Spy0944		0.074	COG2813 [J]
		0.491 ±	Phosphate transport ATP-binding protein -
Spy0951	<i>pstB</i>	0.046	COG1117 [P]
		0.373 ±	Maltose/maltodextrin-binding protein -
Spy1058	<i>malE</i>	0.135	COG2182 [G]
		0.422 ±	
Spy1076	<i>glnH</i>	0.047	Transporter - COG0765 [E/T]
		0.468 ±	
Spy1084		0.118	Outer surface protein - COG3589 [S]
Spy1161		0.346 ± 0.12	Formate transporter - COG2116 [P]
		0.283 ±	
Spy1270	<i>arcC</i>	0.152	Carbamate kinase - COG0549 [E]
		0.278 ±	
Spy1271		0.104	Xaa-His dipeptidase - COG0624 [E]
		0.315 ±	
Spy1272		0.125	Arginine/ornithine antiporter - COG1288 [S]
		0.402 ±	Ornithine carbamoyltransferase - COG0078
Spy1273	<i>arcB</i>	0.091	[E]

		0.483 ±	
Spy1286		0.056	DNA polymerase - COG1518 [L]
		0.461 ±	
Spy1303	<i>aroE</i>	0.149	Shikimate 5-dehydrogenase - COG0169 [E]
		0.306 ±	
Spy1304	<i>lacZ</i>	0.174	Beta-galactosidase - COG3250 [G]
		0.243 ±	
Spy1305	<i>trxR</i>	0.158	TCS response regulator - COG4753 [T]
		0.345 ±	
Spy1306	<i>trxS</i>	0.162	TCS histidine kinase - COG2972 [T]
Spy1307		0.22 ± 0.145	Hypothetical membrane spanning protein
		0.168 ±	
Spy1308		0.201*	Sugar-binding protein - COG1653 [G]
			Sugar transport system permease protein -
Spy1309		0.137 ± 0.18	COG0395 [G]
		0.184 ±	Sugar transport system permease protein -
Spy1310		0.146	COG4209 [G]
		0.454 ±	Transcriptional regulator, GntR family -
Spy1315		0.053	COG1609 [K]
		0.459 ±	
Spy1316		0.082	Hypothetical protein - COG3538 [S]
		0.234 ±	
Spy1376		0.182	Transaldolase - COG0176 [G]

		0.239 ±	
Spy1377		0.136	<i>trans</i> -acting positive regulator
		0.322 ±	
Spy1378		0.099	NADH peroxidase - COG0446 [R]
		0.209 ±	Glycerol uptake facilitator protein - COG0580
Spy1379	<i>glpF</i>	0.184	[G]
		0.181 ±	Alpha-glycerophosphate oxidase - COG0578
Spy1380	<i>glpO</i>	0.133	[C]
		0.085 ±	
Spy1381	<i>glpK</i>	0.255	Glycerol kinase - COG0554 [C]
Spy1539	<i>scrK</i>	0.32 ± 0.088	Fructokinase - COG1940 [K]
		0.176 ±	Endo-beta-N-acetylglucosaminidase F2
Spy1540	<i>endoS</i>	0.105	precursor
		0.409 ±	
Spy1596	<i>glnA</i>	0.112	Glutamine synthetase - COG0174 [E]
		0.389 ±	Transcriptional regulator, MerR family -
Spy1597	<i>glnR</i>	0.078	COG0789 [K]
		0.392 ±	Multiple sugar transport ATP-binding protein
Spy1682	<i>msmK</i>	0.131	- COG3839 [G]
Spy1758		0.5 ± 0.099	Probable dipeptidase B - COG4690 [E]
		0.242 ±	
Spy1771	<i>hutU</i>	0.146	Urocanate hydratase - COG2987 [E]
Spy1772		0.22 ± 0.192	Glutamate formiminotransferase - COG3643

			[E]
			Formiminotetrahydrofolate cyclodeaminase -
Spy1773		0.16 ± 0.178	COG3404 [E]
		0.136 ±	Formate--tetrahydrofolate ligase - COG2759
Spy1774	<i>fhs.2</i>	0.138	[F]
Spy1775		0.15 ± 0.16	Hypothetical cytosolic protein - COG3758 [S]
		0.154 ±	
Spy1776		0.182	Amino acid permease - COG0531 [E]

^aSpy numbers from MGAS5005 genome.

^bWhen available, gene name is provided.

^cArray mean ± standard error. Numbers with an asterisk represent the average of array means obtained from 2 or more distinct probes for the same locus.

^dPutative function using nomenclature from the J. Craig Venter Institute (JCVI) CMR database. ABC, ATP-binding cassette; CoA, coenzyme A; GB, Glycine betaine; MDR, multiple drug resistance; PTS, PEP-dependant phosphotransferase system; TCS, two-component system. Further information relative to the gene-encoded protein is provided using the NCBI Clusters of Orthologous Groups (COG) database. Function categories are given using the letter-based nomenclature from the COG database. Information storage and processing: J, translation, ribosomal structure and biogenesis; A, RNA processing and modification; K, transcription; L, replication, recombination and repair; B, chromatin structure and dynamics. Cellular processes and signaling: D, cell cycle control, cell division, chromosome partitioning; Y, nuclear structure; V, defense mechanisms; T, signal transduction mechanisms; M, cell wall/membrane/envelope biogenesis; N, cell

motility; Z, cytoskeleton; W, extracellular structures; U, intracellular trafficking, secretion, and vesicular transport; O, posttranslational modification, protein turnover, chaperones. Metabolism: C, energy production and conversion; G, carbohydrate transport and metabolism; E, amino acid transport and metabolism; F, nucleotide transport and metabolism; H, coenzyme transport and metabolism; I, lipid transport and metabolism; P, inorganic ion transport and metabolism; Q, secondary metabolites biosynthesis, transport and catabolism. Poorly characterized: R, general function prediction only; S, unknown function.

Appendix D: Supplementary Figures

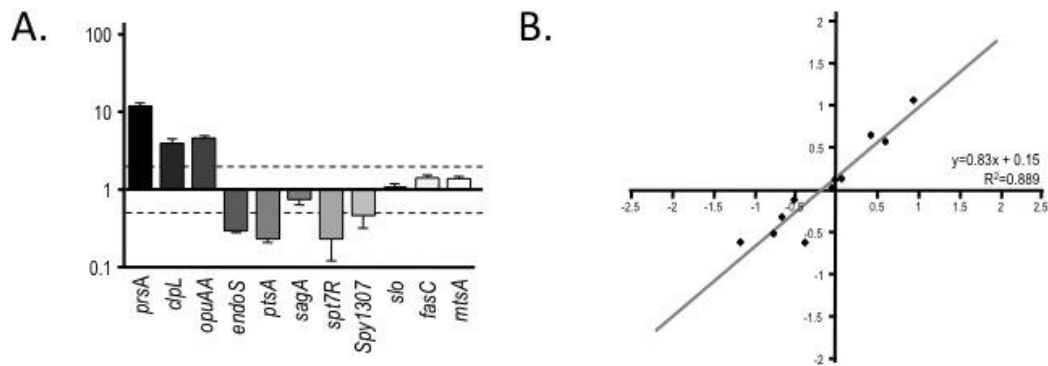


Figure 1: Microarray data validation.

A. A set of 11 genes representing the range of possible changes, i.e. increase (*prsA*, *clpL*, *opuAA*), decrease (*endoS*, *ptsA*, *sagA*, *spt7R*) and no effect (*slo*, *fasC*, *mtsA*) were selected and their expression analyzed by real-time RT-PCR. **B.** Plotting the log value of the array on the *x*-axis against the log value of the real-time RT-PCR on the *y*-axis revealed strong correlation (calculated $R^2 = 0.892$) between the two datasets.